A PERFORMANCE MODEL OF A WANKEL ENGINE, INCLUDING THE

EFFECTS OF BURNING RATES, HEAT TRANSFER, LEAKAGE AND

QUENCHING COMPARED WITH MEASURED PRESSURE TIME HISTORIES

by

Guido A. Danieli

Diploma di Laurea in Ingegneria Meccanica
Universita' degli Studi di Napoli
1971

M.S. in M.E., M.I.T.
1973

Mech. Eng. Deg., M.I.T.
1974

SUBMITTED IN PARTIAL FULFILLMENT

OF THE REQUIREMENTS FOR THE DEGREE OF
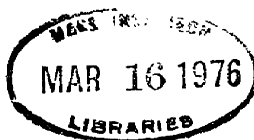
DOCTOR OF PHILOSOPHY

at the

MASSACHUSETTS INSTITUTE OF TECHNOLOGY

January, 1976

Signature of Author..
Department of Mechanical Engineering

Certified by..
Thesis Supervisor

Accepted by..
Chairman, Departmental Committee on Graduate Students

A PERFORMANCE MODEL OF A WANKEL ENGINE, INCLUDING THE
EFFECTS OF BURNING RATES, HEAT TRANSFER, LEAKAGE AND
QUENCHING COMPARED WITH MEASURED PRESSURE TIME HISTORIES

by

Guido A. Danieli

Submitted to the Department of Mechanical Engineering on January 14, 1976, in partial fulfillment of the requirement for the degree of Doctor of Philosophy.

ABSTRACT

A new performance model of the Wankel engine was developed in which the chamber was modelled as an open thermodynamic system exchanging mass, heat, and work with the environment. Real engine geometry, with the approximation of a linearized rotor cavity was included, together with a flame propagation model based on the work by Blizard and Keck. Quenching was computed from burned gas position and heat transfer studied via gas motion induced by the changing engine geometry, flame presence, and inlet and exhaust flows and relative induced turbulence. Experiments performed on a Toyo Kogyo model 12B engine were compared to the model predictions. The agreement was generally good.

Heat transfer and leakage appear to be the most significant loss mechanisms. The first, coupled to long burning times due to geometrical constraints, increases the quenched fraction while absorbing a significant fraction of the energy of the system. The second also was a severe problem, but this was probably more a problem of the engine tested than a general one. In the particular case examined, however, great improvements could be obtained especially at low speed conditions by leakage reduction.

Finally, turbulence generation due to gas motion was found to have a great influence on the flame propagation mechanism itself. This being a rather new field, more work is needed to understand the relation between gas motion and turbulence generation.

Thesis Supervisor: James C. Keck
Title: Ford Professor of Mechanical Engineering

-3-

ACKNOWLEDGMENTS

It is nice and sad at the same time to be writing this part
of my thesis. On the one hand, it is nice because it means that
I am "finally through," but on the other hand, it is sad because
it also means that I have to leave many of my friends not knowing
when I shall have the opportunity to see them again. Since this
seems to be a fact of life as much as the moment a child leaves
his father and mother, I am thankful to God for allowing our friend-
ships, and I am also thankful to Him for giving me this wonderful
educational opportunity and experience.

My father, Sergio, for his encouragement and support deserves
my everlasting gratitude.

To my wife, Renata, and my children, Giorgio, Giovanna, and
Paolo, just thanks for being such a wonderful family.

Of those who assisted in my professional undertaking, the
first person to be thanked is Professor Jim Keck, for his perennial
smile and his way of teaching things while talking to a friend.

Professor John Heywood comes next, and I should thank him for
the many suggestions as well as for "pushing" me always to give the
best of myself.

My other committee members, Dr. D. P. Hoult and Professor
B. B. Mikic are acknowledged for their contribution.

Colin Ferguson, the guy with whom I shared my battles--my few
highs and my many lows--comes next as a most authentic friend.

At this point I must apologize for not mentioning all my friends in the lab, but thanks anyway for being my friends and for being yourselves because I like you all as you are.

Among the lab personnel, a particularly deep thanks goes to Don Fitzgerald. I will always remember his professional effectiveness and competence and his human kindness.

Of my many American friends, I wish to mention Gloria and Bill Saltzberg, my host family of one time and friends forever.

No experimental work can get off the ground without the help of expert machinists. Ray Johnson and his crew fulfilled that role in my case, and I am grateful for their experienced help.

Finally the assistance of Charles Jones and Vincent Pohlmeyer of Curtiss Wright, who answered my many questions, is gratefully acknowledged.

Dr. Keniki Yamamoto of Toyo Kogyo for providing all the useful information about the geometry of my engine.

And thanks to my friend, Lucille Blake, who struggled through this manuscript to come forth with a typed edition of it.

This work was supported by James C. Keck, Ford Professor in Mechanical Engineering. The engine tested was provided by Curtiss Wright.

TABLE OF CONTENTS

Page

INTRODUCTION

The need for a complete performance model of the Wankel engine, able to take into account such effects as leakage, quenching, heat losses, and the real engine geometrical constraints have been recognized for a long time. Previous work by Bracco and Sirignano (1973) was very valuable from many points of view but did not include leakage nor quenching, and was limited to the combustion cycle alone.

Eberle and Klomp (1973) did not take into account flame quenching and especially did not consider the real engine geometrical constraints.

Danieli, Ferguson, Heywood, and Keck (1974) also neglected the geometry effects and, moreover, their model was not a complete engine simulation since they needed an experimentally measured pressure diagram. A following article by the same authors (1975) indicated that heat losses are the main loss mechanism in the Wankel engine. This coupled with long burning times indicates that gas motions and flame propagation are extremely important.

A new model is hence needed which includes real engine geometry and its effect on heat transfer during both motoring and firing by means of relations more appropriate to a Wankel than the Woschni correlation (1967). This is certainly valid for reciprocating engines, but only qualitative when applied to a rotary engine. A flame propagation model based on the work of Blizard and Keck (1974) upgraded with the use of variable laminar speed (Ferguson, 1976) a quenching and a leakage model, a better approximation to real gas properties (Martin,

1975) are also part of the simulation. Finally, to close the loop, a

gas exchange model is also needed, icluding the effect of gas motion,

induced by the process, on heat transfer. Such model, by incorporating

the real engine geometry, is able to predict the effect of rotor cavity

shape on heat transfer, flame propagation, and consequently quenching.

By allowing a change in number, position, and timing of spark plugs,

one could find "a priori" the best location for these. Finally, to

mention another possibility, by changing port location and timing, one

could study the effect on exhaust loss, volumetric efficiency and

residual gas mass fraction.

Since theoretical models are only good as long as they are

proven true, a set of experimental data was obtained to compare with

predictions.

Purpose of the present work is to show how this model is formu-

lated, what assumptions were required, and to present the results

obtained.

Chapter I describes the theoretical bases of the model, while

Chapter II presents the experimental data obtained from a Toyo Kogyo

series 12B Wankel engine. Finally, Chapter III contains the results

of the theoretical model and its comparison with experimental data.

This enables us to draw conclusions on the reason why the engine in

the present configuration is not very efficient.

CHAPTER I

THEORETICAL ANALYSIS

This chapter presents the various parts of the theory developed
to predict performances of the Wankel engine. The assumptions are
listed at the beginning of each paragraph in order to clarify as
much as possible the discussion of the theory. Moreover, when too
much algorithm is required to obtain a certain result, this is pre-
sented separately in the appendices.

1. Thermodynamic Model of the System

    Assumptions

    a. The chamber can be considered as an open system, containing

        different gaseous zones (burned, unburned, and quenched

        gases), subject to quasistatic processes and obeying the

        thermodynamic laws.

    b. Pressure is uniform at each instant of time throughout the

        system.

    c. The average enthalpy, energy, and specific volume of each

        zone can be computed at each instant of time from its average

        temperature, pressure, and composition.

    d. The enthalpy associated with any mass flux between the system

        and the environment or between zones can also be computed from

        the average thermodynamic properties of the given zone or

        environment.

    e. Chemical composition of any gas leaving the system or any

        zone can be computed from its average chemical composition.

f. "Species" that will be taken into consideration will

be only of two kinds: a mixture of air and fuel vapor

of frozen chemical composition,and burned gases (whose

composition can be either "frozen" or "equilibrium"

depending on the temperature).

Let us now examine carefully the assumptions. The first is a

definition which says that we are dealing with a thermodynamic sys-

tem in which each process can be treated as a sequence of equilibrium

conditions. Figure 1 shows a schematic of the engine in which the

ongoing processes in each chamber are shown: induction, combustion,

and exhaust. Each of the three chambers is considered as a separate

system in the thermodynamic models. The model will at any time com-

pute the processes ongoing in a single chamber, while information

about the thermodynamic state of the other chambers are needed only

to compute leakage rates. For the system considered, therefore,

other chambers are different "environments." From the same picture

one can also notice that different zones are present in both the

chamber in which combustion is occurring and the exhausting one.

The second assumption is quite standard and experimentally veri-

fied for reciprocating engines. For rotary engines the matter is

more complex since there is a flow field which does indeed produce

minor disturbances to the pressure field. In order to estimate the

error connected with the constant pressure assumption, a model was

developed based on momentum equations and the use of the perturbation

method. The description of the method is given in Appendix A while

Figure 2 shows a plot of the pressures inside the engine as a
function of time and position along the rotor face for the engine
examined rotating at 2,000 RPM. As can be seen, even if the pres-
sures are indeed non-uniform, the assumption is justified for engineer-
ing purposes since the maximum error is only of the order .5 per cent
for a very short time.

The third assumption is also very good. Note that this assump-
tion reduces to an identity if one makes use of the constant speci-
fic heat assumption. To check this assumption a test was made to
determine the error involved. Four different elements of burned gas
at temperatures of 2,800, 2,600, 2,400, and 2,200 ^{o}K were allowed to
expand adiabatically from a pressure of 1,000 k Pa to 500 k Pa. In
the meantime a mixture of the four gases starting from the initial
average temperature was expanded adiabatically from the same pressures.
The difference between the average temperature of the mixture after
expansion and the average temperature of the gases after the separate
expansions was the error connected with our assumption. The error
found was less than 0.1 per cent, hence once again negligible for engineer-
ing purposes. To test the assumption that density could be computed
also from the average temperature, the total volume occupied by the
four elements of the previous model was computed, together with the
volume occupied by an equal mass of gases having the average tempera-
ture. Although the error in this case was bigger (0.6 per cent) than
the previous case, it was still negligible for engineering purposes.
Note that the fourth and fifth assumption are very similar in nature.

Finally the sixth assumption is more than anything else a matter of definition.

Let us now examine in detail the thermodynamic model. It will be first derived in completely general terms for a system containing n zones, and then specialized for the particular cases encountered in the engine. Figure 3 is a schematic representation of the system considered; index i refers to the zone examined, and j to any other including the environment. Since a clear understanding of the symbols used in this derivation is needed, a list follows.

List of Symbols

$\bar{c}_{p_i}$ = average specific heat at constant pressure

$\bar{c}_{T_i}$ = specific enthalpy derivative with respect to p at const. T

$\bar{e}_i$ = average specific energy of zone i

E_i = total energy

eq = number of zones at thermochemical equilibrium

$\bar{h}_i$ = average specific enthalpy of zone i

h_{ij} = specific enthalpy of the gases flowing from zone i to j

h_s = specific enthalpy of species s

m_i = mass of zone i

$\dot{m}_{ij}$ = mass flux from zone i to j (zero if gas flowing in the opposite direction)

$\dot{m}_{sij}$ = mass flux of species s in the i to j direction (same convention as before for the flow direction)

MW_i =   average molecular weight of zone i

n   =   number of zones

ne   =   number of environments

ns   =   total number of gaseous species

p   =   pressure

$\dot{Q}_{ij}$ =   heat flux from zone i to j (negative if heat flow-

ing in the opposite direction)

R_s =   specific gas constant of species s

$\bar{R}_i$ =   average specific gas constant of zone i

$\bar{T}_i$ =   average temperature of zone i

t   =   time

V_i =   volume of zone i

$\dot{W}_{ij}$ =   work done by zone i on j (negative if work done by j

on i)

x_{si} =   mass fraction of species s in zone i

μ_{p_i} =   derivative of the logarithm of the molecular weight

with respect to the logarithm of the temperature

of zone i at constant p

μ_{T_i} =   derivative of the logarithm of the molecular weight

with respect to the logarithm of the pressure at constant T

Given the symbols, we can now express the third assumption as

$$\bar{h}_i = \sum_{s=1}^{ns} h_s (\bar{T}_i) x_{si} \tag{1.1}$$

$$\bar{e}_i = \sum_{s=1}^{ns} e_s (\bar{T}_i) x_{si} \tag{1.2}$$

$$V_i = (m_i \bar{T}_i \sum_{s=1}^{ns} R_s x_{si})/p \tag{1.3}$$

and the fourth and fifth as

$$h_{ij} = \bar{h}_i \;. \tag{1.4}$$

The energy equation for an open system (zone i) provides

$$\dot{E}_i = \frac{d}{dt} (m_i \bar{e}_i) = \frac{d}{dt} (m_i \bar{h}_i - p V_i)$$

$$= - \sum_{j=1}^{n+ne} (\dot{Q}_{ij} + \dot{W}_{ij}) + \sum_{j=1}^{n+ne} (\dot{m}_{ji} h_{ji} - \dot{m}_{ij} h_{ij}) \;. \tag{1.5}$$

Note that the sum is extended to n + ne element to include the presence of the different environments (ports, other chambers, walls, etc.). The net mass flux of zone i will be given by

$$\dot{m}_i = \sum_{j=1}^{n+ne} (\dot{m}_{ji} - \dot{m}_{ij}) \;. \tag{1.6}$$

Equation (1.6) can then be substituted into (1.5) to obtain

$$\sum_{j=1}^{n+ne} (\dot{m}_{ji} - \dot{m}_{ij}) \bar{h}_i + m_i \dot{\bar{h}}_i - \dot{p} V_i - p\dot{V}_i$$

$$= - \sum_{j=1}^{n+ne} (\dot{Q}_{ij} + \dot{W}_{ij}) + \sum_{j=1}^{n+ne} (\dot{m}_{ji} h_{ji} - \dot{m}_{ij} h_{ij}) \;. \tag{1.7}$$

Next, by noticing that

$$\dot{p V_i} = \sum_{j=1}^{n+ne} \dot{W}_{ij} \tag{1.8}$$

and that

$$\dot{Q}_i = \sum_{j=1}^{n+ne} \dot{Q}_{ij} \, , \tag{1.9}$$

and using equation (1.4), we can rewrite equation (1.7) as

$$m_i \dot{\bar{h}}_i = \sum_{j=1}^{n+ne} \dot{m}_{ji} (\bar{h}_j - \bar{h}_i) + \dot{p V_i} - \dot{Q}_i \quad . \tag{1.10}$$

Now for each zone

$$\sum_{s=1}^{ns} x_{si} = 1 \quad . \tag{1.11}$$

Since as mentioned in the assumptions we basically consider only two species, only three possible compositions in a single zone can occur:

a. Unburned mixture of air and fuel vapour

b. Burned gases

c. Mixture of the previous.

Of these (a) and (c) are always considered of frozen composition while (b) can either be in "equilibrium" of "frozen" composition depending on the average zone temperature.

The time rate of change of the enthalpy for a zone of frozen composition can be written as

$$\dot{\bar{h}}_i = \bar{c}_{p_i} \dot{\bar{T}}_i + \sum_{s=1}^{ns} (h_s - h_{ns}) \dot{x}_{si} \quad . \tag{1.12}$$

Substituting (1.12) into (1.10) and solving for the temperature time rate of change, one obtains

$$\dot{T}_i = [\sum_{j=1}^{n+ne} \dot{m}_{ji}(\overline{h}_j - \overline{h}_i) + \dot{V}_i p - m_i \sum_{s=1}^{ns} (h_s - h_{ns})\dot{x}_{si}$$

$$- \dot{Q}_i]/m_i \overline{c}_{p_i} \quad . \tag{1.13}$$

For the case of a zone containing gas in thermochemical equilibrium, the rate of change of the enthalpy can be written as

$$\dot{\overline{h}}_i = \overline{c}_{p_i} \dot{T}_i + \overline{c}_{T_i} \dot{p} \tag{1.14}$$

from the definition of c_p and c_T given in the list of symbols. The time rate of temperature of a zone in equilibrium can hence be written as

$$\dot{T}_i = [\sum_{j=1}^{n+ne} \dot{m}_{ji}(\overline{h}_j - \overline{h}_i) + (V_i - m_i \overline{c}_{T_i})\dot{p}$$

$$- \dot{Q}_i]/m_i \overline{c}_{p_i} \quad . \tag{1.15}$$

Now that a first equation in terms of time rate of change for pressure, temperature, and chemical composition has been obtained, we will use the perfect gas law to obtain a second. Multiplying both sides of equation (1.3) by the pressure and summing over all zones, we obtain

$$pV = \sum_{i=1}^{n} m_i \overline{T}_i \sum_{s=1}^{ns} R_s x_{si} = \sum_{i=1}^{n} m_i \overline{R}_i \overline{T}_i \tag{1.16}$$

where

$$\overline{R}_i = \sum_{s=1}^{ns} x_{si} R_s = R/MW_i \quad . \tag{1.17}$$

Next by differentiating with respect to time

$$\frac{d}{dt}(pV) = \sum_{i=1}^{n} (\dot{m}_i \overline{R}_i \overline{T}_i + m_i \dot{\overline{R}}_i \overline{T}_i + m_i \overline{R}_i \dot{\overline{T}}_i) \quad . \tag{1.18}$$

The time rate of change of the gas constant $\overline{R}_i$ can be expressed as

$$\frac{d}{dt}(\overline{R}_i) = \sum_{s=1}^{ns} (R_s - R_{ns})\dot{x}_{si} \tag{1.19}$$

for a frozen zone and as

$$\frac{d}{dt}(\overline{R}_i) = -\overline{R}_i \left(\frac{\partial \ln MW_i}{\partial \ln \overline{T}_i} \frac{\dot{\overline{T}}_i}{\overline{T}_i} + \frac{\partial \ln MW_i}{\partial \ln p} \frac{\dot{p}}{p} \right) \tag{1.20}$$

for th e equilibrium case.

We then define

$$\mu_{p_i} = \frac{\partial \ln MW_i}{\partial \ln \overline{T}_i} \tag{1.21}$$

and

$$\mu_{T_i} = \frac{\partial \ln MW_i}{\partial \ln p} \ . \tag{1.22}$$

Substituting (1.19) to (1.22) into (1.18) and reordering the terms, we obtain

$$\dot{p}V + p\dot{V} = \sum_{i=1}^{n} \dot{m}_i \overline{R}_i \overline{T}_i + \sum_{i=1}^{eq} (1 - \mu_{p_i}) m_i R_i \dot{T}_i$$

$$+ \sum_{i=eq+1}^{n} m_i R_i \dot{T}_i - \sum_{i=1}^{eq} V_i \ \mu_{T_i} \ \dot{p} +$$

$$\sum_{i=eq+1}^{n} \left(\sum_{s=1}^{ns} (R_s - R_{ns})\dot{x}_{si} \right) m_i \overline{T}_i \ . \tag{1.23}$$

Combining then (1.23) together with (1.13) and (1.15), we obtain the final expression for the pressure time rate:

$$\dot{p} = \left\{ - p\dot{V} + \sum_{i=1}^{eq} \left\{ \frac{\bar{R}_i}{\bar{c}_{p_i}} (1 - \mu_{p_i}) \left[\sum_{j=1}^{m+ne} \dot{m}_{ji}(\bar{h}_j - \bar{h}_i) \right. \right. \right.$$

$$\left. - \dot{Q}_i \right] + \sum_{i=eq+1}^{n} \frac{\bar{R}_i}{\bar{c}_{p_i}} \left[\sum_{j=1}^{n+ne} \dot{m}_{ji}(\bar{h}_j - \bar{h}_i) - m_i \sum_{s=1}^{ns} (h_s - h_{ns}) \right.$$

$$\left. \dot{x}_s - \dot{Q}_i \right] + \sum_{i=1}^{n} \dot{m}_i R_i T_i + \sum_{i=eq+1}^{n} m_i \bar{T}_i \sum_{s=1}^{ns} (R_s - R_{ns}) \dot{x}_{s_i} \right\} \right\}$$

$$/ \left\{ V + \sum_{i=1}^{eq} \left[V_i \mu_{T_i} - \frac{\bar{R}_i}{\bar{c}_{p_i}} (V_i - m_i \bar{c}_{T_i}) (1 - \mu_{p_i}) \right] \right.$$

$$\left. - \sum_{i=eq+1}^{n} \frac{\bar{R}_i}{\bar{c}_{p_i}} V_i \right\} . \tag{1.24}$$

Finally the equations for $\dot{x}_{si}$ are given by mass conservation of the species

$$\dot{x}_{si} = \frac{\dot{m}_{si} - x_{si}\dot{m}_i}{m_i} = \frac{1}{m_i} \sum_{j=1}^{n+ne} (x_{sj} - x_{si}) \dot{m}_{ji} . \tag{1.25}$$

Since the volume dependence on time is known, if some initial conditions are given at a given instant of time, the system of equations can be integrated from the initial condition.

Note that these equations are in dimensional form since they have to be integrated continuously and possibly for some consecutive cycles. Hence, since each process starts from different initial conditions, it is easier to keep the dimensional form rather than keep on changing the initial conditions. For instance, it would be meaningless to nondimensionalize the equations during the exhaust process with respect to the

energy of the system before combustion, and equally meaningless it would be during the following combustion cycle, that will presumably start from different initial conditions, giving that the process is going toward steady state.

The following sections of this chapter will then show the way the other time rates are computed. But, before going any further, let's examine how these absolutely general equations are applied to the various conditions characteristic of the engine cycle.

a. Inlet and Compression

One zone of frozen composition was considered, in which two species were allowed, pure unburned (pure mixture of air and fuel vapours) and burned. Six different "ports" or environments considered, inlet and exhaust port, tailing and leading chamber, housing and rotor walls. Since only one zone is considered, only one temperature is defined. Note that if no fuel vapours are allowed and no burned gases present, this reduces to a motoring simulation.

b. Combustion and Expansion

Three zones were considered, two of frozen composition (unburned and quenched); one of equilibrium (burned gases). Two species are allowed as before. Note that the unburned region (frozen) is then composed by both species, pure unburned, coming from the fresh mixture introduced into the engine during intake, and burned gases (residual). This time since three zones are considered, three different temperatures are defined.

No diffusion was allowed between burned and quenched regions. Heat Transfer, computed with the method described in a following

paragraph was subtracted only from the burned gas after its mass fraction was becoming significant. Before this time, it was subtracted from both unburned and burned. Hence unburned and quenched were essentially treated isentropically after the initial stage.

Note that this is what was done in the particular case of the computations presented in this work, but in the model provision was made to allow to change the heat loss distribution if desired.

c. Exhaust

This part was treated substantially as combustion; the only difference being that after the end of the combustion, quenched gases were discarded as a separate region and two regions only considered, unburned and burned.

2. Combustion Model

Assumptions

a. Mechanisms of combustion inside an eddy is laminar

b. Mechanism of transfer of combustion is turbulence dominated through transfer of radicals.

The Blizard and Keck model of combustion (1974) for a reciprocating engine is here reviewed and then used with obvious adaptations for the case of a Wankel engine.

Let us first observe that, if one assumes that an eddy will burn at a rate which is dominated by the laminar speed (which strictly speaking can only be true if the size of the eddy is many times bigger

than the laminar flame thickness), its characteristic burning time will be given by $\tau = \dfrac{\ell_e}{S_u}$ where ℓ_e is the eddy characteristic size before combustion while S_u is the laminar flame speed. If we now consider an element of turbulent flame propagating in a duct (Figure 4) of thickness by, given A, total cross-sectional area, and A_u, cross-sectional area still occupied by unburned gases, the rate at which mass will be burning at the given section will be given by

$$\dot{dm}_{b_{local}} = \frac{A_u \rho_u \, dy}{\tau} \tag{1.26}$$

since all of the unburned gases are in eddy form. Clearly the total mass contained in the element of thickness dy will be given by

$$dm_{local} = (A_u \rho_u + A_b \rho_b) dy \; . \tag{1.27}$$

By dividing the two relationships (1.26) and (1.27), one obtains

$$\dot{x}_{b_{local}} = \frac{1}{\tau} \frac{A_u \rho_u}{A_u \rho_u + A_b \rho_b} \; . \tag{1.28}$$

On the other hand, it is also true that

$$x_{b_{local}} = \frac{A_b \rho_b}{A_u \rho_u + A_b \rho_b} = 1 - \frac{A_u \rho_u}{A_u \rho_u + A_b \rho_b} \; . \tag{1.29}$$

By combining (1.28) with (1.29), one obtains

$$\dot{x}_{b_{local}} = \frac{1 - x_{b_{local}}}{\tau} \; . \tag{1.30}$$

By separation of variables and upon integration

$$x_{b_{local}} = 1 - e^{-\int_{t'}^{t} \frac{dt}{\tau}} \tag{1.31}$$

where time t' corresponds to the beginning of the entrainment for the element of mass examined.

By making use of a lagrangian representation in which the element dy considered is a constant mass element and observing that, when the gas is first entrained

$$dy = u_e \, dt \tag{1.32}$$

where u_e is the entrainment speed, we can write the global burning rate as

$$\dot{m}_b = \int_o^t A \, \rho_u \, u_e \, e^{-\int_{t'}^t dt/\tau} \, dt'/\tau \tag{1.33}$$

where A is the area entrained by the flame front.

This, in the further assumption of τ - constant, can be integrated by parts starting from the expression

$$m_b = \int_o^t \dot{m}_b \, dt = \int_o^t e^{-t'/\tau} \int_o^{t'} A \, \rho_u \, u_e \, e^{t''/\tau} \, \frac{dt''}{\tau} \tag{1.36}$$

to obtain the final form

$$m_b = - \tau \, \dot{m}_b + m_e \tag{1.35}$$

where

$$m_e = \int_o^t A \, \rho_u \, u_e \, dt \tag{1.36}$$

is the entrained mass.

Note that equations (1.33), (1.35), (1.36) are identical to the ones given by Blizard and Keck (1974). The same answer can be obtained with a two-step algorithm by Ferguson (1975) and without the need to assume constant burning rate.

By noticing that at each cross section the mass still unburned can be written as

$$dm_u = A_u \rho_u \, dy \quad , \tag{1.37}$$

we can rewrite (1.26) as

$$dm_{b_{local}} = \frac{dm_u}{\tau} . \tag{1.38}$$

In the assumption that τ is time dependent but spatially constant, one can integrate over space to obtain

$$\dot{m}_b = \frac{m_u}{\tau} = \frac{m_e - m_b}{\tau} \tag{1.39}$$

which is the same as (1.35).

While for the time being we will make use of constant entrainment speed and burning times in our first attempt to match the data, let's try to build a rationale beyond the values that we will assume by trying to study how these variables should be defined. After our analysis of the experimental data will be completed, we will try to see if the following models do answer our needs or if this is not the case, why? Since we are given a value for the laminar speed (Ferguson, 1976), let's first try to build an understanding for the eddy "characteristic" size.

Given a turbulent flow through a duct of integral scale ℓ, with u' the turbulent fluctuation velocity, the Taylor microscale for the turbulence λ can be written following Tennekes and Lumley (1972) as

$$\frac{\lambda}{\ell} = \frac{15}{A} \left(\frac{u'\ell}{\nu}\right)^{-1/2} \tag{1.40}$$

where A is an unknown constant of order 1, and ν the viscosity.

On the other hand, the eddy size ℓ_e can be written as a function of the laminar speed S_u and the Taylor Microscale as (Ferguson (1975))

$$\frac{\ell_e}{\lambda} = \left(\frac{S_u}{u'}\right)^3 \left(\frac{u'\lambda}{\nu}\right) \frac{1}{15} .$$

(1.41)

Combining (1.40) with (1.41) and defining a new constant K which again should be of order 1, one obtains

$$\ell_e = K \left(\frac{S_u}{u'}\right)^3 \ell.$$

(1.42)

Next, by assuming that the integral scale corresponded to the engine average chamber height defined as

$$\ell = V/S_r$$

(1.43)

where S_r is the rotor surface, and V the instantaneous volume, the eddy length is defined minus a constant if the turbulent fluctuation velocity is known. We then need to define the entrainment speed. As a first attempt, we will identify the turbulent fluctuation velocity with the entrainment speed.

$$u_e = u'$$

(1.44)

since indeed transfer of radicals should be governed by the turbulent fluctuation velocity.

To estimate the value of u', the following algorithm is then suggested.

In a turbulent flow of mean speed V, the friction coefficient is defined according to Rohsenow (1961)

$$f = \frac{\tau_o}{\frac{1}{2} eV^2} .$$

(1.45)

Meanwhile the Reynolds analogy says that

$$\frac{h}{\rho c_p V} = \frac{f}{2} \qquad \text{,} \qquad (1.46)$$

where h is the heat transfer coefficient. Combining the two relationships, we obtain

$$\frac{\tau_o}{\rho} = \frac{hV}{\rho c_p} \quad . \qquad (1.47)$$

Introducing next the Von Karman similarity hypothesis, we can define the friction velocity

$$u_* = (\frac{|\tau_o|}{\rho})^{1/2} \qquad (1.48)$$

as a "measure of turbulence eddying," Schlichting (1968).

Now, since we do compute heat transfer, it follows that we have the theoretical possibility of computing entrainment speeds. Hence, except for the constant of the eddy length and for a second constant in the expression

$$u' = c \, u_* \qquad , \qquad (1.49)$$

our problem is now fully specified.

Now that physical models have been constructed for burning times and entrainment speeds, we will use them to check upon the values (constants) that will actually be assumed in the computation.

3. Flame Propagation Model

Assumptions

a. Hemispherical flame surface during initial combustion stages.

b. "Plane waves" propagation after the end of the initial stage till the end of combustion.

c. Combustion center moving with surrounding gases from the
    moment the entrained volume grows bigger than the spark
    plug cavity.

In analogy with what was done by Blizard and Keck (1974), the
flame will be assumed to propagate initially in hemispherical shape.
Noticing next that the spark plugs in a Wankel are located in a
recess, away from the region of gas motions, we conclude that from
the moment ignition first occurs, there will be a certain time during
which flames will develop inside the spark plug cavity. But from the
moment they enter inside the chamber, the assumption is made that
they will move with the mean gas flow (due to the changing geometry).
Let us consider as an example a flame propagating in hemispherical
shape inside a constant velocity field. If one takes a series of
pictures of the flame at diffent times, and then superimposes them,
the result will be similar to the one shown in Figure 5. By analogy,
since the burning gas cannot be a flow restriction, the center of the
flame, propagating in hemispherical shape, will move with the speed
of the surrounding gases

Obviously the shape of the flame will not be a true hemisphere,
since boundary layers and different gas velocities from point to point
will distort the shape. But, since the error in evaluating entrain-
ment surfaces introduced by a shape distortion is small, the "exact
hemisphere" assumption is kept.

Another possibility which is to be examined is that the "hot bubble"
of gases, coming out of the spark plug recess, will be broken up by

the flow creating a "multiple-kernel" system that will move with

the gas flow and might increase the entrained volume and hence

surfaces, thus accelerating the initial stage. On the other hand,

by the nature of the combustion model used here, entrainment areas

are not a region in which everything is burning orderly; hence even

a multiple-kernel system can still be treated as a growing "bubble."

The validity of the assumption will be clear when comparing experi-

mental data with the model predictions.

Clearly the hemispheric propagation, given the geometrical

constraints, cannot last forever. Three reasons will hence modify

the flames' shape.

a. Flames are touching the rotor face.

b. Flames are touching the housing sides.

c. Flames are touching the other flames generated by combustion on

the other spark plug.

Let us examine the first condition. Notice that usually the

rotor cavity is not as wide as the chamber and is located at the center

of the rotor. Hence, the flame can grow essentially undisturbed till

it touches the bottom of the cavity. But, when this happens, depend-

ing on the actual cavity shape, it is very likely that flames will

also be touching the sides of the cavity (Figure 6, flame front 1).

Note that the continuous line represents the actual cavity profile

while the dotted line represents the one-dimensional approximation.

In this event, to simplify the algorithm, the flame is transformed

into a half sphere truncated at the top, but whose height is determined

by the distance h between the housing and the rotor face in the one-dimensional cavity assumption. Hence the newly defined flame front (2 of Figure 6) will have a different generating radius.

The truncated sphere is then again allowed to grow till it reaches position 3 (being tangent to the housing sides). When this occurs, the initial combustion stage is considered completed, and a one-dimensional model for flame propagation is used (Figure 7).

In the third case, another simplification is made by letting flames grow undisturbed by the adjacent ones, but stopping the process of growth when the volume enclosed between the combustion centers is entirely entrained (Figure 8). When this happens two flame fronts are computed from this instant on, one proceeding from the trailing spark toward the trailing apex, and one proceeding from the leading spark toward the leading apex.

Note that while the first and second conditions always occur, the last can occur while the flame is still hemispherical only for particular values of timing and spark position.

Now that the problem of the transition from the initial stage to the plane-waves phase has been clarified, let us see how the computation of the volumes is actually carried on.

As mentioned at the beginning, once the flame is big enough to move out of the spark plug hole, the assumption is made that the combustion center will move with the remaining gases. Hence, if we compute the ratio between the mass contained in the region enclosed between the trailing apex and spark plug location when the flame enters

into the main chamber, and the total mass in the chamber at the same time, in absence of leaks, this fraction would always represent the original combustion center. The presence of leakage complicates the picture, however. If one assumes that it is concentrated at the apex seals and identifies by $m_{o_{t,1}}$ the mass present in the chamber at the instant the flames generated by the trailing or leading ignition first entered the chamber, then the mass fraction of the center of combustion will be given at each instant of time as

$$x_{cen_{t,1}} = \frac{x_{cen_{o_{t,1}}} * m_{o_{t,1}} - (m_{o_{t,1}} - m)/2}{m} \qquad (1.50)$$

where x represents mass fraction, indexes t and 1 are used to refer to trailing or leading flames, index cen refers to the combustion center, o to the time in which flames first entered the chamber, and m is the mass. The actual computation of $x_{cen_{o_{t,1}}}$ is explained in the geometrical notes of Appendix B. Once the combustion center of mass is located, actual flame surface and positions are obtained following different algorithms depending on the combustion phase. For instance, for the very initial stage, for the time in which the half sphere approximation is assumed, the flame surface is computed by equating the entrained volume to the volume of half a sphere. This equality is then used also for other possible stages of the flames. The volume entrained is computed by the expression

$$V_{e_{t,\ell}} = \left(\frac{x_{e_{t,1}} - x_{b_{t,1}} - x_{q_{t,1}}}{\rho_u} + \frac{x_{b_{t,1}}}{\rho_b} + \frac{x_{q_{t,1}}}{\rho_q}\right) m \qquad (1.51)$$

where index e refers to entrained, u, b, and q to unburned, burned, and quenched properties.

The position of the flames will in this case be located w/r to the position of the center of the entrained sphere. To do this, one first computes the volume enclosed beween the trailing apex and the combustion center which can be written in the form

$$V_{cen_t} = (\frac{x_{cen_t} - x_{b_{tt}} - x_{q_{tt}}}{\rho_u} + \frac{x_{b_{tt}}}{\rho_b} + \frac{x_{q_{tt}}}{\rho_q}) \quad m \tag{1.52}$$

where index tt refers to the trailing position of the flame generated by the trailing spark.

From the knowledge of this, by equating V_{cent} to the volume enclosed between the trailing apex and a variable position along the rotor surface, the center of the flame is found.

The same is done for the case in which the flames can be considered one-dimensional. For instance, the volume enclosed at each instant of time between the trailing apex, and the trailing moving flame is given by

$$V_{fl_{tt}} = (\frac{x_{cen_t} - x_{e_{tt}}}{\rho_u}) \quad m \ . \tag{1.53}$$

Once the flame positions are located, entrainment surfaces are computed according to what is described in Appendix B and then used in the equation that provides time rate of change of the entrained mass.

4. <u>Heat</u> <u>Transfer</u> <u>Model</u>

Basic assumptions of this model are:

a. Uniform pressure in the chamber

b. Thin boundary layers

c. Heat flux regulated by

$$N_u = c_1 R_e^{c_2} .$$ (1.54)

It is a well-known fact that heat transfer grows with gas speeds (forced convection). To determine the gas speed at any given cross section along the rotor surface (Figure 9), one needs to write mass conservation applied to the volume enclosed by an apex seal (the trailing in our case) and the given section. The result is

$$\frac{dm}{dt} = \int_s \rho u dA + \dot{m}_{\ell t}$$ (1.55)

where index ℓ refers to leakage and t to trailing apex. In the meantime, if the density of the control volume is uniform, we can also write that

$$\frac{dm}{dt} = \rho \frac{dV_c}{dt} + V_c \frac{d\rho}{dt} .$$ (1.56)

If then one computes time rates of change of the control volumes and obtains $\frac{d\rho}{dt}$ from the thermodynamic model, it is possible to compute the velocity profile inside the engine by marching from one end of the chamber to the other.

Notice that this is basically an inviscid solution, and that boundary layers are assumed to be thin in order to use a uniform velocity profile. This could be used as a zero-order solution to

compute boundary layers, which could be subtracted from the flow
area to obtain a new inviscid solution. But, for the purpose of
the present work, the inviscid solution is enough, at least to
give the initial idea of the magnitude of the flow involved. The
combustion process, during which three gaseous regions are present,
is then treated in basically the same way, if one divides the chamber
into regions of different properties. Actually, since quenched
and burned gases occupy basically the same region, they are mixed
adiabatically and at constant pressure. Appendix C contains all
formulas used to compute the mixing of the gases. Doing so, we can
then subdivide the chamber into five regions (Figure 10): three
fully unburned and two of mixed burned and quenched gases, divided
by "equivalent" flame surfaces, where equivalent represents the fact
that, for heat transfer only, the model assumes always plane waves,
that divide the chamber in fully burned and fully unburned portions
(completely different hence from the flame front as defined in the
combusion model).

Partial volumes enclosing the various flame fronts are then
computed, and the "equivalent" flame position located. The previous
algorithm is then applied, but by subdividing the chamber in control
elements that will then be of constant properties. To pass from one
side of the flame to the other, one first defines the combustion speed
at the equivalent flame front from

$$\rho_u A_{e_{tot}} S_{tu} = \dot{m}_{b_c} + \dot{m}_q \qquad (1.57)$$

where index t_u refers to turbulent propagation in the unburned

mixture, $\dot{m}_{b_c}$ to time rate of change of burned gases due to the

combustion alone, $\dot{m}_q$ is the time rate of change of the quenched

gas, and $A_{e_{tot}}$ is the total surface of the "equivalent" flame fronts.

Once this is done, the speed on the other side of the flame

front is computed from the equation

$$V_b = V_u - S_{tu} \ (1 - \frac{\rho_u}{\rho_b}) \tag{1.58}$$

which is derived in Appendix D.

During gas exchange processes the gas motion induced by the

addition or subtraction of mass at the ports is also computed. In

addition, during intake, the effect on heat transfer of the turbulence

induced by flow is computed by noticing that the kinetic energy of

the gas inflow will take the form of turbulent motion. Hence, if u

is the speed of the incoming gas, the time rate of change of the

energy that will be transformed into turbulent motion will be

$$\dot{E} = \frac{1}{2} u^2 \ (1 + 3(\frac{u_i'}{u})^2) \ \dot{m} \tag{1.59}$$

where u_i' is the turbulent fluctuating velocity inside the incoming

flow. Neglecting this term and introducing a dissipation rate

(obtained from dimensional analysis)

$$\varepsilon \sim \frac{(2/3 \ e)^{3/2}}{\ell} \tag{1.60}$$

where ℓ is some characteristic length, and e is the turbulent kinetic

energy. The energy e of the gas motion in the chamber is given at each

instant of time by

$$e = \int_o^t [\frac{1}{2} u^2 \frac{\dot{m}}{m} - \frac{(2/3 \ e)^{3/2}}{\ell}] \ dt \ . \qquad\qquad (1.61)$$

Since ℓ is not known a priori, but we know from the experiments of
Windsor and Patterson (1973) the decay time in an engine, we can
fit the value of ℓ to obtain the proper decay. Once this is deter-
mined, all during intake and compression, given the randomness of
the turbulent motion, defining

$$u' = \sqrt{2 \ e} \ , \qquad\qquad (1.62)$$

the turbulent fluctuation velocity, this vector will be added
orthogonally to the computed gas speed due to changing shape and
intaking mass, and on the basis of this "equivalent speed." vector,
heat transfer will be computed with the usual algorithm.

One more question could be raised about the fact that this model
assumes a linear rotor cavity, while the actual shape of the rotor
could generate a "squish" like effect when the rotor cavity is
directly facing the housing with very little clearance in between.
Let us point out that in a Wankel engine, gas flows are very high
because of mass transfer between different regions of the engine.
Now, if there is a local flow restriction, due to the actual shape
vs. the idealized one (Figure 11), the gases that are contained in
the trailing side of the chamber will migrate toward the rotor center,
and this will be before the actual restriction, since the restric-
tion will generate a small pressure gradient. Moreover, in both
cases, the average speed will be identical, the only difference being
in the u', turbulent fluctuating velocity. Hence it is probably

true that the heat transfer coefficient is increased by the real
rotor shape vs. the idealized one-dimensional cavity. But, on the
other hand, even to solve the inviscid flow problem, it would be
necessary to further subdivide the chamber in control volumes,
also in the longitudinal direction, and then apply mass conserva-
tion to the control elements so obtained. This could be done in
the future, but probably the result obtained would not be very far
from the present estimate.

Once the velocity field is known, by subdividing the chamber
into control volumes, the local hydraulic diameter is computed as

$$d_h = (A_1 + A_2)/((A_1 + A_2)/2b + b) \qquad (1.63)$$

where A_1 and A_2 are the flow areas limiting the considered control
volume and b the housing width. Next, by introducing the speed
relative to the rotor

$$V_r = \frac{V_1 + V_2}{2} \qquad (1.64)$$

as the average between the gas speed computed at the flow areas A_1
and A_2, and the speed relative to the housing

$$V_h = V_r + \frac{2\pi r}{3} \frac{RPM}{60} \qquad (1.65)$$

where r is the rotor generating radius, the Reynolds numbers of the
gas flow relative to both rotor and housing are computed, and then,
through (1.54) Nusselt obtained for both rotor and housing surfaces.
For the surface temperature constant values were assumed, based on
some measurements by Yamamoto (1969). Heat losses are then computed
through the help of the expression

$$\dot{Q} = k \ Nu \ S \ \Delta T/dh \qquad\qquad (1.66)$$

where S is the surface of the element considered, and ΔT the temperature difference between the gases and the wall temperature, and the conductivity k computed by assuming that Prandtl is constant and defining the viscosity from the Sutherland relationship.

$$\mu = 1.548 \times 10^{-6} \ \sqrt{T}/(1 + 110.4/T) \qquad\qquad (1.67)$$

where μ is in kg m^{-1} sec^{-1} if T is expressed in deg $^\circ$K.

5. Quenching Mechanism

Ferguson (1976) proposes for quenching distance the use of the relation

$$q = c \ Pe \ \alpha_u/S_u \qquad\qquad (1.68)$$

where c is a constant, α_u the thermoconductivity, S_u the laminar flame speed, and Pe is the Peclet number. Notice that the Peclet number at quenching is a relatively weak function of the thermodynamic variables; hence as a first cut, one could even assume Pe = const. However, this assumption is not made, and Peclet computed at the location at which the rate of energy release due to the combustion exactly balance the rate of energy loss due to heat transfer.

This relation was chosen because it contains, built into α_u and S_u, the dependence on pressure, temperature, as well as air fuel ratio and exhaust gas recirculation. Once a quenching thickness is hence computed through this algorithm, since areas covered by the burned gases (remember the definition of the "equivalent" flame front of the heat transfer model) are known, the mass quenched can be computed at each instant of time from the expression

$$m_q = \int_o^t \rho_u \, q \, \frac{dA}{dt} \, dt \; .$$
<div align="right">(1.69)</div>

To express the time rate of cha .ge of quench&ng, needed by the thermodynamic model, the expression was developed

$$\dot{m}_q = \rho_u q \, \dot{A}_b \sim q\rho_u A_b \, \dot{V}_b/V_b$$
<div align="right">(1.70)</div>

where q is the quenching distance, and A_b is the surface "wetted" by the burned gases. Note that the last is only an approximate expression particularly valid for Wankel engines, given the "stretched" configuration of the combustion chamber, not good for reciprocating engines.

6. <u>Leakage</u> <u>and</u> <u>Gas</u> <u>Exchange</u> <u>Mechanisms</u>

Assumptions

a. Constant leakage area concentrated at the apexes

b. Quasi one-dimensional isentropic flow

c. Gas flowing out of a chamber during combustion is unburned till burned gases reach the corresponding seal.

d. Ports were assumed to be open and closed linearly with crank angle

e. Intake and exhaust are plena

The first assumption is of capital importance both for simplicity and because in any case one cannot know any better than that. It is a well-known fact that leakage is one of those processes which are much talked about, but extremely difficult to eactly pin down, given the variable geometry and, more than anything else, the fact that if it is difficult to measure the leakage area from the disassembled

parts, it is absolutely impossible to do any better than an order

of magnitude estimate during running conditions. Hence the best

approach is indoubtedly to assume a value and keep on changing it

to obtain the best fit to the data. The second assumption is quite

standard and almost universally accepted. Finally, the third assump-

tion is actually perfectly true, if one admits that leakage areas

are concentrated at the apexas of the chamber, since the flame

will reach them only when combustion is completed.

As mentioned in the second assumption, mass fluxes between

chambers or between chamber and intake or exhaust plena are com-

puted according to

$$\frac{\dot{m}_{jk}}{m_j} = \frac{C_d A_{jk}}{V_j} \; \gamma_j R_j T_j \; \left\{ \frac{2}{\gamma_j - 1} \left[\left(\frac{P_k}{P_j}\right)^{2/\gamma_j} - \left(\frac{P_k}{P_j}\right)^{(\gamma_j+1)/\gamma_j} \right] \right\}^{1/2} \quad (1.71)$$

for

$$\frac{P_j}{P_k} < \left(\frac{\gamma_j + 1}{2}\right)^{\gamma_j/(\gamma_j-1)} \quad (1.72)$$

and

$$\frac{\dot{m}_{jk}}{m_j} = \frac{C_d A_{jk}}{V_j} \; \gamma_j R_j T_j \; \left(\frac{2}{\gamma_j + 1}\right)^{(\gamma_j+1)/2(\gamma_j-1)} \quad (1.73)$$

for

$$\frac{P_j}{P_k} \geqslant \left(\frac{\gamma_j + 1}{2}\right)^{\gamma_j/(\gamma_j-1)} \quad (1.74)$$

where indexes j and k denote upstream and downstream conditions, respec-

tively, and C_d is the discharge coefficient of the communication area

A_{jk}.

Flow coefficients used in the calculations were 1 for all leakage areas, given that we could not measure the flow area anyway. For exhaust the coefficients of .75 and 1 were used for outflow and inflow, respectively, while for intake the values were .5 in outflow and 1. in inflow. This choice was done to try to reproduce as much as possible the observed pressures in the gas exchange processes.

One last observation is to be done here concerning the period of port overlap. Since intake and exhaust are opened for a certain period and it is likely that some residual gas could be sucked into the intake manifold, in order to try to reproduce as much as possible the reality, the outflow of residual gases was integrated during port overlap and then the burned mass reintroduced into the engine during the intake process.

7. Geometrical Model

Let's consider the housing and rotor equations in parametric form, v being the independent variable for the rotor profile, and α for the housing (Figure 12) (Ansdale (1968)).

$$x_{R_o}(v) = R \cos 2v - \frac{3e^2}{R} \sin 6v \cos 2v + 2e[1 - \frac{9e^2}{R^2} \sin^2 3v]^{1/2}$$

$$\cos 3v \cos 2v \tag{1.75}$$

$$y_{R_o}(v) = R \sin 2v - \frac{3e^2}{R} \sin 6v \cos 2v + 2e[1 - \frac{9e^2}{R^2} \sin^2 3v]^{1/2}$$

$$\cos 3v \sin 2v \tag{1.76}$$

$$x_R(v) = x_{R_o}(v) \cos \frac{\pi}{6} + y_{R_o} \sin \frac{\pi}{6} \tag{1.77}$$

$$y_R(v) = - x_{R_o}(v) \sin \frac{\pi}{6} + y_{R_o} \cos \frac{\pi}{6} \qquad (1.78)$$

$$x_H(\alpha) = e \cos 3\alpha + H \cos\alpha + a \cos(\alpha + \phi) \qquad (1.79)$$

$$y_H(\alpha) = e \sin 3\alpha + H \sin\alpha + a \sin (\alpha + \phi) \qquad (1.80)$$

where $\phi = \tan^{-1} [3 \, e \sin 2\alpha/(H + 3 \, e \cos 2\alpha)]$ \qquad (1.81)

being R the rotor generating radius, e the shaft eccentricity, H

the housing quenching radius, a housing displacement from the true

epitrocoidal, and v defined between $\frac{\pi}{2}$ and $\frac{\pi}{6}$, and α between $-\pi$ and $+\pi$.

Note that equations (1.77) and (1.78) represent the rotor surface

on TDC position. Next a rotor cavity shape is given as v coordinate

along the rotor surface, and y coordinate, displacement from the true

epitrocoidal when the rotor is at TDC (points A to F). Note that the

profile is given in the relative size, while actual values of the

cavity are computed in order to respect the given compression ratio.

Once the coordinates of the rotor surface are computed, with the

correction for the rotor cavity, the rotor is then moved to the

proper crank angle with the help of the expressions

$$x_R(v, \theta) = x_R(v) \cos \theta/3 - y_R(v) \sin \theta/3 - e \sin \theta \qquad (1.82)$$

$$y_R(v, \theta) = x_R(v) \sin \theta/3 + y_R(v) \cos \theta/3 + e \cos \theta \; . \qquad (1.83)$$

Next the rotor surface is subdivided into n − 1 sections by dividing

the independent variable v in n − 1 equal intervals. (Points R_1 to R_7

on Figure 13). The perpendiculars to the original rotor profile (with

no cavity) are computed at R_1 .... R_7 with the help of the formula

$$\tan \xi = - \frac{x_R'(v)}{y_R'(v)}$$

then rotated to the proper crank angle. By computing the intercept between the perpendicular from the point on the rotor surface whose coordinates were evaluated at the same v, and the housing profile (H_1 to H_7), the corresponding value of α is determined. The algorithm of this determination is presented in Appendix E. Doing so we determined n-1 different control elements of which we know the 4 x n coordinates of the extremes.

Finally by further subdividing each given interval and integrating between the extremes of each control element, its volume together with housing and rotor surfaces enclosed and flow areas are determined.

CHAPTER II

EXPERIMENTAL RESULTS

This chapter presents the experimental apparatus that was designed in order to obtain the best accuracy in the measurements together with the widest possible range of data. Also presented is the philosophy behind certain choices and the techniques used in the various measurement. Finally, results are presented and then analyzed in an exhaustive search for consistency checks that could validate the data obtained.

To acquire a wide range of data, while performing the minimum number of actual experiments, load, speed, and air fuel ratios were varied. A base run was assumed at 2,000 RPM, equivalence ratio $\Phi = 1$ (stochiometric) and MID load. A spatial mesh of experiments was then performed changing load first (MAX and LOW), then air fuel ratios ($\Phi = .85, 1.26$), and finally speed (1,000 and 4,000).

1. Experimental Apparatus and Techniques

The engine tested was a Toyo Kogyo series 12B twin rotary Wankel engine. Table 1 contains the main geometrical parameters of the engine tested. Figure 14 is a schematic representation of the experimental apparatus. Since one of the aims of this study was to measure performance changes as one varies air fuel ratio independently of load and speed, the original carburator of the engine was removed in order to be able to externally control the exact air and fuel flows and ratios. Furthermore, in order to be able to reduce to the minimum the inhomogeneities in the mixture, a heated mixing tank together with fuel atomizers were used to mix the gases thoroughly before introducing them into the

chamber. The fuel atomizers used (Delavan) had also the characteristics to provide a fuel flow that was a known function of the atomizing pressure. This then provided also an extremely reliable way of measuring fuel flows. Three fuel atomizers were used to cover the entire speed and load range of the engine, allowing in addition the atomizers to operate always in the pressure range that would assure a small enough maximum droplet size.

Fuel was also measured with a Flowscan 200A flow counter, but this proved to be unreliable for this particular application since vibrations induced by the high pressure pump were actually recorded as more fuel flowing through the system than actually was.

Air flows were measured with two ASME Squared Edged Orifices for high and low speed, in order to minimize errors on the low-speed end of the scale.

Torque was measured with a standard M.I.T. hydraulic scale.

Ignition was provided by using the standard ignition system of the engine, but timing was chosen at each condition to obtain maximum torque.

Water and oil cooling systems were modified by providing external electric pumps and heat exchangers able to exchange heat in both directions. This was done in order to warm up the engine before starting, reduce wear and allowing the motoring of the engine in a "hot walls" condition.

Angle measurements were made with a digital clock, coupled to a counter and a trigger reset. The electronic circuit used is shown

in Figure 15. Table 2 contains the list of the electronic components used. The system was calibrated both statically, by making sure that the reset signal was corresponding to a known engine position (TDC mark on the front pulley for the front rotor) and dynamically, by triggering a strobe light out of the reset signal and shining on the front pulley while the engine was rotating at different speeds, while checking on the scope that the strobe light was actually operating exactly during the period in which the reset signal was on "high" (reset of the counter). No speed dependence was shown (hence no appreciable signal delay), and the position was found to be only slightly off from the exact center of the TDC mark (estimated error < .5° C.A.). Hence the system was judged satisfactory. Temperatures were measured with iron-constantane thermocouples, individually cali-brated before introduction in the engine setup.

Exhaust gas temperatures were measured with a chromel alumel thermocouple manufactured by Omega Co.

Pressures were measured with manometers (water or mercury) for mixing and exhaust tanks and intake orifice while five different pressure transducers were used to record pressure inside the chamber; four mounted on the rear rotor (Figure 16) and one on a spark plug adapter mounted on the front rotor.

The first four transducers were installed in the chamber to provide a continuous pressure record of the full engine cycle while the fifth was installed to provide the possibility of checking how the second rotor was performing. The transducer on the rear rotor was monitoring pressure variations during the combustion phase.

Therefore, it was probably in the best position to detect differences in the performance of the two rotors, if any.

The transducers used were (referring to Figure 16):

i.   Transducer 1   Kulite   Model XTMS-1-190-50

ii. Transducer 2   PCB   Model 111A24

iii. Transducer 3   AVL   Model 8QP 500 ca

iv. Transducer 4   Kistler   Model 601A

The fifth transducer, installed on the front rotor, was a PCB Model 111 A 24 with spark plug adapter No. 65 of PCB catalog. The reason for this wide variety of transducers and manufacturers is partially to be found in different spatial constraints (presence of studs that made necessary the use of narrow transducers) or requirements (we wanted a strain gauge on the intake side in order to evaluate the absolute value of the pressure at some point of the cycle) and partially to save as much money as possible by using what was currently available.

Figure 17 represents the scope records of the pressure measured in the engine while Figure 18 shows the same run with the four transducer outputs sawed together and their relative fields.

Two separate exhaust tanks were provided to allow independent exhaust measurements on both rotors. The exhaust measurements were carried on the M.I.T. cart, which includes the following instruments:

i.   Scott Paramagnetic Oxygen Analyzer Model 150

ii. Beckman Infrared CO Analyzer Model   864

iii. Beckman Infrared CO_2 Analyzer Model   315 A

iv. TECO Chemilumenscent NO Analyzer Model   10 A

v.   Scott Heated Hydrocarbon Analyzer Model   215

Finally the engine was fueled with a mixture of pure isooctane mixed with 2 per cent of Texaco Ursa Oil L.A.3 in order to compensate for the suppression of the oil metering pump, necessary since the mixing tank was used.

2. Results and Their Analysis

A. Exhaust Analysis Compared to Air and Fuel Flow Measurements

Exhaust concentrations of CO, CO_2, O_2, and HC were measured together with NO. By imposing the species conservation in the global combustion equation, and with the help of a constant determined experimentally (Spindt, 1965), one is then able to compute air fuel ratio of the original mixture. Now since this is also given by individual flow measurements of air and fuel, the two results can be compared. Since it is known that the ASME Squared Edged Orifices are good to about $\pm$ .5 per cent, in order to be sure that the measured air flow was indeed representing the true air flow to the engine, tests on the intake line were performed to make sure that there were no leaks, while the fuel atomizers were recalibrated since the fuel was containing 2 per cent of oil in it. Since only one intake system was used, given geometrical considerations, the mass was assumed to be evenly distributed between the two rotors.

Results showed practically no difference at all between the air fuel ratios computed from exhaust gas analysis on the two rotors separately, while an average error of - 1.6 per cent was registered between flow measurements and exhaust analysis (the measured air flow being richer). The agreement obtained is judged excellent.

B. Measurement of Pressures in the Chamber

a. Transducer Calibration

As described before four pressure transducers were used to record
pressures during the cycle Given the geometrical constraints,
only one of the transducers was provided with an independent
water cooling system, while all the other were operated at the
water jacket temperature. By doing so we knew in advance that
the calibration of the transducers, obtained at room temperature
by making use of a dead-weight tester, had to be corrected for
the temperature effect.

To avoid "thermocycling" (Danieli, 1975) of the transducers, a
coating of RTV was provided to damp the effect of the gas tempera-
ture on the transducer surface. In order to solve the problem
of finding the proper calibrations, the following system was
devised. First, transducer 1, which was facing the inlet port
and for which pressure variation was minimal, was simply cali-
brated with the dead-weight tester, and no further corrections
were made since the error introduced by it was in any event
very small.

The level of T1 was then adjusted to satisfy the requirement
that in the part of the cycle in which the volume was increas-
ing, the level should have been lower than the measured pressure
in the inlet tank. This method to obtain the absolute pressure
level was used rather than the zero voltage line since it was
observed that the zero pressure signal of the transducer was not
very stable.

The traces of transducer T2 were then joined to the ones of

T1 using for T2 the calibration of the dead-weight tester as

a first trial. In order to set the level of T4 it was first

observed that, since the exhaust tank was relatively far from

the engine, due to wave propagation phenomena, the pressure in

the engine can occasionally drop below the pressure in the tank,

even if, on the average, the pressure in the engine is higher

than the one in the tank. The absolute level of T4 was hence

determined accordingly to what said.

As trial value for the calibration of T4, the dead-weight tester

was used. Finally, T3 was connected to T4, and the first trial

pressure diagram obtained for all runs.

This given, the calibration on T4 was changed by comparing its

output with the one of T3 and performing a least-square fit of

the two outputs for all runs. This was done since T3 was the

independently water cooled one, and previous work (Danieli, 1975)

showed that it was an extremely reliable transducer if one made

sure that the temperature of the cooling fluid was constant.

Finally, T2 was recalibrated by imposing the loop closure in the

average.

The observed deviation from the dead-weight tester calibration

was for T2 + .5 per cent and for T4 - 4.8 per cent, hence acceptable.

b. Results

The experimentally measured pressure diagrams as obtained after

the data reduction for the seven firing cases are shown at the

end of the third chapter in Figures 32 to 38. They are generally

good except the one relative to 4,000 RPM, in which a mismatch

of 2.5 per cent was present in the region of TDC (not shown in

Figure 38). This is believed to be due to passage effects since

the passage of the AVL transducer was in that case partially

obstructed by RTV. But since the error is in any case small, and

it does not affect IMEP computations given that in the region of

TDC the volume variation is smaller, the data were considered

good enough for the purpose of this research.

c. __IMEP Computation__

Given the fact that torque was measured either during firing and

motoring conditions and that we had the pressure diagrams on both

cases, the equality was tried:

$$\text{IMEP} = \int_{o}^{6\pi} P_{fir} dV/V_d = \text{BMEP}_{fir} - \text{BMEP}_{mot} + \int_{o}^{6\pi} P_{mot} dV/V_d . \qquad (2.1)$$

where indexes fir and mot refer to firing and motoring conditions, and

V_d is the displacement volume.

This strictly speaking would turn out to be an equality only if the

friction during motoring and during firing conditions were identical.

This is not absolutely certain since during firing the load on the

crankshaft is higher, but on the other hand, the oil viscosity

drops due to the higher oil temperature.

Nevertheless, it is obvious that if they are not identical, they

should be similar. Table 4 shows the results of this computation.

An average error of − .2 per cent was recorded (the pressure

integral being smaller) while the standard deviation was of about

3 per cent. The agreement is again judged excellent.

C. Global Energy Balance

By writing the energy equation for an open system in steady state, one obtains the following equation

$$[h_u(T_{int}) - h_b(T_{int})]m = [h_b(T_{exh}) - h_b(T_{int})] \ (m - m_{HC})$$

$$+ \ [h_u(T_{exh}) - h_b(T_{int})]m_{HC} + Q_{loss} + W_{usef} \qquad (2.2)$$

where m is the mass flowing into the engine per revolution, h_u and h_b the enthalpies of the gases evaluated at the intake (T_{int}) or exhaust T_{exh}) temperatures, m_{HC} is the mass which leaves the engine still unburned, Q_{loss} is the heat loss, W_{usef} the useful work.

Notice, furthermore, that the first term represents the total energy available, the second the energy wasted as exhaust loss due to temperature in exit higher than the temperature in entrance, and the third term is the energy loss due to incomplete combustion of the charge.

Since in our experiment we were measuring flows to the engine, temperatures and work, one should expect that the energy balance should be a very straightforward one. However, several sources of error are possible. Referring to Figure 19, we see that heat is entering and leaving the system in all sorts of possible ways.

Table 5 presents a complete picture of the various terms to be included in the heat loss term together with relative sizes and possible error. Appendix F contains the computation of the various secondary terms. But the bigger error of all is to be found in the measured exhaust temperature. In fact the term h_b (T_{exh}) ($m - m_{HC}$) should represent the total enthalpy outflow during one cycle. But first there is an experimental error due to radiation because the thermocouple is at

a higher temperature than the walls (see also Appendix F), and secondly, the exhaust process is really composed by two distinct phases--the "blow down," which is very short and characterized by high temperatures, and the rest of the exhaust stroke, when the rotor is pushing out the gas at almost constant pressure and temperature, characterized by a lower temperature. Now a simple thermocouple is not able to time resolve the temperatures, and only takes a time average.

For this reason, if one wants to make a global energy balance in a similar setup, one cannot hope to get good results. The only possible ways out are either use the theory to estimate the actual time-averaged temperature or use a big exhaust tank providing good insulation from the engine to the tank and measure the stagnation temperature in the tank. Then the energy balance equation will balance correctly, not before. Table 6 shows the results of the energy balance for the various runs and the magnitude of the different terms.

CHAPTER III

COMPARISON BETWEEN THEORY AND EXPERIMENTS

Two modes of operation were examined both experimentally
and theoretically, motoring and firing. We shall present first
the results obtained for the motoring runs and then the ones for
the firing runs. Finally, some parametric studies will be made to
assess possible gains to be obtained from reduction of losses.

Many parameters were to be determined in order to correctly
match the data. First of all, the constant of the Nusselt de-
pendence on the Reynolds number (equation (1.54)), the leakage area
per apex seal(A_ℓ), the characteristic decay length of the tur-
bulence induced by the intake process (equation (1.62)), finally
entrainment speed, and the characteristic laminar burning time.
Quenching computation, according to what is explained in Chapter I
did not contain any unknown and hence was not to be determined.

Luckily we had many different ways to determine them, and this
made the work at one time more difficult and precise. First item
in the agenda was the determination of the turbulence decay length,
and this was done, as mentioned already in Chapter I by fitting
the data by Windsor and Patterson. Next the heat transfer constant
could be checked either by matching the pressure diagrams or by
matching the global heat transfer to the engine with the experimentally
measured value. But while the first process contained as an unknown,
the leakage area, global heat transfer was a relatively weak function
of the leakage area. This allowed the independent determination of

of the heat transfer coefficient by first requiring agreement with the global heat transfer rate and then of the leakage area by matching the pressure. Another factor proved to be effective in decoupling the two phenomena: the different speed dependence of the two. In fact, while leakage is an extremely strong function of the speed, the same is not true for heat transfer.

Moreover, the value found for the heat transfer coefficient for both motoring and firing conditions (.047), is reasonable if one remembers that while the McAdams correlation (Rohsenow, 1961) provides for this constant the value of $\sim$ .02 (if one eliminates the dependence of the Prandtl number), such correlation is valid only for pipes in fully developed flow. Now it is fairly evident that an engine, and particularly the Wankel, is far from being a pipe in fully developed flow. In fact, gas speeds induced by the inlet jet, flame propagation, and chamber shape variation are continually changing not only in intensity but also in direction. Given this general overview on the problems encountered, let us now examine in detail the two cases studied.

1. Motoring Conditions

Figure 20 shows the pressure in the engine as a function of time as experimentally measured (continuous line) and the model prediction (dashed lines). Figure 21 is another way to look at the same data by plotting $pV^{\gamma}/p_o V_o^{\gamma}$ vs. crank angles. (γ being the ratio of specific heats, 1.4 for air), and index o referring to conditions at the beginning of the compression. This time experimental data are plotted as points while the theory is as before--the dashed line. The leakage area

used in the model was $A_\ell = 1.5$ mm^2, and the heat transfer co-
efficient $C = .047$ as mentioned before. The reason for this choice
will be clarified later on in this chapter. As can be seen the
agreement is generally good except at early crank angles. The
reason for this disagreement is to be found in an oscilloscope error,
which was distorting the signal by summing other signals to the
transducer output. This could not be immediately detected given the
fact that the error was small. The error started to become pro-
gressively worse and recently (long after the measurements were
taken) a bad capacitor was discovered in the oscilloscope's amplifier
circuit. However, because the error was in any event small, at the
time these experiments were performed, and only apparent at the low
end of the scale (low pressure), it was decided not to take new data.
The disagreement between theory and experiments, at early crank
angles also clarifies the reason why it was chosen to plot the data in
pV^γ form. In fact this form has the ability of magnifying the errors
while providing a way to locally verify the rate of losses due to both
heat transfer and leakage.

As can be observed, the pV^γ plots are not antisymmetric about
TDC. This is due to many combining factors. First, the turbulence
induced during the intake process (and hence heat transfer produced
by the turbulent motion) decays during the compression. Hence this
is a first factor contributing to the nonsymmetricity of the engine
behaviour.

Second gas motions due to the changing geometrical shape of the

chamber are particularly high at three locations, about $-\pi/3$, TDC and $\pi/3$ of crank angle position,(Figure 21B). But the first two peaks will clearly take a much higher toll in terms of heat; hence when the gases will be at the third peak in gas speed, not much heat will be lost.

Figure 22 shows the heat transfer due to gas motion induced by the changing geometry as a function of time and position along the rotor surface. Notice how "peaky" is heat transfer at $-\pi/3$ and how much lower it is on the other side of the stroke. Figure 23 further shows this behaviour by a contour plot.

Since these are two basic unknowns in the motoring performance of a Wankel, leakage area and heat transfer coefficient, it was decided to make a parametric study by varying them one at a time.

A first parametric study was made to see what the effect of leakage alone was, and, to make the matter more evident, heat transfer was held to zero. Figure 24 shows the pV^γ plots for three cases at constant speed and varying the leakage are to 0, 1, and 2 mm^2 per apex seal.

In all cases presented here pV^γ was always computed, for sake of simplicity, using a constant value of γ - but the program, as stated in the description of the thermodynamic model, did not contain any specific heat assumption. Consequence is that the curve generated for the isentropic case (top curve of figure 24) presents a minimum in the region of TDC, where temperatures are higher and hence γ lower. Notice that this fact further enhances the nonsymmetricity of the curves about TDC when there is leakage and heat transfer.

A second set of theoretical curves was then generated, assuming
now as a trial value for the constant of the heat transfer relation
the value given by Woschni (1967) which was developed by matching
piston engine data. This time speed was also varied (Figure 25). A
final set of curves was then generated holding constant the leakage
area to 1 mm^2 and varying the heat transfer coefficient (Figure 26).
The last two sets of curves can then be represented on still another
plot which presents peak pressure in the motoring engine as a
function of speed and for variable leakage area and heat transfer
coefficient together with the experimental values (Figure 27). Given
hence the experimental data, on the basis of the curves generated,
it was found that the overall best fit to the data should have been
obtained for $A_\ell \sim 1.5$ mm^2 per seal and $Q \sim 1.5$ W where W represents
the Woschni constant (.035). The values so determined were to be
considered as a first trial value. In fact, while no major changes
were expected for the leakage area during motoring, the value of
the constant of the heat transfer coefficient was only determined
as a first trial to be ~ 1.5 W (or .052). A better value for it
was to be determined by comparing global heat losses from the engine
during firing with model predictions. This was done as explained
in the following paragraphs, and hence the final values of $A_\ell = 1.5$ mm
and $Q = 1.35$ W (.047) were determined. These are the values of
the parameters with which the curves presented at the beginning of
this section were calculated.

One more observation is to be made before moving to the

discussions of the firing conditions. Mass flows were recorded

during experiments, and a disagreement was found between mass flow

predicted and measured, the predicted being too low by about 10 per

cent of the average, the error decreasing with speed, as it should be

expected. The reason for this rather important discrepancy is to be

found in the fact that the model does not take into account leakage

past the side seals but assumes all leakage is past the apex seals.

Now the error induced by assuming that all leakage goes into the

other chambers is completely negligible when one tries to match

theoretical predictions with experiments in the region of high pres-

sures. This is because in that region, since leakage is outgoing, it

is not important where the gas goes as long as it will leave the

system. On the other hand, if side seal leakage is present, the gas

will leave the high pressure chamber and go into the "side seal re-

servoir," created by the volume defined between the crankshaft and the side

gas seals on the rotor surface. Now what happens is that not all the

mass that leaves the high pressure chamber will then leak from the

"side seal reservoir" into the inducting chamber, but a part of it will

be lost through the oil pan into the atmosphere. Hence globally less

mass will leak into the inducting chamber, and as a consequence more

mass of fresh mixture will enter the system. Given these considerations,

the error induced by neglecting the side seal leakage becomes completely

negligible during motoring, since in any event it is always air that is

circulating around the engine. On the other hand, during firing the

error could be more important since it could influence the computed

residual gas mass fraction. However, since most of the mass that
leaks into the inducting chamber is unburned, on the balance also in
this case the error should be a minor disturbance. Hence, the only
real shortcoming of neglecting leakage through the side seals is that
predicted and measured mass flowrates do not match, and that con-
sequently thermodynamic efficiencies computed from the model are
higher than the ones computed from the experimental data.

2. Firing Conditions

As mentioned in the previous paragraph, a first trial value
for the heat transfer constant was determined for the motoring runs.
A better value was expected to be determined by matching global heat
transfer rates predicted with measured values during firing. The
value was then to be used also for the motoring runs since there is no
apparent justification for a different value of it from motoring to
firing, once the flow field is determined for both.

The situation is quite different for leakage. In fact, it is to
be expected that engine clearances will vary between motoring and
firing conditions, since, during the latter, all components of the
engine will be hotter while the housing will not be able to expand in
the same way as the other parts. This is because it is constrained in
longitudinal direction by the presence of the studs which hold the
engine together and which are basically at the same temperature during
either firing or motoring, as long as the water jacket is kept at the
same temperature. Hence, we were not surprised when we discovered that
the use of the same leakage area found for motoring led to pressures

during firing which were too low. This different behaviour between
motoring and firing conditions has also been found and reported by
Eberle and Klomp (1973). A leakage area of 1 mm^2 per apex seal was
then used. The reasons for this choice will be clearer when a
parametric study of the pressure dependence on the leakage area will
be presented.

If we then accept as a first trial value for the leakage area
A_ℓ = 1 mm^2 and for the heat transfer coefficient .052 (or 1.5 W),
we can next proceed to the computation of the values of the entrain-
ment speed (U_e) and of the characteristic burning time (τ) that fit
best our data. Since only one condition should be examined in these
preliminary studies, it was decided to use the base condition of the
experimental runs, corresponding to 2000 RPM, MID throttle setting
and stoichiometric air-fuel ratio. This corresponds to Run # 9. A
parametric study was then done to find the point of best fit by
first varying the entrainment speed between 12 and 6 m/sec while
holding for the characteristic burning time the value of .4 m sec
(corresponding to a combustion delay of about 5 degrees of C.A. at
this speed). Figure 28 presents the results of the simulations com-
pared to the actual pressure trace that was the goal to be matched
(solid line). On the same picture the mass fraction burned, defined
as the ratio between the total mass burned from ignition and the mass
in the chamber of the same time, is plotted. Note that in no case does
it reach 1, due to the fact that quenching prevents the flame from
burning the mixture near the walls. Notice also that if the combustion
is faster (and higher peak pressures occur), less mass is quenched

given the dependence of the quench thickness on pressure and
temperature. The same results are then displayed in a pV^γ plot
(same figure, upper graph) where now index o refers to ignition
conditions, and the γ used are different for the compression stroke
and the combustion-expansion parts. The values of γ (constant) used
here were the ones given by Danieli et al (1974), obtained through a
fit to enthalpy data for real gases, using constant specific heats.
These data are presented in Appendix B of the surnamed paper. Next
the entrainment speed was held constant while τ was varied from .8 m sec
to .04 m sec. The results of these simulations are shown in Figure 29.

On the basis of the results obtained in these parametric studies,
the "best values" of τ = .6 m sec and u_e = 7 m/sec (note that the
rotor tip average speed 7.3 m/sec at this speed) were determined.
This was done by looking more at the combustion period and rise in
pressure and pV^γ than by trying to match the level of the jump in
pV^γ between end conditions. In fact, it was felt that since the
magnitude of the jump was not such a strong function of the values
assumed for the entrainment speed and the burning time, the most
important part to be matched "as a first cut" was the burning law
itself.

Following this, by matching global heat transfer measured and
predicted (Table 7), the value of the constant in the Nusselt re-
lations was determined to be approximately 1.35 the value given by
Woschni. Note from Table 7 that while as mentioned before the error
on the mass induced match is big, the same is not true for work out-
put (expressed as IMEP) and global heat losses. Particularly if

one discards runs 11 to 13 (that had some problems as explained later)
the average error on work and heat transfer is surprisingly good.
This further confirms what previously was stated about the fact that
the mass mis-match,due to neglecting leakage through the side seals,
does not play a major role in the evaluation of the global per-
formances.

On the other hand, both Figure 28 and 29 display a mis-match
between experimental values and theory, in the jump of pV^{γ}. To
understand the possible reasons for it it was decided to try to see if
the choice of a different value for the heat transfer coefficient or
the leakage area (and note that we thought that the values we had
assumed were correct,at least as a first cut), could have been the
cause for it. First we changed the heat transfer coefficient, to see
the sensitivity to it of pV^{γ}. The result was (Figure 30) that the
jump was substantially independent on whatever value for the heat
transfer coefficient one would choose. The reason for this behaviour
is to be found in the fact , as it is explained in detail in Appendix
G, the leading term in the pV^{γ} jump is proportional to the heating
value of the fuel (ΔH) multiplied by the ratio between the mass in
the chamber at the given instant of time and the mass in the chamber
at ignition (m_o), further divided by the temperature of the mixture
at ignition (T_o). Now this last quantity (T_o) is strongly influenced
by the value of the heat transfer coefficient assumed. To this term
the heat lost (Q) from the system during combustion, divided by the
product of the initial pressure and volume, is to be subtracted. Equally
subtracted should be the work done by the system in the period (W) and

the integrated enthalpy loss (H) due to leakage. Table 8 presents
the heating value and heat loss term, multiplied by the appropriate
quantities. Work and integrated enthalpy loss are not present since
they are almost constant. Note that ΔH and γ were once again com-
puted according to Danieli et al (1964).

A totally different behaviour in the jump in pV^γ is observed
when one changes the leakage area holding the other parameters con-
stant. As can be clearly seen in Figure 31, the jump is now extremely
sensitive to the value of the leakage area assumed. This is due to
the fact that, as mentioned before, the heating value of the fuel is
multiplied by the ratio between the mass in the chamber and the
initial mass. Again, the terms Q and H are minor disturbances, and
W can be considered almost constant for the various runs. Hence the
consequence is that the pressure ratio is this time a strong function
of the leakage area. Now if it is true that the jump in pV^γ is a
strong   function of the leakage area assumed, it is also true
that one should not be tempted to jump to the conclusion that the
value assumed for the leakage area is wrong. In fact, notice again
from Figure 31, that if one judges from pV^γ alone he could find him-
self in serious trouble when matching the pressure diagrams. In fact,
while the simulation for $A_\ell = 1 \text{ mm}^2$ match rather nicely the pressure
data , the same is not true for $A_\ell = .5 \text{ mm}^2$, which is in a better
agreement with pV^γ measured. Also this time it is good to have
several ways to obtain the same result, but attention must be paid
to the way to use them.

At this point, since the values for U_e = 7 m/sec, τ = .6 msec, A_ℓ = 1 mm^2 and Q = 1.35 W (or .047) were determined, at least for one case, it was felt necessary to see how the model could predict other running conditions. While leakage and heat transfer scaling factors were from this point on not subject to further change, some decisions had to be made about the way the entrainment speed and the laminar burning time should scale with engine operating conditions. As a first approach it was decided that the entrainment speed had to scale linearly with speed. Meanwhile, the characteristic burning time, τ, was kept as a free parameter although the relation was also tried

$$\tau = \frac{\tau_{ref}}{S_u} S_{u_{ref}} \tag{3.1}$$

where ref indicates reference to the base run (#9) and the laminar speed was evaluated at some average pressure and temperature. This relation had embedded the assumption of constant characteristic eddy length, and was discarded after a few trials. A different approach was also tried, computing U_e and τ with the help of equations (1.42) and (1.49) at each instant of time, where for the constant of equation (1.42) the value of 10 (non-dimensional number) was assumed. The values for U_e and τ used in the computation (constant) together with the burning time deduced from equation (3.1) and the average value of entrainment speed and burning time computed from equations (1.42) and (1.49) are then displayed on Table 9. As it results, the model predictions are correct at lease as order of magnitude. Note that if it is true, that τ varies quite widely in the case of the

computed values, it is also true that the same behaviour is displayed

by the assumed values for it. Furthermore, one should not look at the

values of U_e and τ alone, but should also remember(as also shown in

Figures 28 and 29) that by increasing U_e or decreasing τ one obtains

almost the same result. Remembering this, the agreement looks even

better. Nevertheless, a warning is necessary at this point. The pre-

dicted values were generated on the basis of a combustion that was

generated through the use of constant values for both U_e and τ.

Hence it is not certain what would happen if one lets the predicted

values of entrainment speed and burning time drive the combustion.

Furthermore, the value of the constant in the definition of the eddy

length, equation (1.42), was assumed,as mentioned before, 10, but

if one wants to use the computed values of τ and U_e a more careful

choice of the value of the constant would be necessary. Figures 32 to

38 show the model predictions together with the experimental results

for the seven experimental conditions. Plotted on each figure are

pressure (continuous line for experimental; dashed for model), pV^γ

(data points for experimental; dashed-dotted for theoretical) and

finally, the mass fraction predicted by the model (dotted line). Also

marked on each picture is the average peak pressure (horizontal line)

obtained by computing the average peak over several traces, together

with standard deviation (dash as above and below the horizontal line).

Table 10 contains the ignition timing for the different runs.

As can be seen in some of the pressure diagrams, not all traces

coincide with the average peak pressure. This is because traces to be

analyzed were chosen quite randomly when the cycle to cycle variation

was small, and only later average peak heights were computed. As

a result, some traces are "atypical", even if data for more "typical"

conditions are available, but not presented here. Consequence of

this is that the values, determined through the "best fit", of en-

trainment speed and laminar burning time are not appropriate for trace

having peak pressure equal to the average, but rather appropriate

for the particular condition. Nevertheless one should observe that

even in the case of a not completely "typical" trace, all physical

phenomena (like heat transfer and leakage) evolve in the engine

exactly in the same way, except for the apparent combustion speed.

Worth of notice is that, except for one case, run 12 (Figure 36),

the compression stroke was correctly matched for all conditions.

Clearly something mattered in the case of run 12, and not apparent

explanation can be found except, if possible, an experimental error.

For the **expansion** strokes all of them were matched, more or less

correctly, except for run 13, which was a 1000 RPM run. We will

return later to examine this condition more carefully. Moreover also

the combustion part is matched for runs 8 - 9 - 10 - 14, except for

minor differences. Again, the matching of compression and expansion

strokes implies that the leakage and heat transfer treatments are

correct, or at least very close to actual values. The matching of

the combustion part implies that values of U_e and τ good for the

particular condition examined were chose. As a consequence, we can

claim that our model does reproduce fairly well reality. But for one

point.

Again, observing figures 32 to 38, note that the predicted

values of pV^γ are almost always lower than the experimental ones

after the end of the combustion. The explanation for this can be of

two kinds:

a. First and more obvious explanation could be an error in digitizing

the pressure data. Generally digitizing errors have the tendency

of being of the random type, while this is a systematic one. Now

systematic errors are usually more difficult to justify. Still

in the particular case of these experiments one should remember

that these pressure diagrams have been obtained by sewing

together different transducer outputs. (See Figure 17.) Moreover,

while ignition is always a point of the trace of transducer T2,

the jump is always computed on the trace of transducer T3.

Hence even a small systematic error, like imperfect value for

the calibration of T2 could be the cause of the mismatch. Now

this error is not displayed on the matching of the pressures,

since pressures (and IMEP) are far less sensitive to small errors.

But the result on pV^γ is indeed felt.

b. The second possible explanation is more subtle, but should not

be discarded "a priori". One of the parameters that enter in

the computation of the pressure at ignition is the decay of

turbulence induced by the intake stroke. Now this parameter

enters in defining the rate of heat losses all during the com-

pression stroke. From thetheory presented in the heat transfer

treatment, (equations (1.59) to (1.62)), and from the data by

Windsor and Patterson (1973) the characteristic length was

determined to be .1 m in order to obtain the proper value for
the turbulent fluctuation velocity. Now and again not enough
data are available for the Wankel engine to establish the
correctness of the assumption that turbulence decays in this
case exactly in the same way. As a consequence, it could be
that heat transfer is not fully correct during the compression
stroke. More work is therefore needed in the area of decay of
turbulence induced by the intake stroke.

Worth particular attention are runs No. 8 (Figure 32) and
No. 13 (Figure 37) for opposite reasons. Run No. 8 shows an extremely
long burning time. The first time the run was compared to the others
by plotting pV^γ, we were rather surprised by the fact that the slope
of pV^γ is not as rapidly rising as all others. The explanation was
found in the model prediction. Since the ignition timing in this
run was quite advanced and hence the mass on the leading side of the
chamber was small, the charge enclosed between the leading apex and
the trailing spark was almost immediately burned up. But after this
rapid first combustion stage, only one flame front was left, the one
originated from the trailing spark and going into the trailing dir-
ection. It is an experimentally verified fact that flames are
much faster in the leading than in the trailing direction. And the
model displays the same difficulty for the flame propagation, mainly
because of the fact that entrainment areas are constantly small in
the trailing moving flame front. We had not equipped our rotor with
ion gaps, so that a direct check on flame positions versus model

predictions is impossible, but at least qualitatively our model

agrees with measurements by Toyo Kogyo (Yamamoto and Kuroda, 1970).

And the particular case of the run mentioned provided us with an

explanation for the experimentally observed behaviour. The other

condition on which we address our attention is run 13 (Figure 37).

This was a low speed run (1000 RPM) and characterized by an ex-

tremely violent cycle to cycle variation. We already know that

small fluctuation in the peak pressure can be handled by the

model changing the value of the entrainment speed and of the

laminar burning time. But we were unprepared to accept the ex-

tremely long laminar burning time characteristic of this run.

Again in Figure 37 the horizontal line represents the average peak

pressure while the two dashes above and below it represent the

standard deviation on height of the peak. Notice that the lower

bound is lower than the motoring peak pressure, which implies that

in many cases the combustion peak pressure was lower than the

motoring peak pressure.   Here for motoring peak pressure we intend

the maximum pressure that the engine would have reached if no com-

bustion were present, and for combustion peak pressure we intend

the second pressure peak on the same curve. Again the dashed line

represents the model prediction. As can be seen the model does not

predict two distinguished peaks in pressure, and this was due to the

fact that the maximum delay (or laminar burning time) that we allowed

was 4 m sec with U_e = 3.5 m/sec. Notice instead that the model

predictions (Table 9) show a smaller value for the entrainment speed

(U_e = 1.7 m/sec) and an even longer delay (5.1 m sec). Now the fact that as a consequence of this the expansion stroke is mismatched should not surprise. In fact, if the combustion is delayed the pressures attained in a later stage (as during expansion) should be higher. Moreover, this being a low speed run, possible errors in leakage are twice as severe as in the case of a 2000 RPM.

Few more words should be spent on analyzing run 11 (Figure 35). As can be seen while the compression stroke is correctly matched, the combustion failed to reach the same peak pressure and the expansion stroke was lower than the experimental one. Notice also that this is one of the cases in which the error in the mass (Table 7) is more severe. Could be that in this case the error in the mass could have affected the residual gas recirculation or something similar had happened. The result is a faulty matching of the data.

Some preliminary conclusions can be drawn at this point. As can be seen globally the model does follow the general trend of the data. Local discrepencies between the two are displayed, indicating that more work is needed, especially on the areas of the definition of entrainment speed and laminar burning time. Moreover, experimental errors are displayed (see the pV^γ mismatch). Nevertheless, the model seems able to explain most of the conditions occurring in the engine, and in particular is able to predict consequences of too advanced ignition timing. The model of entrainment speed as equivalent to the friction velocity seems adequate while some doubts are still on the correctness of the eddy length, and hence burning time computed

according to equation (1.42). The use of constant entrainment

speed and burning times seems adequate to a first analysis, but

the same fact that one, upon modifying them can predict pressures

different from the "average" pressure trace indicates that one

should try to build a consistent algorithm   only, as a

first stage, to predict average pressures. Then in a following

time one could try to use statistics to compute which kind of

perturbations can be admitted, and as a consequence complete

"atypical" traces.

At this point since the model was predicting both quenching and

leakage, an attempt was made to compare measured average hydrocarbon

concentrations with model predictions, based on the assumption that

at each instant of time what leaves the chamber has the average

composition of the systems. These results are displayed on Table 11,

and distinction is made between quenching and leakage-generated

hydrocarbons. On the same table also the error between experimental

and theoretical values is displayed, together with air fuel ratios

and exhaust temperature. As can be seen we constantly overpredicted

hydrocarbons. This should not surprise anybody since our model does

not take into account oxidation. Which of course is a function of

the air fuel ratio and the exhaust temperature. For instance, the

run which presents the bigger error is also the one which has the

higher exhaust temperature. Furthermore notice how the trend in

quenching is also correct. Run 8 had the smallest quenched fraction.

This is due to the fact that it was an almost stoichiometric condition

characterized by very high pressures and temperatures (being a WOT case) hence no surprise for the smaller quenched fraction. Runs 9 and 14 were also partly throttled cases near stoichiometric. Hence again the similitude in their quenched fraction is understandable. Runs 10 to 13 were characterized either by lower temperature and pressures or air fuel ratios quite different from stoichiometric. Hence again no surprise for their higher quenched fraction. Next examining the leakage dependence also in this case we notice that leakage hydrocarbons are almost constant at constant speed (runs 9-12) and of about 6%. When the speed is the half (run 13) the leakage contribution doubles, and when the speed doubles (run 14) the leakage contribution halves. Finally, run 9 has a very low leakage. But we already know the reason, since we said before that due to the advanced ignition timing the mass on the leading side of the chamber burned completely in a short time. Hence it should be expected that the unburned leaked into the exhausting chamber were less, given that from an early point during the cycle only burned gas was present at the leading apex seal. To conclude this discussion, we can say that our hydrocarbon production model seems to be in very reasonable agreement with experimental measurements, which in turn implies that our models for quenching and leakage are correct. Worth mentioning again is the fact that the quenching model seems to be very reasonably predicting the correct trends with air fuel ratio, pressure and temperature. Only things still missing in the hydrocarbon model are a model of oxidation and a

model of the vortex roll up to match the time resolved hydrocarbons data by Ferguson et al (1975).

3. Some Parametric Studies on Engine Performances

Two more parametric studies were done--the first to see how big an improvement could be obtained in our engine by a leakage or heat transfer reduction. Notice that while the first one is easier to accomplish, the second can only be obtained through the change of the material of the housing, like by using steel instead of aluminum, or even ceramics. While a change in geometrical shape of the chamber was here not taken into consideration, it should be considered as still another possibility to change the global heat losses from the engine. At any rate, the model was first run with both zere heat transfer and leakage area; then heat transfer was allowed but leakage kept to zero. Finally both were included. Runs were made holding constant the intake plunum pressure, and ignition timing. The results of this simulation are displayed in Figure 39. Table 12 presents the indicated thermal efficiencies of the previous simulations. As can be seen from the pictures, and even more from the table, indeed a big improvement could be obtained if leakage were drastically reduced. On the other hand, one has to remember that, first, leakage is a strong function of speed, and this was certainly a low speed run (2000 RPM); then, our engine was probably partially abused by us when it was dis-assembled to provide all the holes necessary for the pressure measurements, since not all gauges and instruments were available

to insure that the engine was reassembled according to specifications. Hence it could be that normal engines have better performances than ours. Worth of notice at this point is that the conclusions that can be drawn on the basis of the present analysis basically coincide with previously obtained by Danieli et al (1975). Heat transfer is the biggest loss in this engine, and even a small decarease in it would be very beneficial for the engine performances. Leakage is much smaller a problem, even if by eliminating it one could have indeed a very good efficiency gain. Quenching was here not touched upon since it was felt that it is impossible to eliminate, unless unburned temperatures inside the engine reach so high levels to make quenching impossible (Ferguson, 1976). Finally, crevice volume was not explicitly considered given that previous work (Danieli et al, 1974, 1975) had demonstrated that it was indeed a correction to a correction (the quenching). Before leaving the argument of the comparison between previous and present results notice also that while in the previous work (Danieli et al, 1975) simulations were made holding the brake output constant, here the intake plenum, equivalent to the throttle position, was held constant. Hence this is the reason why numbers in efficiency gain to be obtained from leakage or heat transfer reduction do not appear in agreement, the new ones being much higher.

Last parametric study was done to assess the feasibility of an increase in compression ratio as a possible way to improve engine efficiency. Now if no losses were present, we know from the ideal air cycle analysis that a great improvement can be expected from

higher compression ratios. For instance, for an ideal air cycle the efficiency would go from 49% to 54% upon increasing the compression ration from 9.4 to 13.2 as done here. But in a Wankel engine, given the geometrical constraints, it is fairly obvious that if one increases the compression ratio, it will also decrease the flow areas through which the gases move within the chamber. Hence speeds induced by changing chamber shape as well as flame presence will be increased. Hence if the compression ratio in the Wankel is increased the advantage of a higher thermodynamic efficiency will be at least partly offset through a higher heat loss. Another factor that plays an important role is that, given the flow area reduction, also the entrainment rate is reduced, producing a possibly longer combustion time, which in turn increases total quenched fraction and enthalpy loss in the exhaust. Table 13 shows the comparison between a computer simulation at Cr = 9.4 and one obtained with a compression ratio 40 per cent bigger (13.2). The simulation was done holding constant all parameters to the values assumed for run 9, including spark timing that was not varied to find the best value. As it can be observed, while the total heat loss and exhaust enthalpy were essentially unchanged, the work output from the engine was reduced while also the mass induced dropped due to the smaller volume at intake valve closed. Meanwhile the quenched fraction at the end of the combustion increased, even if lightly. The consequence was that no improvement was obtained in the indicated efficiency, which actually dropped by about 7 per cent going from 26 to 24 per cent. However it may

well be possible that a smaller increase in compression ratio
could indeed improve the engine efficiency and this possibility
is certainly worth studying.

CONCLUSIONS

A model of performance of a Wankel engine was developed.
Its main features are a new thermodynamic treatment, and a careful
geometricl analysis of induced flows and as a consequence a new
proposed mechanism for heat losses and flame propagation. No
assumptions of "plane waves" propagation during the initial com-
bustion stages was necessary, and two spark plugs were included.
Model predictions were compared to experimental data obtained during
both firing and motoring conditions. The agreement obtained was
generally good. Few cases were not in agreement, and generally the
reason for the mismatch was found to be due rather to experimental
errors than to errors in the model. The only point in which the
model was clearly wrong was in the computation of the masses in-
ducted in the chamber, due to the fact that side seal leakage was
neglected. However the error introduced by this was found un-
important for purposes of performance modelling, since it could only
affect, and in an almost insignificant way, the computation of
residual gas fraction.

During this early development of the model, a constant entrainment
speed and "characteristic burning time" (Blizard and Keck, 1974) were
used. An attempt was made of rationalizing through the analogy
to the friction velocity the rather high value of the entrainment
speed that was found by a "best fit" process to the experimental
data. Results were good on the average, but there is uncertitude of their
global reliability since they were predicted from the flow generated

by a combustion propagation driven by a constant entrainment speed and burning time. Moreover, in the present form the model did not contain any information about the effect of turbulence induced during intake on the heat transfer and hence entrainment speed during combustion. Also neglected in this study was the vortex roll up by the trailing apex that should probably increase both heat transfer during compression and that plays a significant role in the time-resolved hydrocarbon emissions (Ferguson et al, 1975). But to include this, a more careful study of the boundary layer growth in this engine will be needed. Finally, quenched layer diffusion and oxidations were also neglected.

Now that some of the deficiencies of this model have been pointed out, let us look at what is good and unique about it. First, the hermodynamic model presented here allows one to study boundary layer growth since it has been purposely developed for an n zone model. Hence the addition of a fourth and fifth zone to take into account an adiabatic core of both unburned and burned will only be a relatively simple change. And this will be needed if one wants to predict NO production, given its sensitivity to the temperature history of the different elements.

Second, the flame propagation model predicts rather nicely the effects of timing on the rapidity with which the engine is able to burn its charge. Third, by incorporating leakage and quenching at one time, the model is also able to show the dependence of the latter on the pressure-time history and the potential improvement that could be obtained from a reduction of the first.

Finally the model showed another intriguing point in the
Wankel engine performances, by showing that an increase in com-
pression ratio, at least if obtained only through a change in the
volume of the rotor cavity, did not increase the efficiency of the
engine as every thermodynamicist would expect. This is because
there is a tradeoff point above which, by increasing the compression
ratio, gas speeds and hence heat transfer become even more
significant than they are, while in the meantime the combustion
time is extended due to the reduction in entrainment surfaces. The
result obtained in this case should in any event not considered a
final one, since only one different value for the compression ratio
was found and spark timing was not set for MBT but rather kept
constant. More work is therefore needed to determine the precise
trade-off point for the compression ratio. Furthermore, also
studies   on the effect of rotor cavity shape should be
conducted to determine its best configuration.

Leakage area used for the model prediction was 1.5 mm^2 per apex
seal during motoring and 1 mm^2 during firing. The reason for the
difference in the values is explained in the third chapter.

Heat transfer, defined according to equation (1.54), was
found to be the most significant loss mechanism. The value for
the constant in the Nusselt dependence on the Reynolds number is
computed from the gas speeds generated by shape variation and com-
bustion presence.

Long burning times, characteristic of this engine, were
found to be a consequence of the "stretched" chamber configuration .

And their effect is to increase the mass fraction quenched and the exhaust loss.

Final result of this work is therefore a model which allows to study parametrically the effects of almost any geometrical change on engine performances. More work is certainly needed to further improve this model, particularly to understand better the turbulence in this engine. But turbulence is such a difficult subject to handle that at least one feels in good company, given the number of researchers of the past and of the present that have dealt with it.

REFERENCES

- R. F. Ansdale, The Wankel RC Engine, Iliffe, London, 1968.

N. C. Blizard and J. C. Keck, "Experimental and Theoretical Investigation of Turbulent Burning Model for Internal Combustion Engines," SAE paper 740191 (1974).

- F. V. Bracco and W. A. Sirignano, "Theoretical Analysis of Wankel Engine Combustion," Combustion Science and Technology, Vol. 7 (1973) pp. 109-123.

- G. A. Danieli, C. R. Ferguson, J. B. Heywood and J. C. Keck, "Predicting the Emissions and Performance Characteristic of a Wankel Engine," SAE Transactions, Vol. (1974), paper 740186.

- G. A. Danieli, "Pressure Measuring Techniques in I.C.E.," Sloan Automotive Lab Internal Report (1975).

- G. A. Danieli, C. R. Ferguson, J. B. Heywood, and J. C. Keck, "Analysis of Performance Losses in a Wankel Engine," I.M.E. Conference in "Combustion in Engines," Cranfield, 1975.

- M. K. Eberle and E. D. Klomp, "An Evaluation of the Potential Performance Gain from Leakage Reduction in Rotary Engines," SAE paper 730117 (1973).

- C. R. Ferguson, G. A. Danieli, J. B. Heywood, and J. C. Keck, "Time Resolved Measurements of Exhaust Composition and Flow Rate in a Wankel Engine," SAE paper 750024 (1975).

- C. R. Ferguson, "Turbulent Flame Propagation in Engines," Seminar of the Sloan Automotive Lab (1975).

- C. R. Ferguson, "On Quenching Generated Hydrocarbons in Engine Combustion," to appear in Combustion and Science.

- M. K. Martin, "Photographic Study of Stratified Combustion Using a Rapid Compression Machine," M. S. Thesis, Dept. of Mech. Eng., M.I.T., January, 1975.

- W. M. Rohsenow and H. Y. Choi, Heat, Mass and Momentum Transfer, Prentice Hall, Englewood Cliffs, 1961.

- H. Schlichting, Boundary Layer Theory, McGraw Hill Co., New York, 1968.

- R. S. Spindt, "Air-Fuel Ratios from Exhaust Gas Analysis," SAE Transactions, Vol. 74 (1965) paper 650507.

- H. Tennekes and J. L. Lumley, A First Course in Turbulence, The M.I.T. press, Cambridge, Mass., 1972.

- R. E. Windsor and D. J. Patterson, "Mixture Turbulence - A Key to Cyclic Combustion Variation," SAE paper 730086

- G. Woschni, "A Universally Applicable Equation for the Instantaneous Heat Transfer Coefficient in the Internal Combustion Engine," SAE Transactions, Vol. 76, paper 670931.

- K. Yamamoto, Rotary Engine, Toyo Kogyo Co., Ltd, Hiroshima, 1969.

- K. Yamamoto and T. Kuroda, "Toyo Kogyo's Research and Development on Major Rotary Engine Problems," SAE Transactions, Vol. 79 (1970)

TABLE 1

Engine Parameters

Maker: Toyo Kogyo Co., Ltd.

Model: 12B

Twin rotary engine, water cooled

Displacement:	573	cm^3 x 2 rotors
Compression ratio:	9.4	
Crankshaft eccentricity:	15	mm
Housing generating radius:	102	mm *
Housing displacement from true epitrocoidal:	3	mm *
Rotor generating radius:	$\sim$ 104.5	mm

Part timing:

Intake opens	$- 508^o$	BTDC
Intake closes	$- 220^o$	BTDC
Exhaust opens	199°	ATDC
Exhaust closes	$- 491^o$ 30'	BTDC

---

*Courtesy of Dr. Kenichy Yamamoto of Toyo Kogyo Co.

TABLE 2

Electronic Components of Angle Indicator Circuit

A_1	1/2	72720		comparator
A_2	1/2	72720		comparator
A_2		P65A		op amp
C_1		1 μ F		capacitor
G_1		7490		divide by ten
G_2	1/4	7400		NAND gate
G_3	1/4	7400		NAND gate
L_1	G.E.	327		lamp
L_2	G.E.	327		lamp
R_1		560	Ω	resistor
R_2		4.3	K Ω	resistor
R_3		5.1	K Ω	resistor
R_4		1.8	K Ω	resistor
R_5		5.1	K Ω	resistor
R_6		7.5	K Ω	resistor
R_7		1.5	K Ω	resistor
R_8		15	K Ω	resistor
R_9		3.3	K Ω	resistor
R_{10}		180	Ω	resistor
T_1				photo electric transistor
T_2				photo electric transistor
Z_1		4.3V		Ziener diode

TABLE 3

Analysis of Experimental Data
Air Fuel Ratios and Engine Efficiency

Load	Run	RPM	Φ_{flow}	Φ_{front}	Φ_{rear}	$(\Phi_{ave} - \Phi_{flow})/\Phi_{flow}$ %	η %
Max	1	1000	.98	.95	.94	− 3.3	20.0
Max	2	1000	1.02	.98	.98	− 3.9	20.2
Max	3	1100	.802	.81	.81	1.0	21.9
Max	4	1970	.892	.86	.86	− 3.6	25.3
Mid	5	1970	.854	.83	.78	− 5.7	23.8
Mid	6	1970	.875	.83	.84	− 4.6	22.5
Max	7	2040	1.03	1.00	1.00	− 2.9	21.0
Max	8	2040	1.04	1.00	1.00	− 3.8	21.0
Mid	9	2070	1.02	1.02	1.02	0.0	21.7
Low	10	2040	.99	.99	1.00	0.5	16.7
Mid	11	2070	1.26	1.23	1.23	− 2.4	17.4
Mid	12	2080	.848	.81	.8	− 5.1	16.7
Mid	13	1020	1.05	1.06	1.08	1.9	16.2
Mid	13	1020	1.05	1.06	1.05	0.5	16.2
Mid	14	3960	1.08	1.05	1.04	− 3.2	21.1

Average error on Φ − 1.45%
Standard deviation 2.5 %
(Runs 8 ÷ 14)

TABLE 4

Analysis of Experimental Data

Run	RPM	BMEP	FMEP	$\int_o^{6\pi} P_{mot} dV/V_d$	$\int_o^6 P_{fir} dV/V_d$	IMEP+	$\dfrac{\int P_{fir} dV - IMEP}{IMEP}$ %
8	2040	468	129	− 94	474 − 484	503	− 4.8
9	2070	324	121	− 93	355	352	.9
10	2040	176	133	− 108	205	200	2.5
11	2070	324	129	− 102	359	351	2.3
12	2080	211	131	− 93 *	264 − 221	248	− 2.2
13	1020	215	133	− 92	247 − 282	259	2.1
14	3960	363	203	− 136	429 − 410	430	− 2.4

* This value was assumed identical to the one of Run No. 9 since it was not integrated for an error

+ IMEP = BMEP + FMEP + $\int_o^6 P_{mot} dV/V_d$

Average error on IMEP − .2 %

Standard deviation 2.9 %

TABLE 5

Magnitude of Terms Appearing in the Energy Balance and their Possible Error

Term	Meaning	Value*	Normalized† %	Maximum Error†† %
H_{tot}	Total enthalpy flux into the system	833	100	± 1
H_{exh}	Total enthalpy flux out of the system	270	32.4	?
W	Net work output	186	22.3	± 1.1
Q_W	Heat lost to the water-cooling system	189	22.6	± 1.1
Q_o	Heat lost to the oil-cooling system	71	8.6	$\pm .4$
Q_{nc}	Heat lost through natural convection	2	.2	$\pm .1$
Q_{fc}	Heat lost through forced convection (fly wheel)	18	2.1	$\pm 1.$
Q_r	Heat lost through radiation	5	.6	$\pm .3$
Q_{c1}	Heat lost through conduction to the engine bed	1	.1	$\pm .05$
Q_{c2}	Heat lost through conduction in the exhaust pipe	3	- .4	$\pm .2$
H_{defect}	Exhaust enthalpy defect due to thermocouple error	8	1.0	$\pm .5$
	Final error on energy balance		- 10.3	± 5.2

* Joules/cycle

† Value/H_{tot}

†† ΔValue/Value $\times$ 100

TABLE 6

Energy Balance for Various Runs
and their Thermodynamic Efficiency

Run	H_{tot}	H_{exh}	H_{umb}	Q_{loss}	W_{usef}	Q_{conv}	E_{error}	η_{TH}
				JOULES/CYCLE			%	%
8	1221	278	83	425	268	25	11.6	21.0
9	833	200	70	260	186	25	11.1	21.7
10	599	131	56	239	101	25	7.9	16.7
11	798	220	66	288	186	25	1.75	17.4
12	719	200	71	257	121	25	6.3	16.7
13	714	98	103	244	123	32	16.0	16.2
14	893	266	47	312	208	22	4.3	21.1

TABLE 7

Run	Mass Kg x 10^{-4}			Work K Pa			Heat Joules/Cycle		
	exp	th	error %	exp	th	error %	exp	th	error %
8	4.69	4.10	- 8.7	503	516	2.6	433	432	- .2
9	3.04	2.74	- 9.9	352	346	- 1.7	268	288	7.5
10	2.20	1.87	- 15.	200	198	- 1.	247	218	- 11.7
11	3.11	2.66	- 14.5	351	303	- 13.7	296	258	- 12.8
12	3.05	2.68	- 12.1	248	287	15.7	266	227	- 14.7
13	2.63	2.31	- 11.8	259	208	- 19.7	252	254	.8
14	3.32	3.11	- 6.3	430	414	- 3.7	295	275	- 6.8
Average error			- 11.2			- 4.5			- 5.4
only runs 8 - 9 - 10 - 14			- 10.0			.95			- 2.8

$$error = \frac{variable_{theoretical} - variable_{experimental}}{variable_{experimental}} \times 100$$

TABLE 8

Analysis of the Terms Affecting the Value of pV^{γ} for Various Runs

A_{ℓ} mm^2	Q W	P_o k Pa	T_{u_o} Deg $^\circ K$	$(\gamma_b-1)\dfrac{\int_{ign}^{\pi/3}\dot{Q}dt}{P_o V_o}$	$\dfrac{\gamma_b-1}{\gamma_u-1}$	$\dfrac{\Delta H(\gamma_b-1)m^*}{R_u T_o m_o}$
0	1.35	995	673	.39	.76	3.27
.5	1.35	965	682	.38	.76	3.1
1	1.35	944	698	.34	.76	2.93
1	1.00	969	734	.26	.76	2.79
1	0.50	1031	813	.14	.76	2.49

TABLE 9

Assumed vs. Average of the Predicted Values for
Entrainment Speed and Characteristic Laminar Burning Time

	assumed			predicted	
Run	u_e	τ	τ^*	u_e	τ
8	7	.34	.34	10	1.5
9	7	.6	.6	5.4	.97
10	7	1.1	1.1	3.71	.54
11	7	.6	.97	5.8	.4
12	7	.86	.86	3.5	.4
13	3.5	4.0	1.25	1.7	5.1
14	14	.45	.6	17.5	.08

u_e (m/sec)

τ (msec)

*   computed with the help of equation 3.1

TABLE 10

Ignition Timing for the Various Runs

Run	RPM (rev/min)	Trailing (deg. ATDC)	Leading (deg. ATDC)
8	2040	− 33	− 28
9	2070	− 14	− 16
10	2040	− 8	− 12
11	2070	− 14	− 16
12	2080	− 9	− 10
13	1020	− 10	− 20
14	3960	− 21	− 20

TABLE 11

Measured vs. Predicted

Hydrocarbon Concentration

Run	HC_{meas}	HC_{pred}[*]	x_q[†]	x_ℓ[**]	error[††]	ϕ[***]	T_e[†††]
	p.p.m		%				Deg ^{o}K
8	7000	7050	2.3	3.7	1	1.04	839
9	8400	9500	4.0	6.4	12	1.02	938
10	9400	11400	5.4	6.7	21	.99	898
11	9500	11500	6.0	6.6	20	1.26	923
12	8100	10300	5.9	5.7	27	.85	953
13	16200	19600	6.3	14.3	21	1.05	718
14	5400	7600	3.9	2.8	41	1.08	1023

* $[HC] = \dfrac{8\,MW_e}{114}\, x_u\, (1-r_f)\, \dfrac{\phi}{15.1 + \phi} \times 10^6$ (p.p.m.)

MW_e — Average moleculer weight of exhaust gases

x_u — mass fraction of unburned in exhaust gases

r_f — residual mass fraction

† x_q — fraction of unburned due to quenching

** x_ℓ — fraction of unburned due to leakage

†† error = $([HC]_{pred} - [HC]_{meas}) / [HC]_{meas} \times 100$

*** equivalence ratio (fuel air ratio/stoichiometric fuel air ratio)

††† exhaust temperature

TABLE 12

Indicated Efficiency Gains from Leakage
and Heat Transfer Reduction

Case	A_{ℓ_2} mm^2	Q^* W	η $\%$	$\dfrac{\eta - \eta_o}{\eta_o}$ $\%$
0	1	1.35	26.	0
1	.5	1.35	27.7	5.6
2	0	1.35	30.3	15.3
3	0	0	38.1	45.2

* Being according to Woschni .035 the value of
the heat transfer coefficient,
$$Q = 1.35 \ W = .047$$

TABLE 13

Compression ratio*	9.4	13.2
Mass Inducted (Kg/cycle)	2.74×10^{-4}	2.69×10^{-4}
Enthalpy Inducted (Joules/cycle)	754	738
Enthalpy Exhausted (Joules/cycle)	270	270
Heat Loss (Joules/cycle)	288	289
Work (Joules/cycle)	198	180
η_{ind}	26.3	24.4
Quenched fraction (%)	4.0	5.0

*Values assumed for both runs were exactly the same and corresponding to the simulation for Run 9, including spark timing and intake manifold pressure

APPENDIX A

Formulation of Momentum Equation to Compute Pressure Differences within the Chamber of a Wankel Engine, Originated by Gas Motion (Program WFLOW)

List of symbols used in this appendix

A	-	flow area (chamber cross section)
$\vec{F}$	-	force acting on the control element
N	-	number of points delimiting the control elements
$\vec{n}$	-	perpendicular to the flow area
R_e	-	Reynolds number
S	-	surface of the engine chamber
v	-	volume
V	-	gas speed
ρ	-	gas density
τ	-	wall friction

Indexes

c	-	refers to control element and to the right-hand side of it
h	-	refers to housing
r	-	refers to rotor
sp	-	refers to housing side plates
tot	-	refers to total chamber
1	-	refers to other side of control element

Assumptions

i. Engine motoring and following isentropic processes

ii. Wall friction given by the relation (Rohsenow, 1961)

$$\tau = .0225 \rho V^2 R_e^{-1/4} \qquad (A.1)$$

The inertia forces acting on a control element from momentum equation can be written as

$$\vec{F} = \int_{v_c} \frac{\partial}{\partial t} (\rho \vec{V}) \, dv + \int_{S_c} \rho \vec{V} \vec{V} \cdot \vec{n} \, ds \quad . \qquad (A.2)$$

This can be written in finite differences form as

$$\frac{\partial}{\partial t} (\rho V) v_c \overset{+}{_-} \rho A_c V_c^2 \overset{-}{_+} \rho A_1 V_1^2 = F \qquad (A.3)$$

where the $\overset{+}{_-}$ sign depends on the sign of the product $\vec{V}_c \cdot \vec{n}$. The picture helps to clarify the use of indexes c and 1.
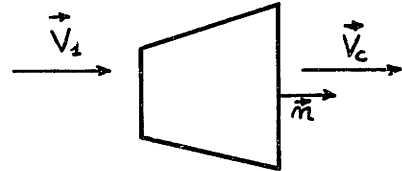
Next, given the isentropic assumption

$$\frac{\partial}{\partial t} (\rho \vec{V}) = \frac{\partial \rho}{\partial t} \vec{V} + \rho \frac{\partial \vec{V}}{\partial t} = - \frac{\rho}{v_{tot}} \frac{\partial v_{tot}}{\partial t} \vec{V} + \rho \frac{\partial \vec{V}}{\partial t} \qquad (A.4)$$

hence upon substitution of (A.4) into (A.3), we obtain

$$F = - \rho v_c (\frac{1}{v_{tot}} \frac{\partial v_{tot}}{\partial t} V - \frac{\partial V}{\partial t}) \overset{+}{_-} \rho_c A_c V_c^2 \overset{-}{_+} \rho_1 A_1 V_1^2 \quad . \qquad (A.5)$$

Now the inertia forces are to be equated to the forces acting on the control volume; being

$$\alpha \sim \tan g \; \alpha \simeq \frac{A_c - A_1}{Sr} \qquad (A.6)$$

We can define an equivalent wall friction stress by summing the various components in the direction of the flow and dividing by the total surface as
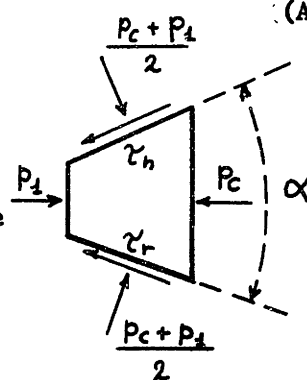
$$\tau \simeq ((\tau_r S_r + \tau_h S_n)\cos \frac{A_c - A_1}{2 S_r} + \tau_h S_{sp})/S_r + S_h + S_{sp}) \qquad (A.7)$$

since the housing sides are parallel to the wall.

The force acting in the direction of the flow is therefore

$$F = p_1 A_1 - p_c A_c + \frac{p_c + p_1}{2} (A_c - A_1) - \tau(S_r + S_h + S_{sp}) . \qquad (A.8)$$

By equating then (A.5) to (A.8) and solving for p_c, we obtain

$$p_c = p_1 + \frac{2}{A_1 + A_c} \left\{ - \underbrace{\tau(S_h + S_r + S_{sp})}_{\text{Friction}} + \right.$$

$$\underbrace{\rho \, v_c (\frac{1}{v_{tot}} \frac{\partial v_{tot}}{\partial t} V - \frac{\partial V}{\partial t})}_{\text{inertia forces}} \qquad \underbrace{\mp \rho \, A_c \, v_c^2 \pm \rho A_1 \, v_1^2}_{\text{kinetic energy of gases}} \left. \right\} . \qquad (A.9)$$

By evaluating all derivatives with the finite differences method and making use of a spatial temporal mesh of five elements in time and N in space, the pressure distribution is hence computed in terms of the initial pressure at the trailing apex seal.

APPENDIX B

Geometrical Notes

This appendix contains linearized algorithms to find partial volumes, flow areas, surfaces, and front positions given all geometrical parameters for the control element, when the control elements have to be subdivided to allow for flame motions[*]

List of symbols

N - 1   number of control elements (Figure B1)

AXH(I)   x coordinate (Figure B2) of the housing point limiting

            the control element at the right-hand side (m)

AAC(I)   flow area at the right of the control element (m^2)

AVC(I)   volume of the control element (m^3)

ASR(I)   surface of the control element belonging to the rotor

ASH(I)   surface of the control element belonging to the housing

XHT   x coordinate of the axes of the trailing spark plug

AV1   unknown volume of a subelement in which the control

            element has been divided (m^3)

AA1   unknown flow area at the section at which the c.e. has

            been divided (m^2)

SR1   surface of the rotor contained in AV1

SH1   surface of the housing contrained in AV1

a. Given the coordinates of a point on the housing profile which

    happens to be inside a given control element, find volume to the

_____

[*]To make life simpler to the potential users of Program WANKEL, the symbols used here are in the majority of cases identical to the ones used by subroutines FLAMES and HTRANS.

left of given point. Following the linearizing[*] assumption, the

unknown cross sectional area at the point XHT

$$AA1 = AAC(I-1) - (AAC(I-1) - (AAC(I)))*$$

$$(XHT - AXH(I-1))/(AXH(I) - AXH(I-1)) \ . \tag{B.1}$$

Also the total volume of the control element (known) must be

$$AVC(I) \sim (AAC(I) + AAC(I-1)) * (AXH(I) - AXH(I-1)/2 \tag{B.2}$$

while the unknown partial volume can be written by analogy

$$AV1 \sim (AA1 + AAC(I-1)) * (XHL - AXH(I-1))/2 \tag{B.3}$$

Substituting (B.1) into (B.3) and dividing by (B.2) one obtains

$$AV1 = AVC(I) * \left[1 - \frac{AAC(I)-AAC(I-1)}{AAC(I)+AAC(I-1)} * \frac{AXH(I)-XHT}{AXH(I)-AXH(I-1)} \right] \frac{XHT-AXH(I-1)}{AXH(I)-AXH(I-1)} \tag{B.4}$$

b. Given the volume enclosed between the trailing apex and a certain

front (VTOTX), determine volume enclosed between the front and the

control element division to the left of it (AV1 of Figure B3).

Starting from trailing apex, define

$$VPAR = \sum_{2}^{I} AVC(I) \tag{B.5}$$

when VPAR $\geqslant$ VTOTX

$$AV1 = VTOTX - VPAR + AVC(I) \ . \tag{B.6}$$

Note that the sum starts from 2 since AVC(1) = 0.

---

[*]From here on, in this appendix everything is treated linearly if
it is not mentioned.

c. Given AV1 find the flow area (AA1) (Figure B2); once again we
can say that

$$AVC(I) \sim (AAC(I-1) + AAC(I)) * \ell/2 \qquad (B.7)$$

$$AV1 \sim (AAC(I-1) - AA1) * \ell_p/2 \; . \qquad (B.8)$$

On the other hand,

$$\frac{\ell_p}{\ell} \sim \frac{AA1 - AAC(I-1)}{AAC(I) - AAC(I-1)} \; . \qquad (B.9)$$

Combining (B.7) to (B.8) and (B.9), we obtain after some algebraic
computations

$$AA1 = AAC(I-1) * \{1 + \frac{AV1}{AVC(I)} * [(\frac{AAC(I)}{AAC(I-1)})^2 - 1]\}^{1/2} \; . \qquad (B.10)$$

d. Find the rotor surface enclosed by AV1

$$ASR1 \sim \ell_p * b \qquad (B.11)$$

where b is the housing width; being also

$$ASR(I) \sim \ell * b \; . \qquad (B.12)$$

Combining these to (B.7) and (B.8), we obtain

$$ASR1 = ASR(I) * \frac{AV1}{AVC(I)} * \frac{AAC(I-1) + AAC(I)}{AAC(I-1) + AA1} \; . \qquad (B.13)$$

3. Rotor housing surface enclosed by AVC1

$$ASHL \sim \ell_p (\frac{AAC(I-1) + AA1}{b} + b) \qquad (B.14)$$

proceeding as in (d)

$$ASH1 = ASH(I) * \frac{AV1}{AVC(I)} * \frac{(1 + b^2/(AAC(I-1) + AA1))}{(1 + b^2/(AAC(I-1) + AAC(I)))} \qquad (B.15)$$

Final Note: These algorithms can easily be modified if one wishes
to know volumes and surfaces on the other side of the flame front;

the modifications are not presented here to reduce the total

amount of material presented.

APPENDIX C

Mixing Gases at Constant Pressure (Heat Transfer Model)

Given x_b and x_q (whose sum is generally not equal to 1), let's first define their equivalent composition (with respect to the mixing).

$$x_{be} = x_b/(x_b + x_q) \tag{C.1}$$

$$x_{qe} = 1 - x_{be} \; ; \tag{C.2}$$

given then $\dot{x}_b$ and $\dot{x}_q$, the "equivalent" rates result after some algebraic computations

$$\dot{x}_{be} = -\dot{x}_{qe} = x_{be} \, x_{qe} \left(\frac{\dot{x}_b}{x_b} - \frac{\dot{x}_q}{x_q}\right) . \tag{C.3}$$

Density of mixture

$$\rho = \frac{\rho_b \, \rho_q}{\rho_b \, x_{qe} + \rho_q \, x_{be}} . \tag{C.4}$$

Time rate of change of the density

$$\dot{\rho} = \frac{\rho^2}{\rho_q^2} (\dot{\rho}_q \, x_{qe} - \rho_q \, \dot{x}_{qe}) + \frac{\rho^2}{\rho_b^2} (\dot{\rho}_b \, x_{be} - \rho_b \, \dot{x}_{be}) \tag{C.5}$$

Average molecular weight

$$MW = \frac{MW_b \, MW_q}{MW_b \, x_{qe} + MW_q \, x_{be}} \tag{C.6}$$

Average temperature

$$T = MW(T_q \, x_{qe}/MW_q + T_b \, x_{be}/MW_b) \tag{C.7}$$

Average specific heat

$$c_p = c_{pq} \, x_{qe} + c_{pb} \, x_{be} \tag{C.8}$$

APPENDIX D

Simple Case of Flame Propagation:
One-dimensional Bomb

flame front
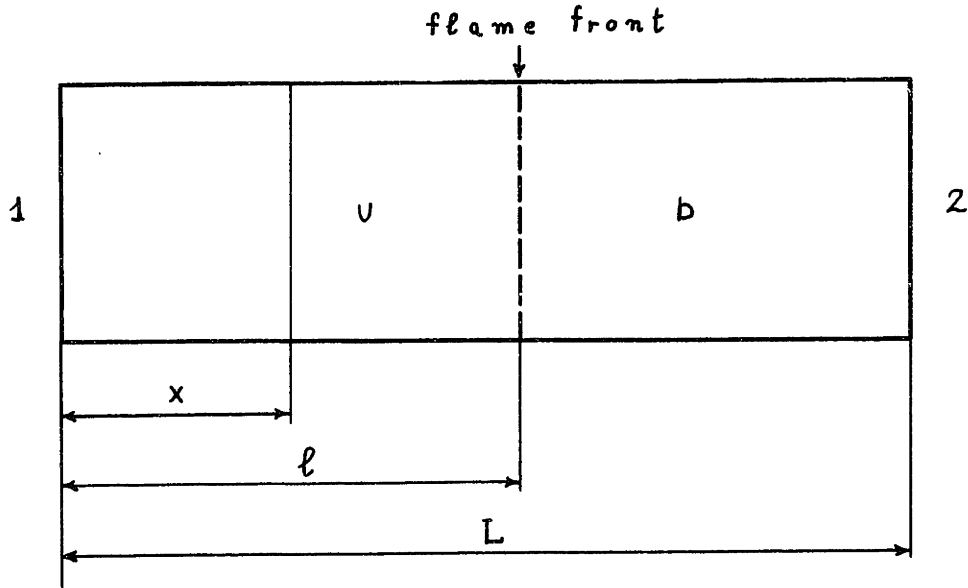
At any given section, the mass enclosed between end 1 of the bomb and abscissa x is given for $x \lessgtr \ell$ by

$$m_x = \rho_u \, x \, A \tag{D.1}$$

and for $x \gtrless \ell$ by

$$m_x = \rho_u \, \ell \, A + \rho_b (x - \ell) \, A \; . \tag{D.2}$$

If we now consider a constant mass element starting from end 1 of the bomb, the rate of change of the mass of the element will be zero and hence

$$\dot{\rho}_u \, x \, A + \rho_u \, \dot{x} \, A = 0 \; ; \tag{D.3}$$

hence

$$\dot{x} = V_{u_x} = - x \frac{\dot{\rho}_u}{\rho_u} \tag{D.4}$$

Let's now consider a second element of constant mass, but this time enclosing both burned and unburned gases. Again the rate of change of the mass provide us with an equation of the form

$$\dot{\rho}_u \ell + \rho_u \dot{\ell} + \dot{\rho}_b (x - \ell) + \rho_b (\dot{x} - \dot{\ell}) = 0 \tag{D.5}$$

and hence

$$\dot{x} = V_{b_x} = \dot{\ell}(1 - \frac{\rho_u}{\rho_b}) + \frac{\dot{\rho}_b}{\rho_b} (\ell - x) - \frac{\dot{\rho}_u}{\rho_b} \ell \quad . \tag{D.6}$$

One more unknown has been introduced by this equation, $\dot{\ell}$, velocity of the flame front.

We will compute it by taking the derivative of the mass balance equation for unburned at locàtion ℓ.

$$\dot{m} = \dot{\rho}_u \ell A + \rho_u \dot{\ell} A \quad . \tag{D.7}$$

Note that

$$V_{u_\ell} = - \frac{\dot{\rho}_u}{\rho_u} \ell \tag{D.8}$$

is the velocity of the unburned gas. Equating the time rate of change of the mass to the combustion rate

$$\dot{m} = - A \rho_u S_u \tag{D.9}$$

(since the unburned is loosing mass due to the combustion); hence

$$\dot{\ell} = V_{flame} = - S_u - V_{u_\ell} \quad . \tag{D.10}$$

Substituting (D.10) into (D.6), we obtain

$$V_{b_x} = - S_u(1 - \frac{\rho_u}{\rho_b}) + V_{u_\ell} - \frac{\dot{\rho}_b}{\rho_b} (x - \ell) \qquad (D.11)$$

in particular for $x = \ell$ (but on the burned gases side)

$$V_{b_\ell} = V_{u_\ell} - S_u(1 - \frac{\rho_u}{\rho_b}) \ . \qquad (D.12)$$

APPENDIX E

Determination of the angle α which determines the housing coordinates of the intercept between the perpendicular to the rotor surface from a given point and the housing.

Calling n_r the tangent of the perpendicular to the rotor surface, being x_r and y_r the coordinates of the given point on the rotor surface, we hence have to find the value of α which satisfies the equation

$$y_h(\alpha) = x_h(\alpha)n_r + (y_r - x_r n_r) . \tag{E.1}$$

We will hence start with a smart assumption as

$$\alpha_1 = \frac{1}{3} \tan g^{-1} \frac{y_r}{x_r} . \tag{E.2}$$

Then we will assume

$$\alpha_2 = \alpha_1 + 2^o . \tag{E.3}$$

Given α_1 and α_2 we will compute $\acute{y}_{h1}$ and y_{h2} from equation (1.80) and then compute

$$\overline{y}_{h1} = x_h(\alpha_1)n_r + (y_r - x_r n_r) \tag{E.4}$$

$$\overline{y}_{h2} = x_h(\alpha_2)n_r + (y_r - x_r n_r). \tag{E.5}$$

This can be visualized from Figure E.1. In the linearity assumption, one then observes that

$$\frac{\alpha_3 - \alpha_1}{\alpha_2 - \alpha_3} = \frac{\overline{y}_1 - y_1}{y_2 - \overline{y}_2} \tag{E.6}$$

which can be solved in terms of α_3 as

$$\alpha_3 = \alpha_1 + (\alpha_2 - \alpha_1)/(1 - \frac{\overline{y}_2 - y_2}{\overline{y}_1 - y_1}) \tag{E.7}$$

The value of α_3 so obtained is then compared to α_1 and α_2 to establish

the nearest of the two to the solution (being α_3 a better guess than

α_1 and α_2). The nearest is kept, the other discarded, and the process

iterated. If something strange should happen (like it will happen

in the neighborhood of the axes), the computation proceeds computing the

α defining x_h and $\bar{x}_h$. The iteration is extremely fast converging and

well behaved.

APPENDIX F

Many are the possible sources of error in the energy balance, since not all heat fluxes were measured. Hence in order to establish the order of magnitude of these, a rough computation will be made. Morever, since there is a possible thermocouple error, this will also be taken into account.

The processes through which our open system can lose heat are basically convection, radiation and conduction; let us examine them in order to estimate their relative importance.

1. Convection

Three terms are present:

a. Natural convection on three vertical faces of the engine.

b. Natural convection on two horizontal faces.

c. Forced convection on the rotating flywheel.

Let us evaluate theyr contribution.

A. Natural convection on a vertical flat plate.

Rohsenow (1961) gives for air:

$$N_u = .685 \ (G_r \ / \ 4)^{.25} \tag{F.1}$$

where the Grashoff number can be written as:

$$G_r = \frac{g \ \beta \ (T_o - T_\infty) \ x^3}{\nu^2} \tag{F.2}$$

where g is the gravity and β coefficient of thermal expansion is given by

$$\beta = - \frac{1}{\rho} \left(\frac{\partial \rho}{\partial T}\right)_p = \frac{1}{T_o} \tag{F.3}$$

for perfect gases. Assuming a room temperature of 38 ^{o}C and a wall temperature of 94 ^{o}C, being the engine dimension of about .3 m, we

obtain:

$$N_u = 53.6$$

from which

$$Q_{nc} = 7. \times 10^{-2} \text{ k W} \qquad (F.4)$$

B. Natural convection on horizontal surface.

i. For plate facing up and

$$20 < L^3 \Delta T < 3000 \quad \text{(in english units)}$$

$$h = .22 \, (\Delta T)^{.33} \qquad (F.5)$$

ii. For plate facing down and

$$.3 < L^3 \Delta T < 30000$$

$$h = .12 \, (\Delta T \, / \, L)^{.25} \qquad (F.6)$$

upon substitution of the engine dimension and summing to the previous

term for natural convection on vertical plates, ve obtain:

$$Q_{nc} = .11 \text{ k W} \qquad (F.7)$$

C. Forced convection on flywheel.

From Shlichting (1968) the friction coefficient for rotating bodies

is given in terms of Reynolds based on tip velocity

$$R_e = \frac{d^2 \, \omega}{4 \, \nu} \qquad (F.8)$$

Substituting the engine geometrical parameters and considering a speed

of 2000 RPM, we obtain

$$R_e = 3.96 \times 10^5 .$$

Based on this value of R_e, from the dyagram on fig 5.13, pag. 98 of the

Shlichting we find

$$c_M = 1.1 \times 10^{-2}$$

The torque can then be written as

$$M = .25 \ c_M \ \rho \ \omega^2 \ R^5. \tag{F.9}$$

We then look for an average value of the friction stress thinking it concentrated at the half radius, such that

$$M = .5 \ R \ a \ \tau_o. \tag{F.10}$$

Substituting (F.9) into (F.10) and rearranging we obtain

$$\tau_o = \frac{1}{2 \ \pi} \ c_M \ \rho \ \omega^2 \ R^2 \tag{F.11}$$

Now, from the Reynolds analogy (Rohsenow, 1961)

$$h = \frac{\tau_o \ c_p}{V} = \frac{c_M}{\pi} \ c_p \ \rho \ \omega \ R \tag{F.12}$$

Once again substituting the engine parameters and remembering that not only the flywheel is rotating, but is inducing gas motion on the engine surface facing it, we obtain for the forced convection on the flywheel and engine surface:

$$Q_{fc} = 1.23 \ k \ W \tag{F.13}$$

2. <u>Radiant heat transfer.</u>

Assume that the engine is a box of .3 m of side, its temperature being of 94 ^{o}C, while the room temperature is of 32° C. The net heat flux will be given by:

$$Q_r = A \ \sigma \ (T_e^4 - T_r^4) = .32 \ k \ W \tag{F.14}$$

3. <u>Conduction.</u>

Two are the ways conduction affects the energy balance, conduction from the engine to the bed and conduction from the exhaust pipes to the engine.

Given the equation to compute heat transfer due to conduction,

$$Q_c = A\ k\ \frac{\Delta T}{\Delta x} \qquad\qquad (F.15)$$

assuming for the first case a bed temperature of 38 $^\circ$C and 94 $^\circ$C for the engine, with a total conducting surface of 36×10^{-4} m^2 and a characteristic conducting lenght of .3 m, we obtain:

$$Q_{c1} = 4.6 \times 10^{-2}\ k\ W \qquad\qquad (F.16)$$

In the second case, assuming for the pipes temperature 700 $^\circ$C, with a characteristic lenght of .15 m and a total conducting surface of 15×10^{-4} m^2, upon substitution into (F.15) one obtain

$$Q_{c2} = -.23\ k\ W \qquad\qquad (F.17)$$

where the minus sign has been used to remember that this is a flux of heat into the engine, rather than out of it.

4. Exhaust thermocouple error.

The thermocouple can be modelled as a sphere sitting in a uniform velocity field (the exhausting gases). In absence of radiation, the "sphere" temperature would be some kind of an average of the one of the surrounding gases. However, since the thermocouple will lose heat through radiation to the pipe's walls, at steady state the heat transmitted from the thermocouple to walls will be equal to the heat transmitted from the gases to the thermocouple.

The first heat flux can be written following the theory of flows over submerged bodies as

$$Q_{conv} = A\ h\ \Delta T = A\ \frac{k}{D_o}\ P_r^{.3}\ \Delta T\ (.97 + .68\ R_e^{.5}) \qquad\qquad (F.18)$$

where A is the thermocouple surface, D_o its diameter, k the conductivity.

Meanwhile, the heat lost to the walls can be written as

$$Q_{rad} = A \sigma (T_{therm}^4 - T_{wall}^4) \qquad (F.19)$$

By then remembering the definition of the Prandtl number, we can express the conductivity in terms of

$$k = \mu \, c_p / P_r \qquad (F.20)$$

Equating (F.18) to (F.19), making then use of (F.20) and rearranging we then obtain

$$c_p (T_{gas} - T_{therm}) = \frac{D_o}{\mu} P_r^{.7} \frac{\sigma (T_{therm}^4 - T_{wall}^4)}{.97 + .68 \, R_e^{.5}} \qquad (F.21)$$

Multiplying both sides by the exhaust mass flowrate we will easily recognize that we found the enthalpy defect in the evaluation of the enthalpy exhausted due to radiation.

$$H_{defect} = \dot{m}_{exh} \frac{D_o}{\mu} P_r^{.7} \frac{\sigma (T_{therm}^4 - T_{wall}^4)}{.97 + .68 \, R_e^{.5}} \qquad (F.22)$$

where the Reynolds number is

$$R_e = \frac{\rho \, V \, D_o}{\mu} = \frac{\frac{4 \, \dot{m}}{\pi D_p^2} D_o}{\mu} \qquad (F.23)$$

Considering a mass flowrate of 2.1×10^{-2} kg/sec, $T_{wall} = 700\ ^oK$,

$T_{therm} = 938\ ^oK$, $D_o = 1 \times 10^{-3}$ m, computing the viscosity μ according to equation (1.67) we obtain

$$H_{defect} = .58 \text{ k W} \qquad (F.24)$$

corresponding to a temperature defect of 25 ^oK.

APPENDIX G

Meaning of pV^γ during combustion.

Referring to equation (17) in the paper by Danieli et al (1974), by considering the condition at end of combustion ($x = 1$, $m = m^*$) and rearranging we obtain:

$$pV = p_o V_o - (Q + W + H)(\gamma_b - 1) + (\gamma_b - \gamma_u) c_{v_u} m_o T_o$$

$$- \Delta H (\gamma_b - 1) m^*. \qquad (G.1)$$

Remembering the perfect gas law and dividing both sides of equation (G.1) by $p_o V_o$ we obtain

$$\frac{pV}{p_o V_o} = 1 - \frac{(Q + W + H)(\gamma_b - 1)}{p_o V_o} + \frac{\gamma_b - \gamma_u}{\gamma_b - 1}$$

$$- \frac{\Delta H (\gamma_b - 1)}{R_u T_o} \frac{m^*}{m_o} \qquad (G.2)$$

Finally, multiplying both sides by $(V/V_o)^\gamma$ and grouping the various terms we obtain the equation

$$\frac{p\, V^{\gamma_b}}{p_o\, V_o^{\gamma_b}} = \left(\frac{V}{V_o}\right)^{(\gamma_b - 1)} \left[\frac{\gamma_b - 1}{\gamma_u - 1} - \frac{(Q + W + H)(\gamma_b - 1)}{p_o V_o}\right.$$

$$\left. - \frac{\Delta H (\gamma_b - 1)}{R_u T_o} \frac{m^*}{m_o}\right]. \qquad (G.3)$$

where

$$Q = \int_o^t dQ$$

is the heat lost by the system from the beginning of combustion,

$$W = \int_o^t p \, dV$$

is the work done by the system since ignition,

$$H = \int_o^t \sum_i c_{p_i} T_i \dot{m}_i \, dt$$

is the integrated enthalpy flux and

$$\Delta H = h_{f_b} - h_{f_u}$$

is the difference in enthalpy of formation between burned and umburned.

Notice that the first term is a constant, the second tends to vanish as the combustion duration decreases while is the third the most important one in determining the size of the jump in pv^γ.
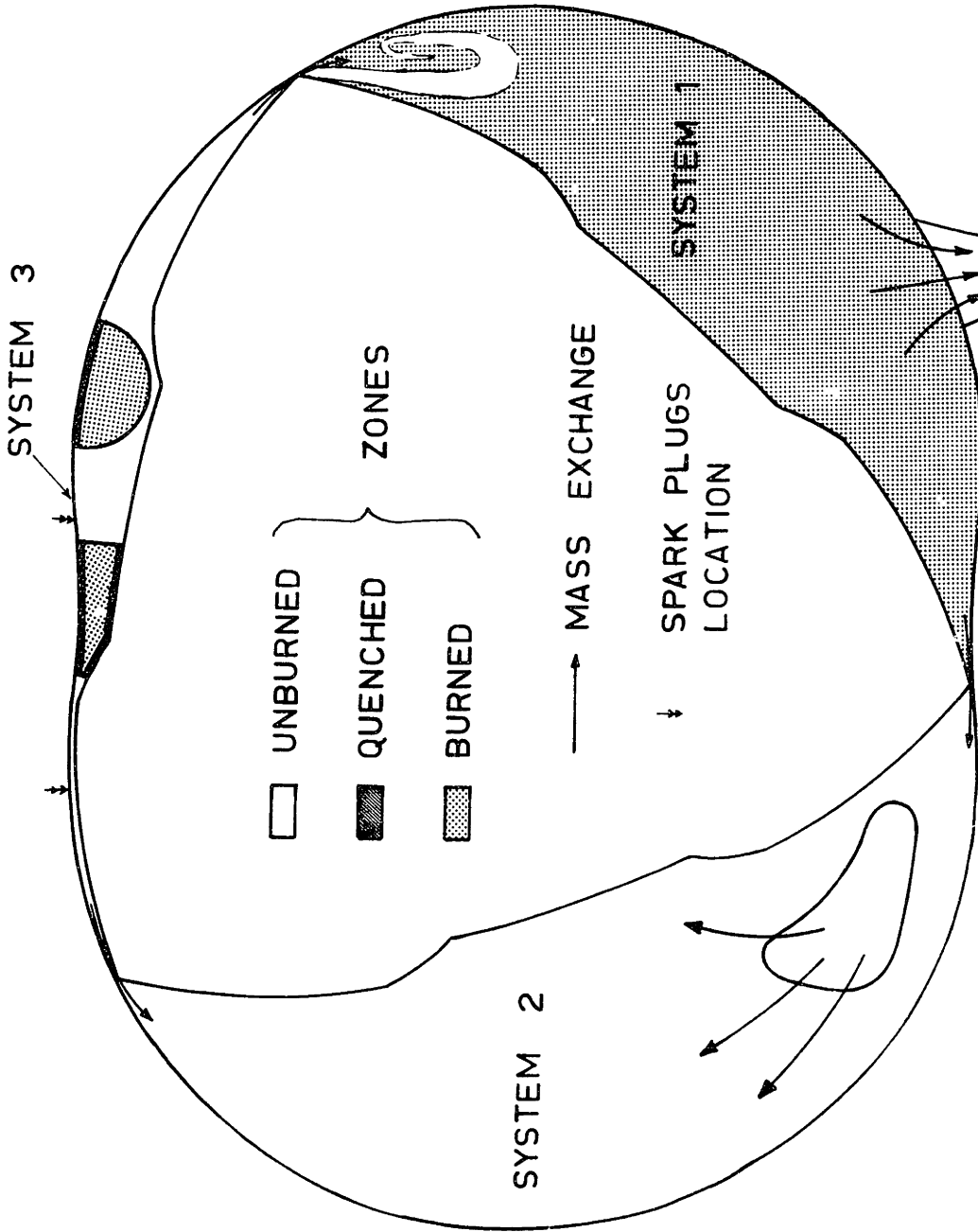
Fig. 1 Schematic of the engine, where the chambers are considered as open systems, interacting with the other systems and the environment; also shown are different zones within each system.
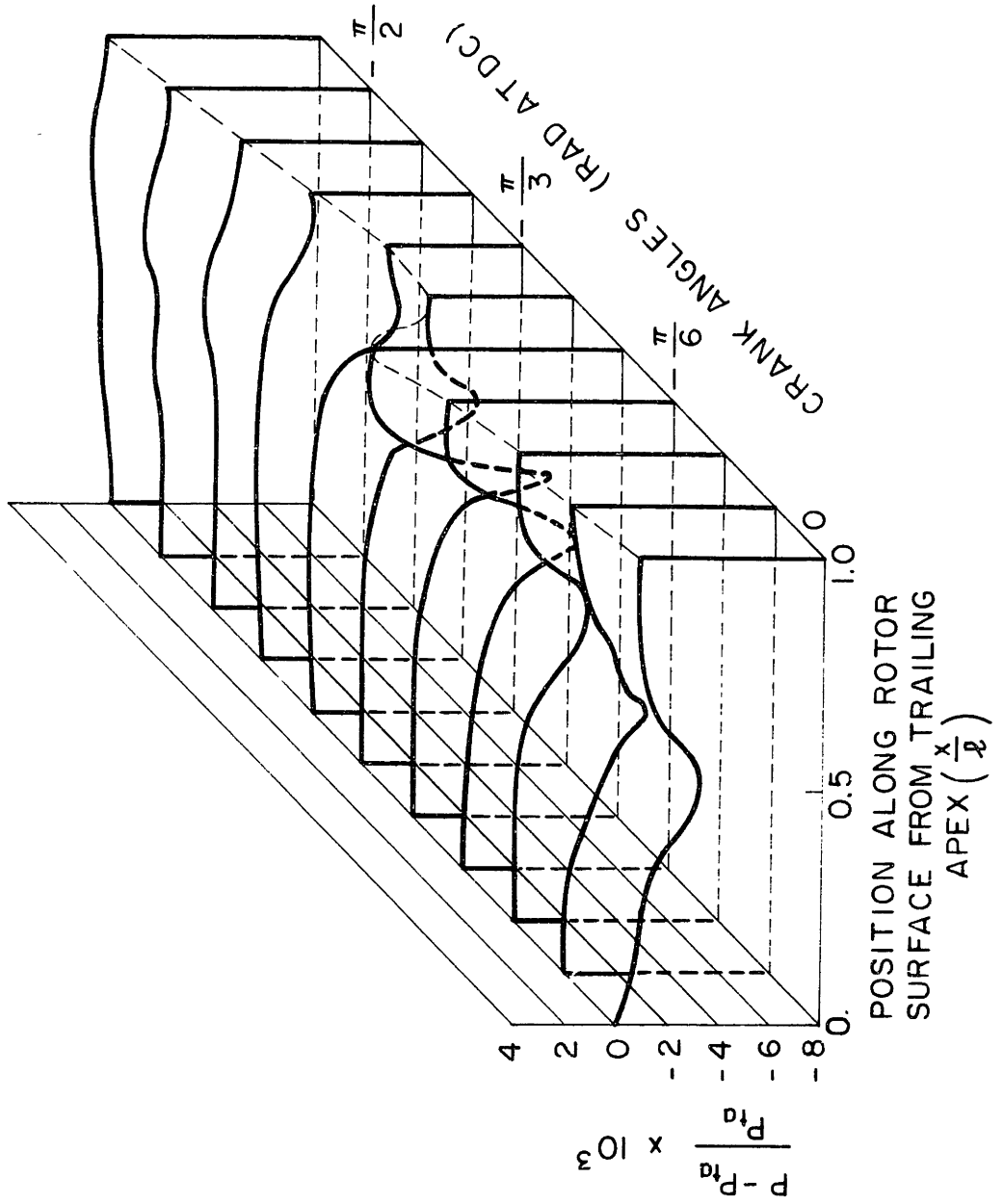
Fig. 2 Pressure disturbances induced by the flow. RPM = 2000, motoring, MID throttle setting.
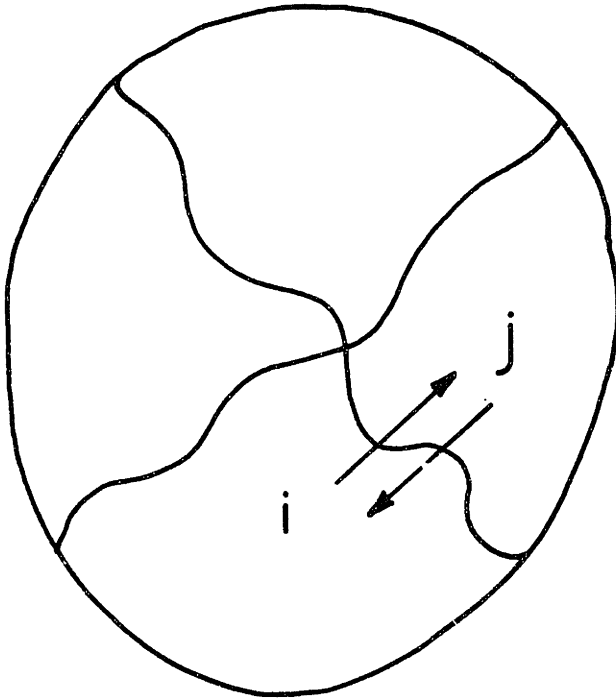
Fig. 3   Schematic representation of interaction between zones or
between a zone and the environment in an open system.
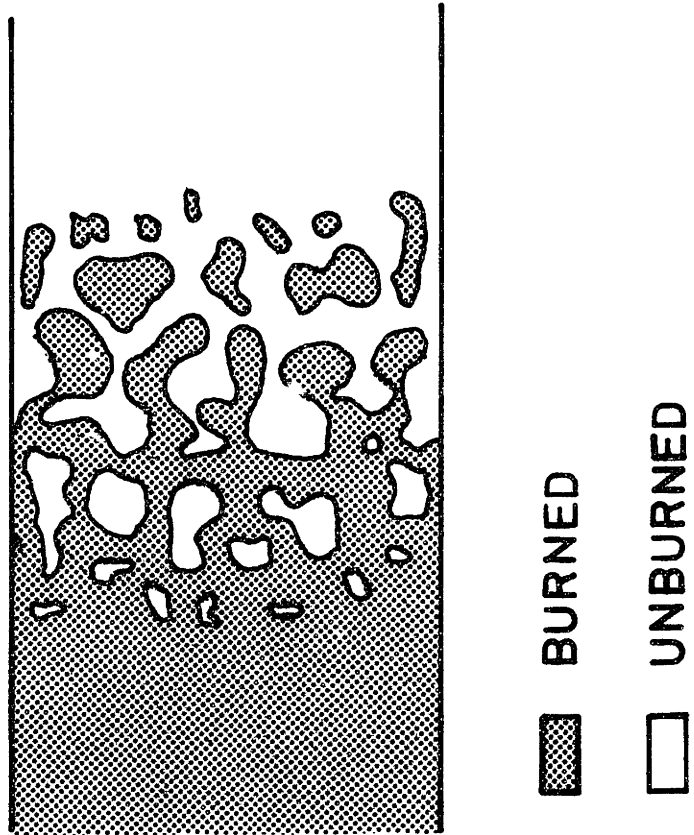
Fig. 4 Propagation of turbulent flame in a duct

BURNED

UNBURNED
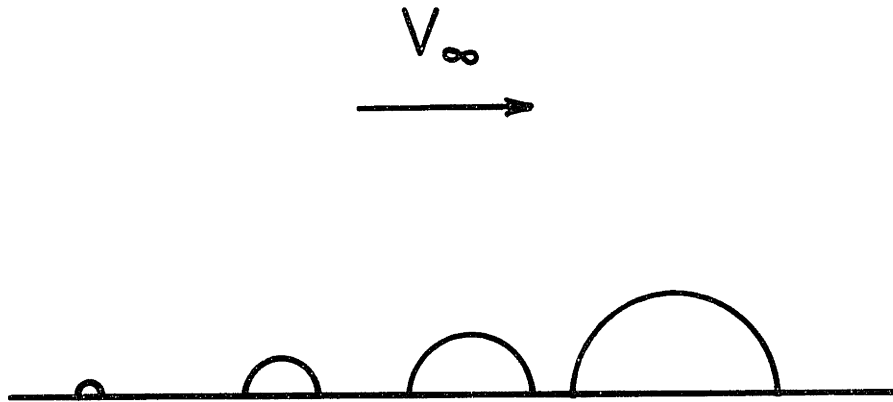
Fig. 5   Hemispherical flame propagation in a constant velocity field.
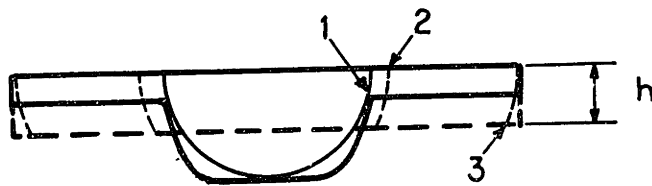
Fig. 6 Transition of flame propagation from pure hemispherical shape
(curve 1), to truncated hemispherical configuration (2).
Transition to one dimensional propagation (3).
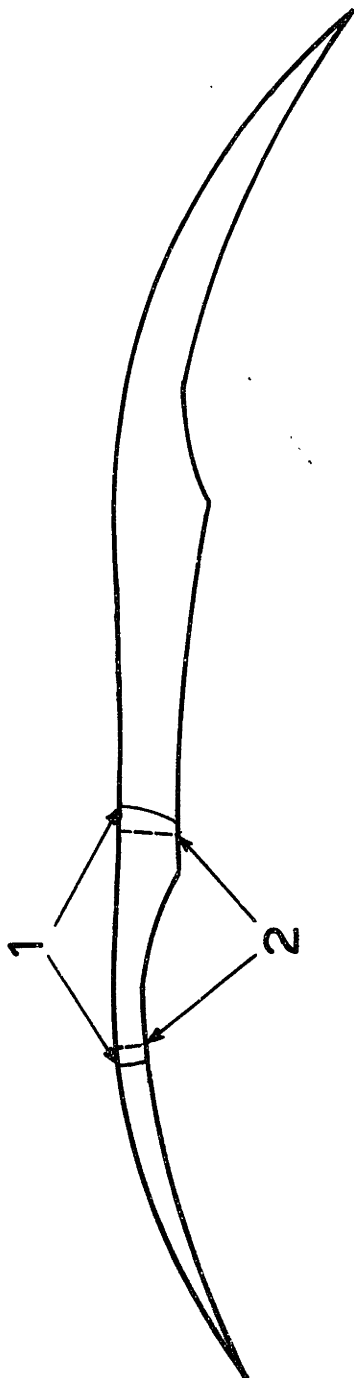
Fig. 7   Transition of flame propagation from hemispherical shape truncated at the top (1) to one dimensional propagation (2), as seen from the side.
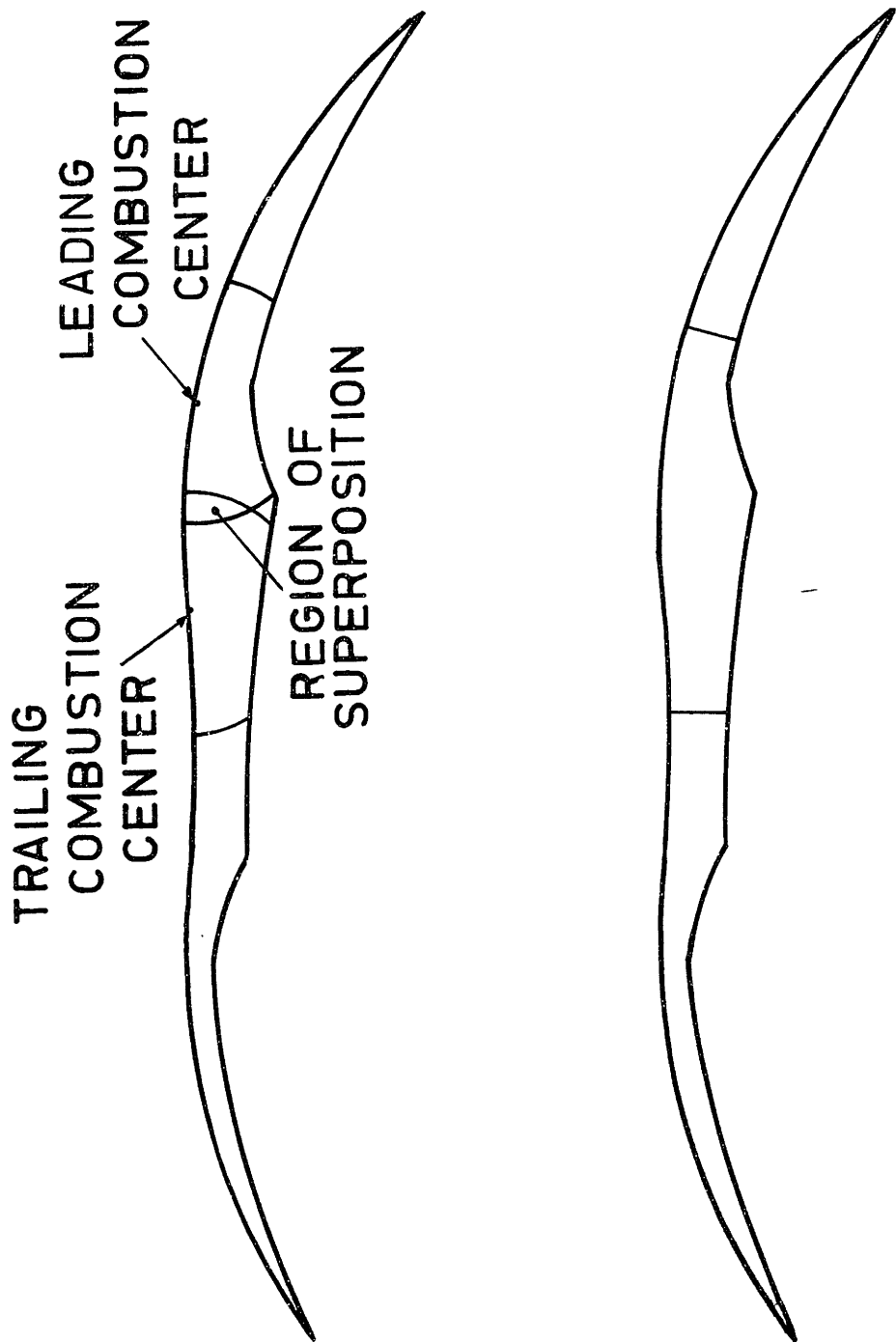
Fig. 8   Transition from hemispherical configuration (upper case) to one dimensional propagation (lower), when flame fronts meet in the region between the spark plugs.

LEADING COMBUSTION CENTER

TRAILING COMBUSTION CENTER

REGION OF SUPERPOSITION
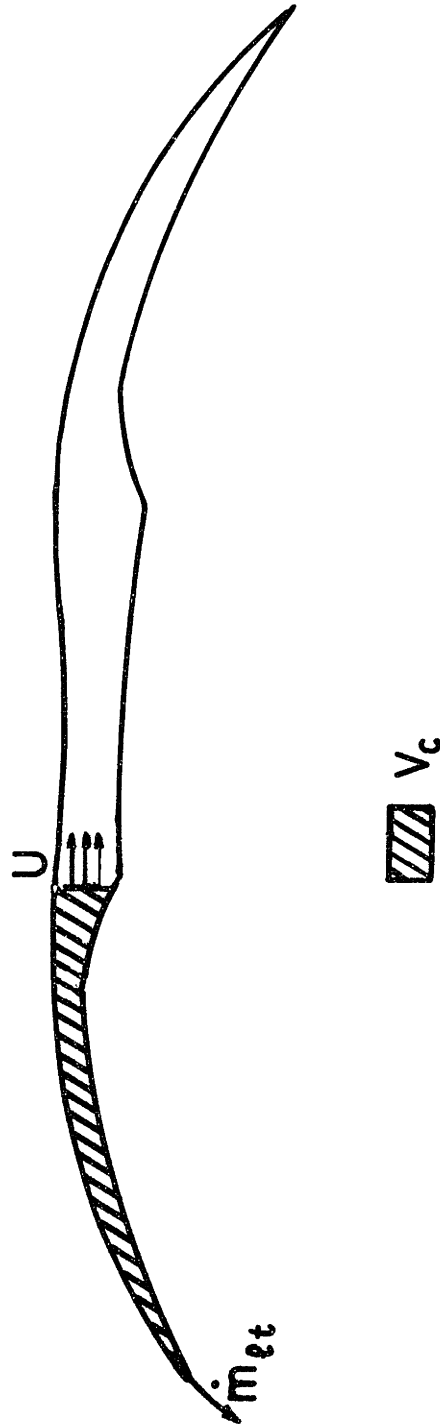
Fig. 9   Schematic representation of the control volume (V_c) used to compute average gas speed (U) at any point along the rotor surface.
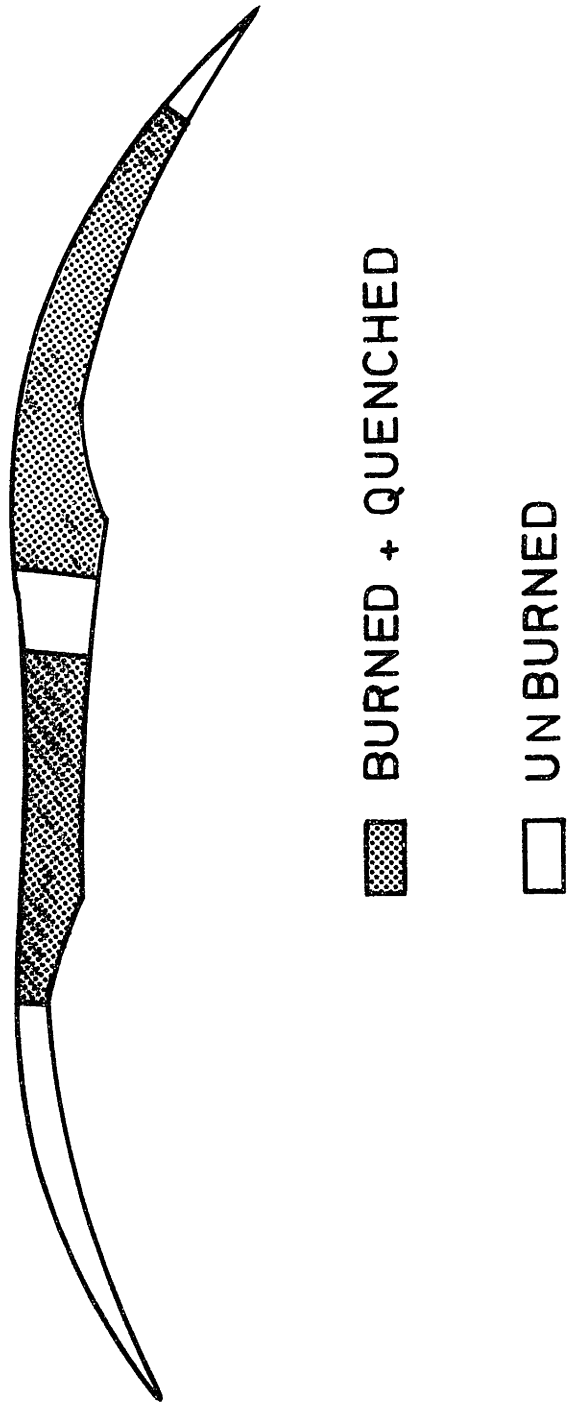
Fig. 10   Schematic representation of the chamber, divided in five different regions to compute heat transfer during combustion.

BURNED + QUENCHED

UNBURNED
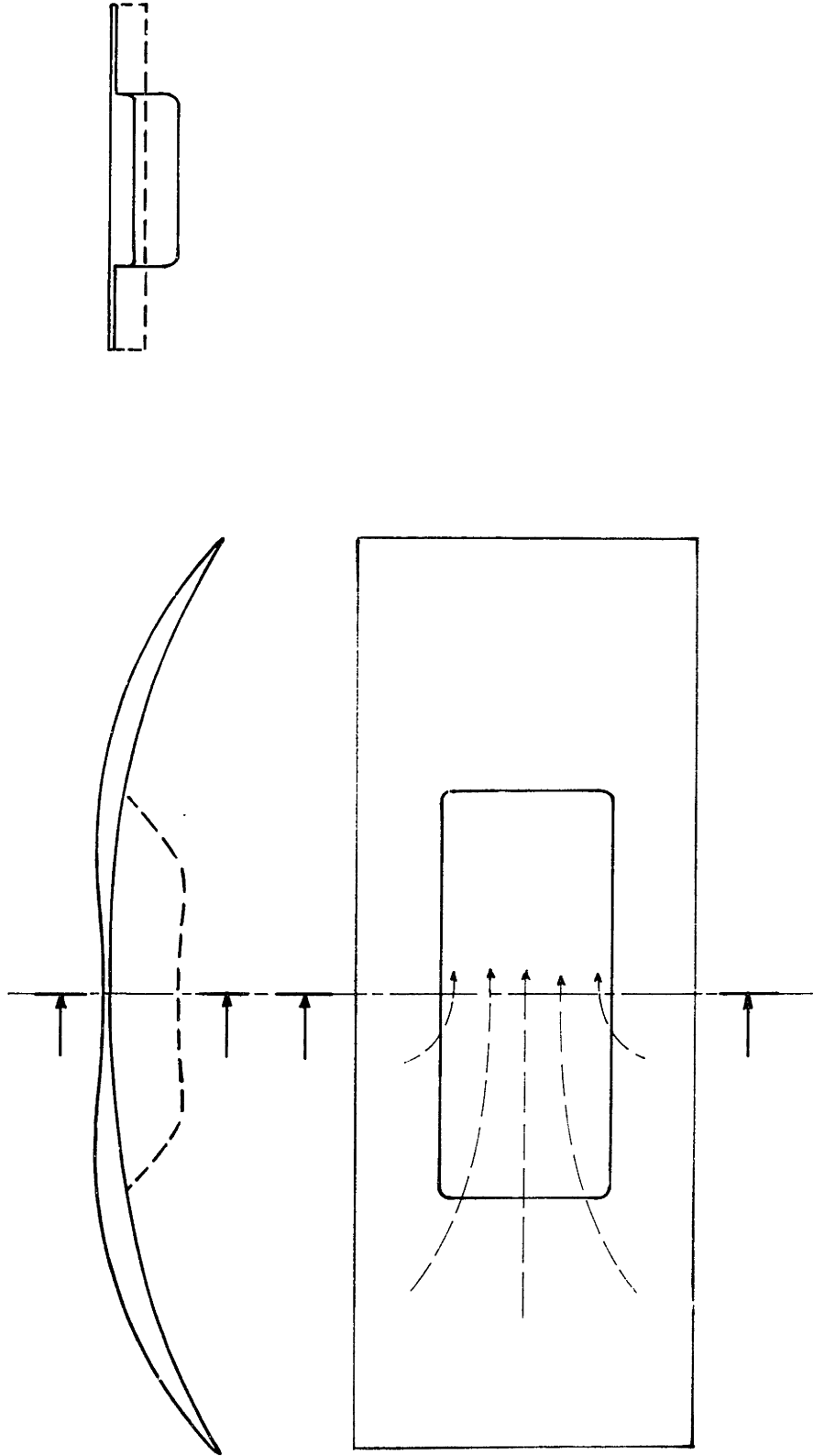
Fig. 11   Real rotor cavity configuration in the region near T.D.C.; dashed lines are gas streamlines.
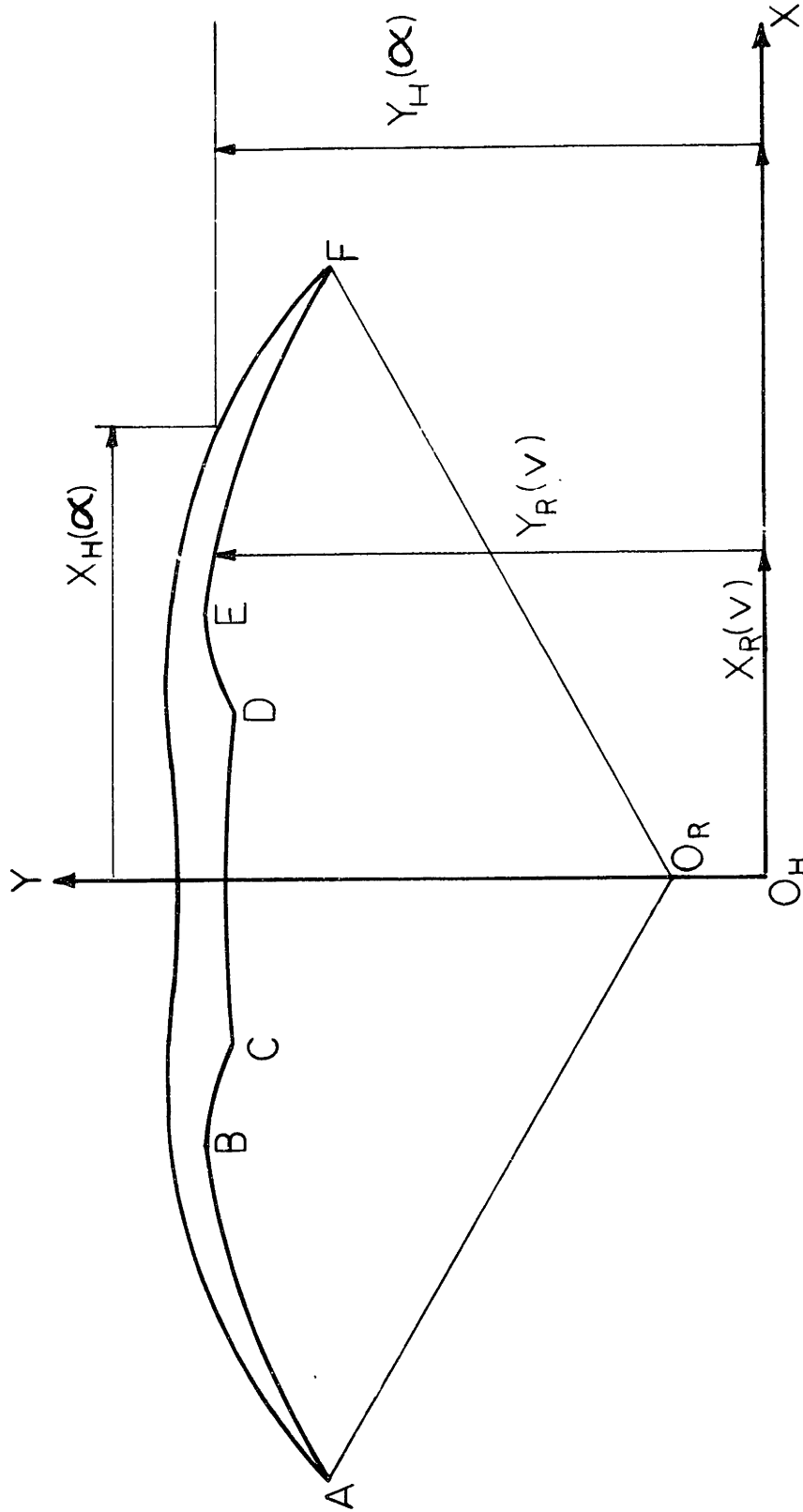
Fig. 12 Rotor and housing coordinates computed with the help of equations (1.75) to (1.83)
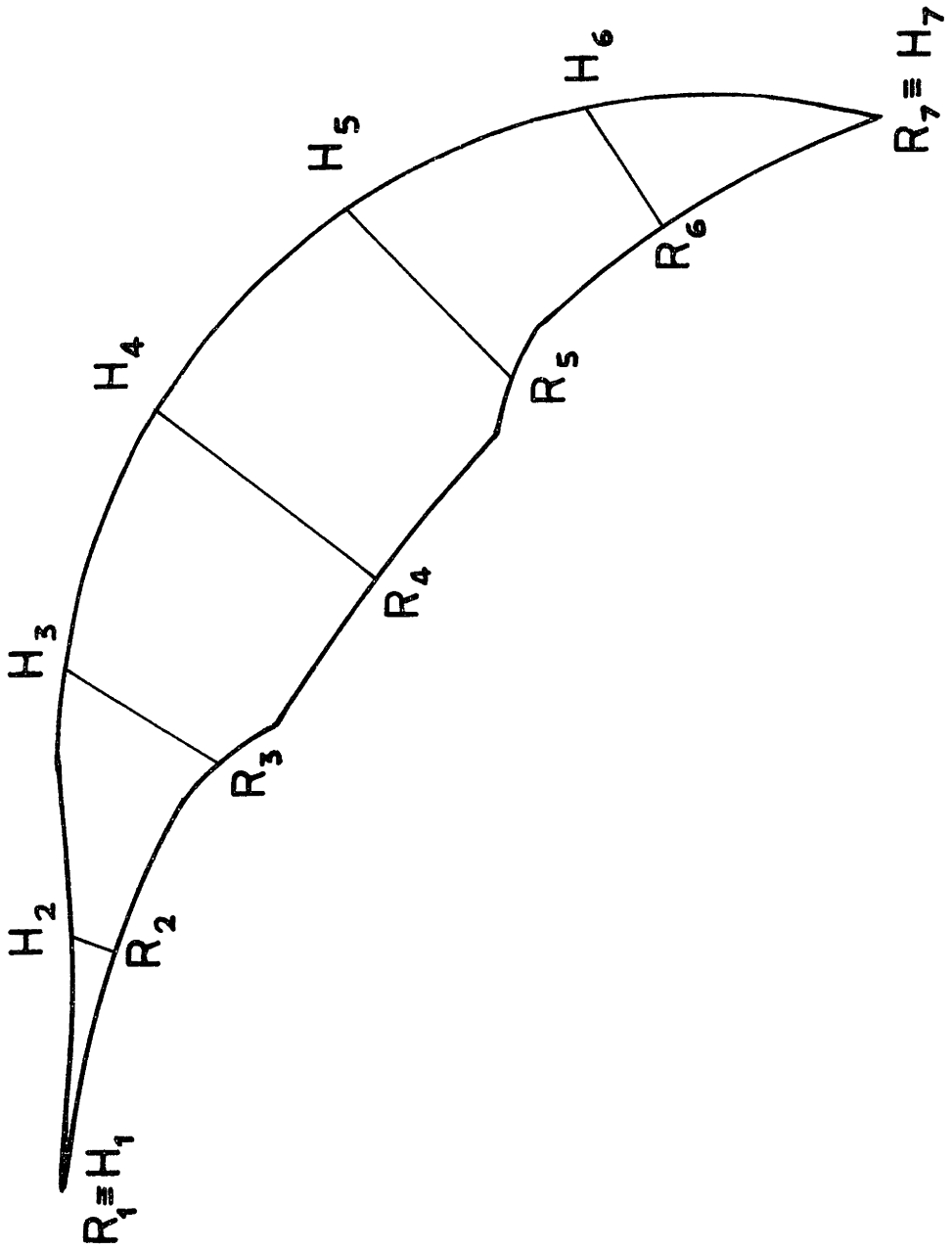
Fig. 13 Representation of the control elements in which the chamber is subdivided.
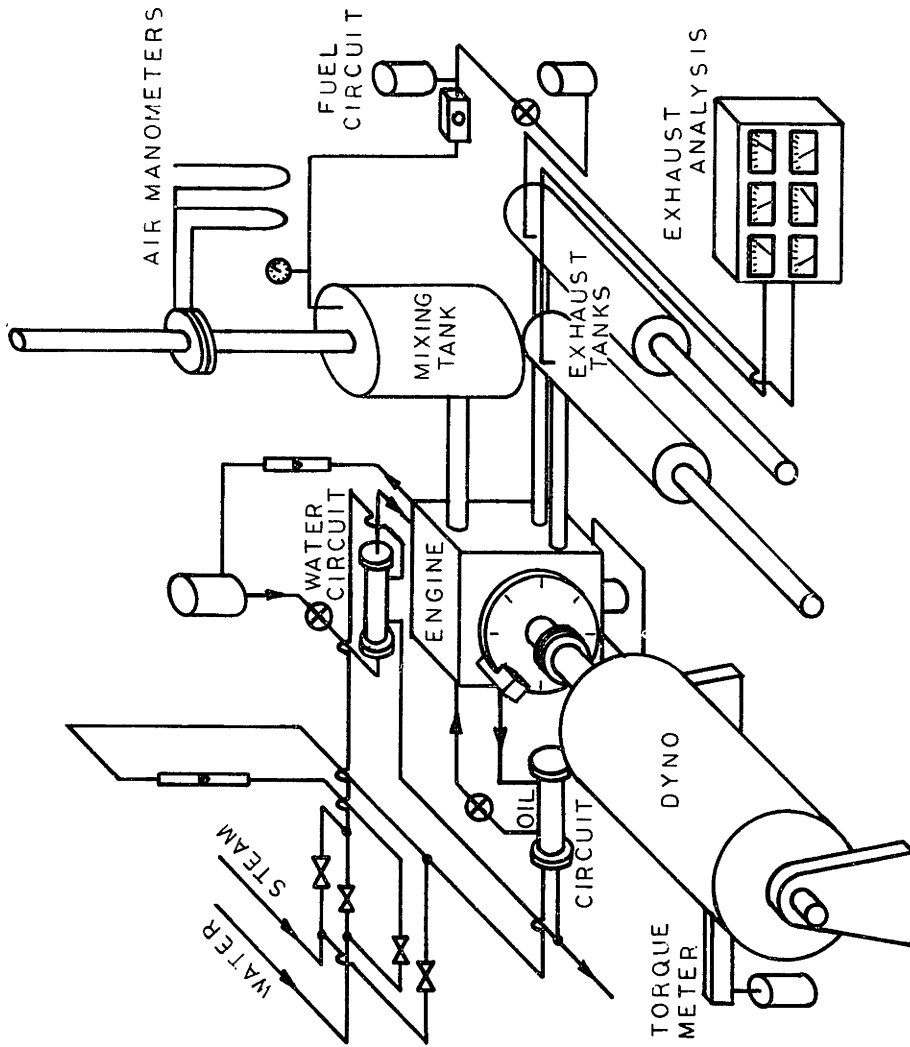
Fig. 14 Experimental apparatus.
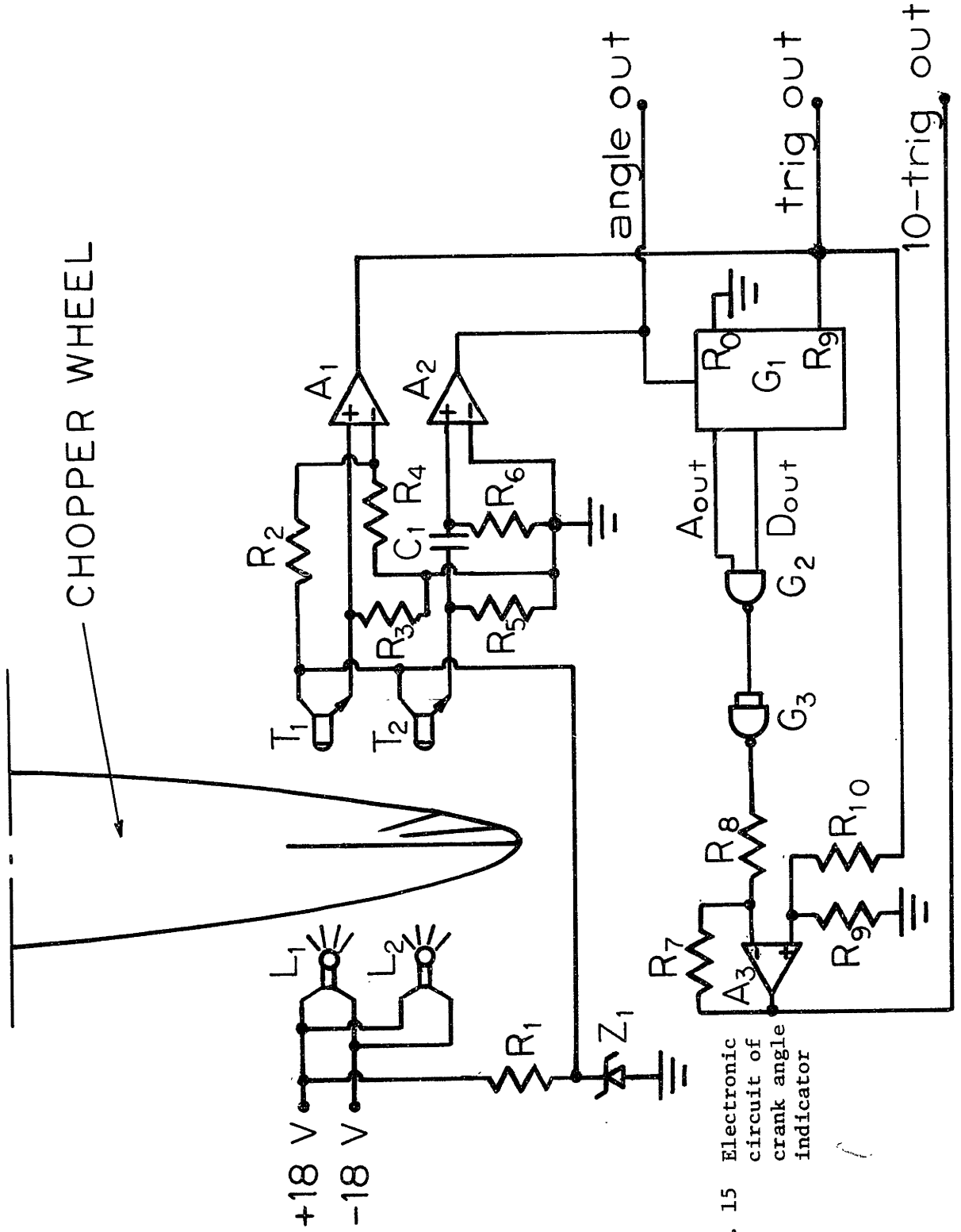
Fig. 15 Electronic circuit of crank angle indicator
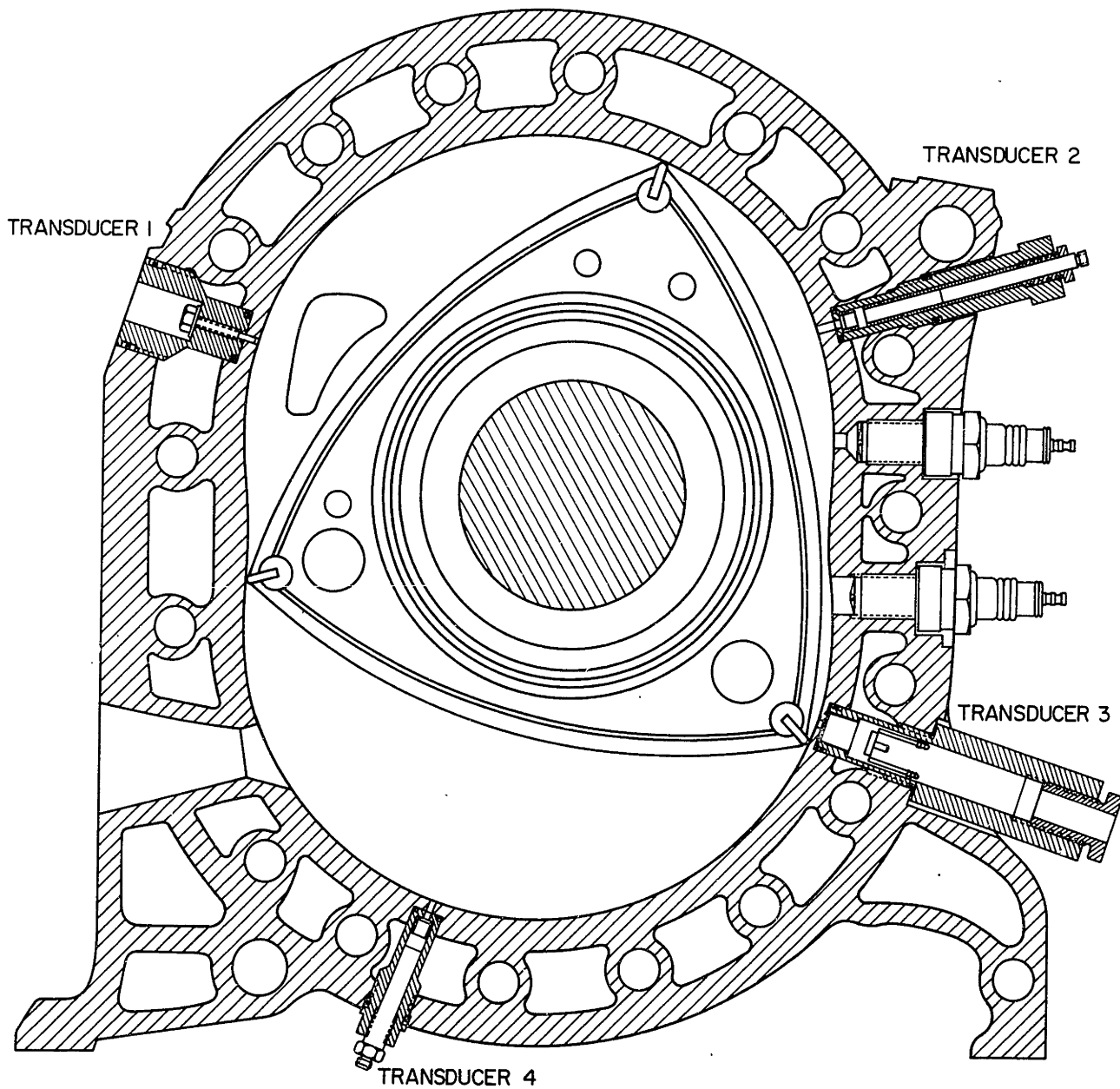
Fig. 16 View of the engine and of the
pressure transducers location.
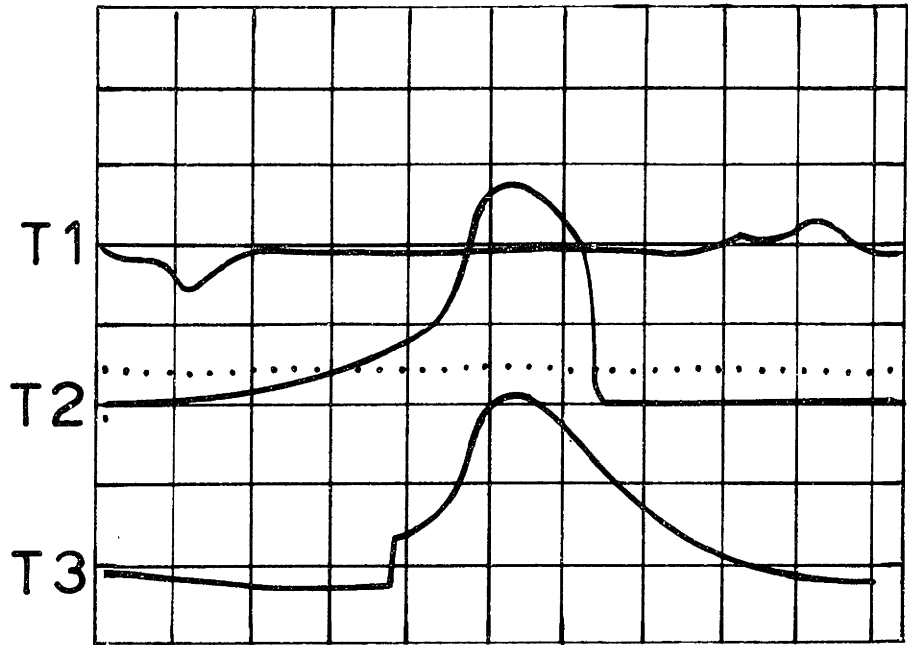
Fig. 17   Oscilloscope records (above and below) showing
          outputs of various transducers and crank angle
          indicator (dots).
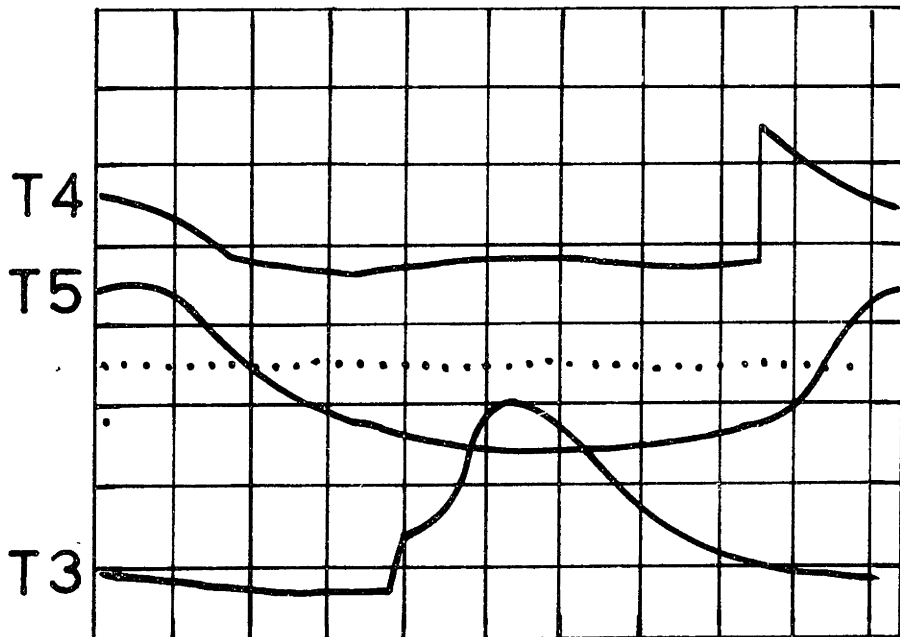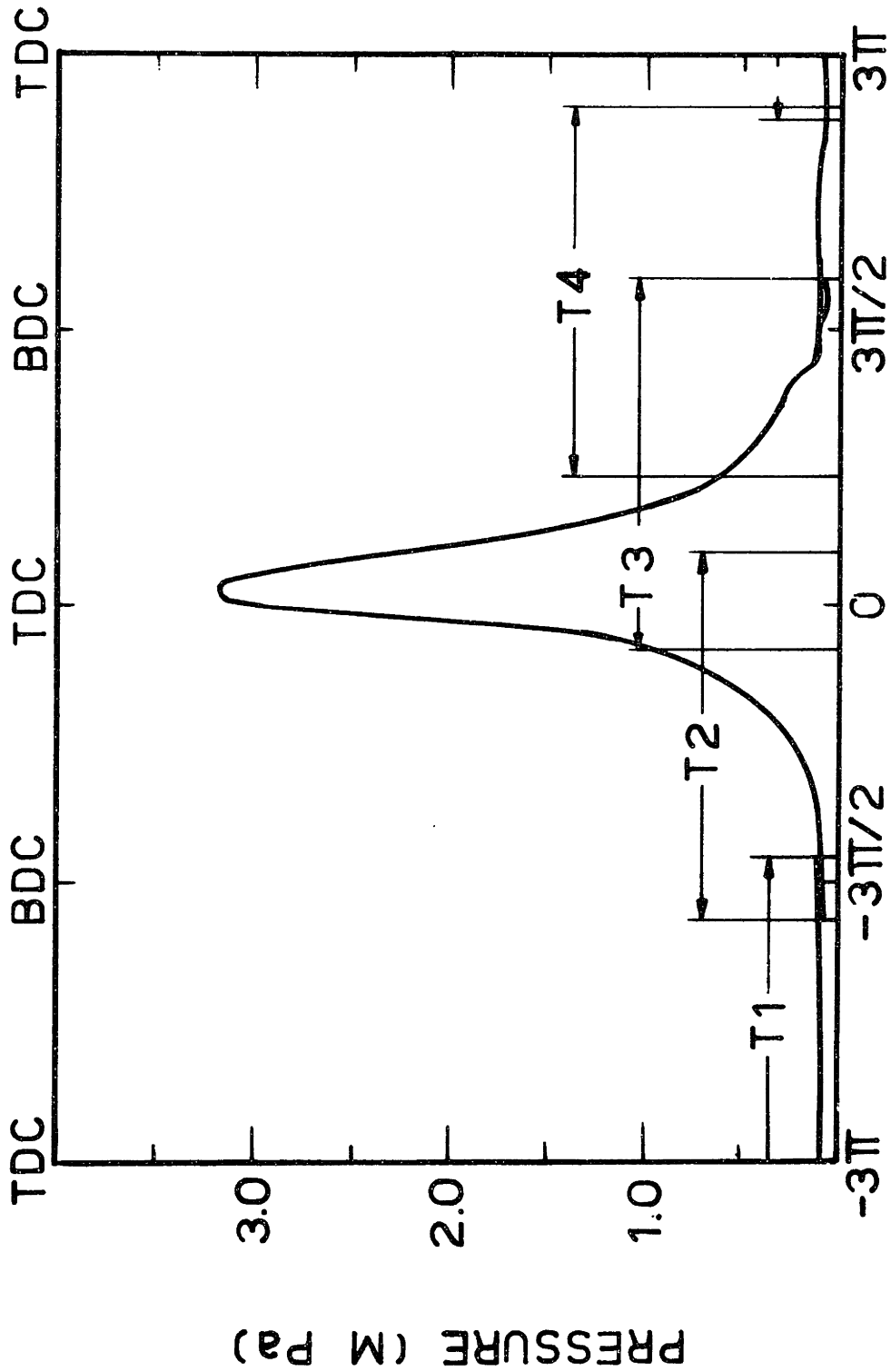
- Fig. 18 Complete pressure diagram obtained from previous record, and regions of transducer recording.
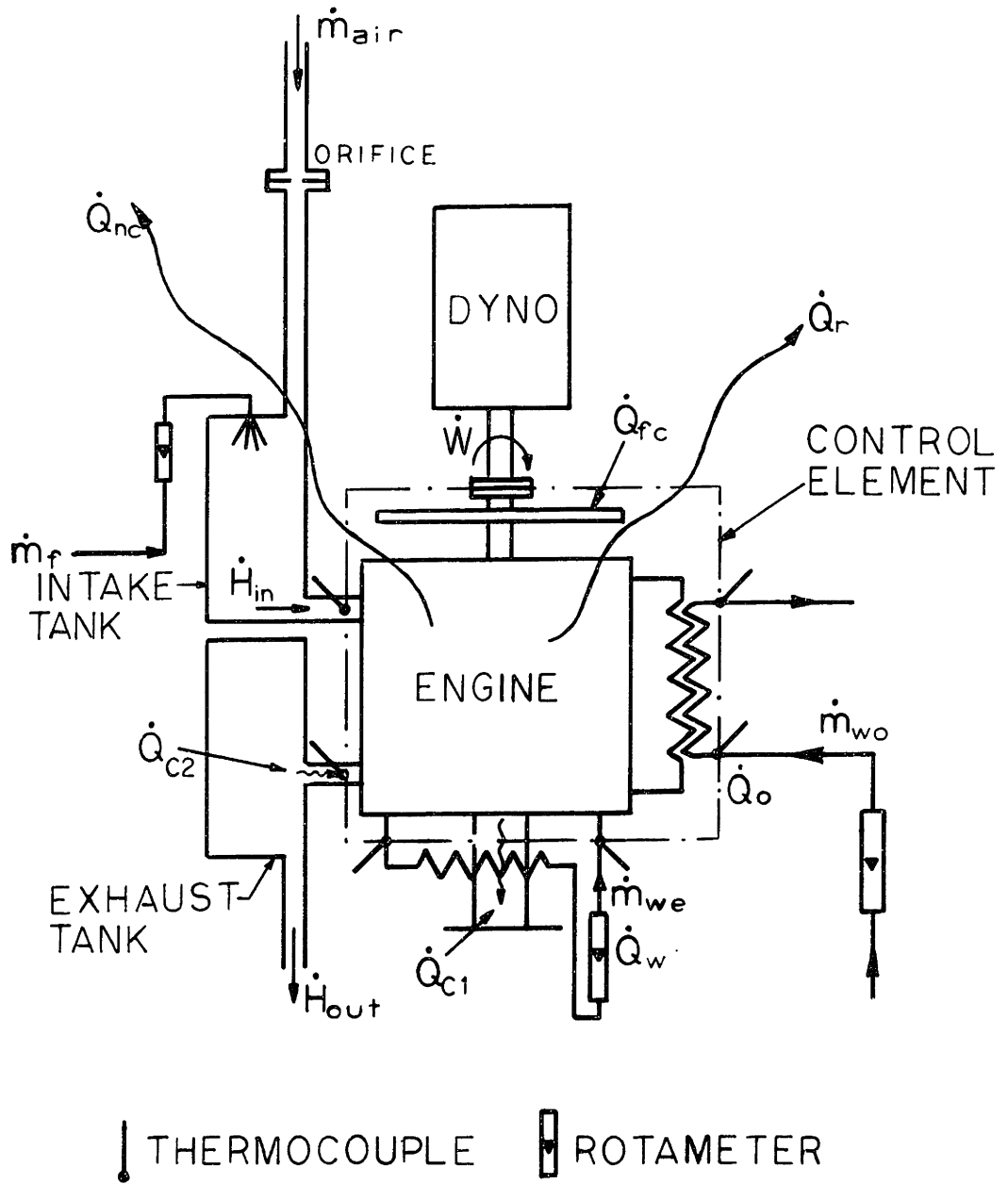
Fig. 19   Schematic of the experimental facility showing all heat
fluxes being exchanged.
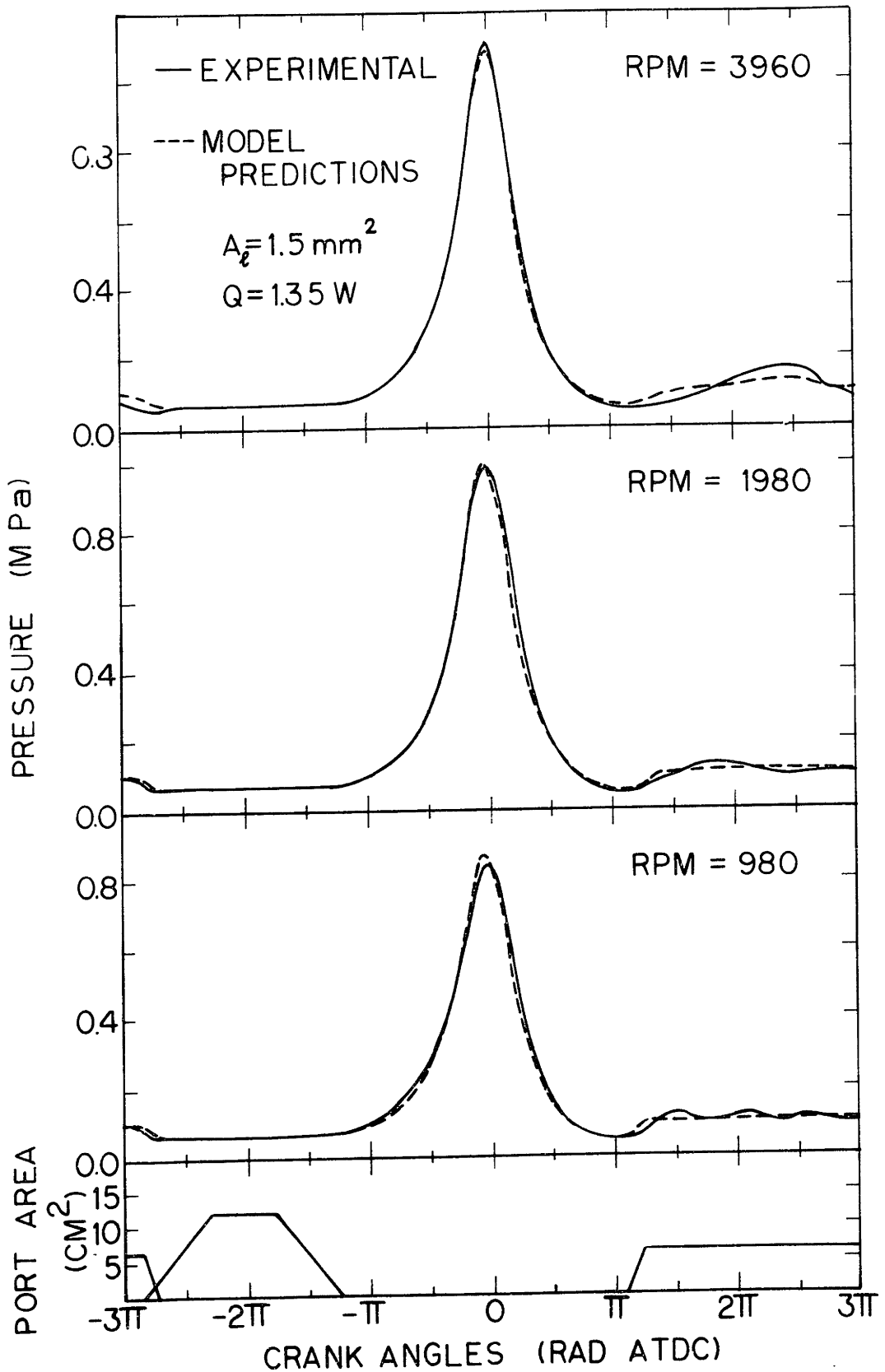
Fig. 20 Pressure diagrams experimentally obtained for the motoring cases versus model predictions.
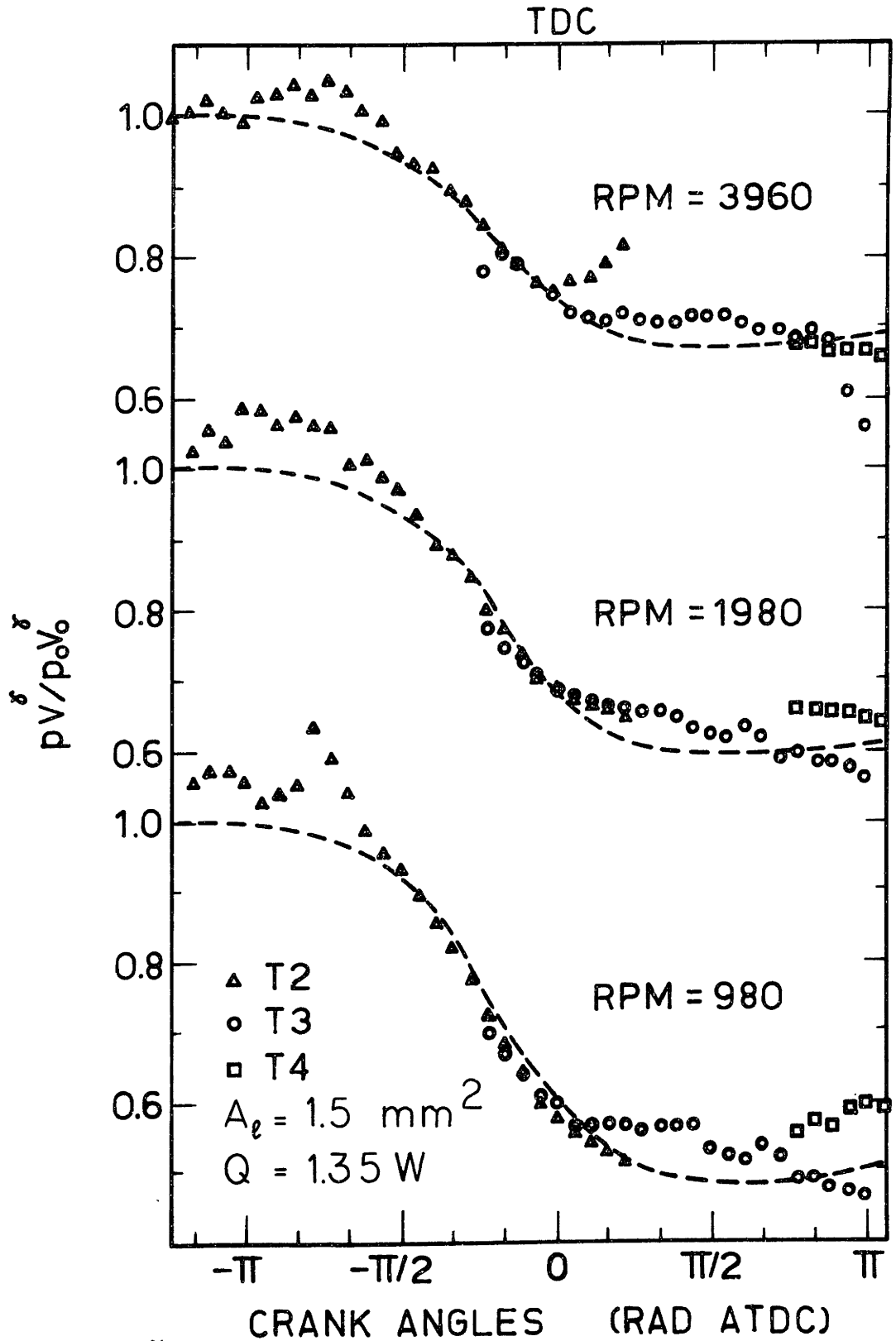
Fig. 21 pV^γ versus crank angle obtained from the various transducers during motoring conditions, versus model predictions (dash).

Fig. 21A Gas motion induced by the changing chamber geometry, relative to the rotor. Positive in the direction of rotation. Nondimensionalized by the average rotor tip velocity.
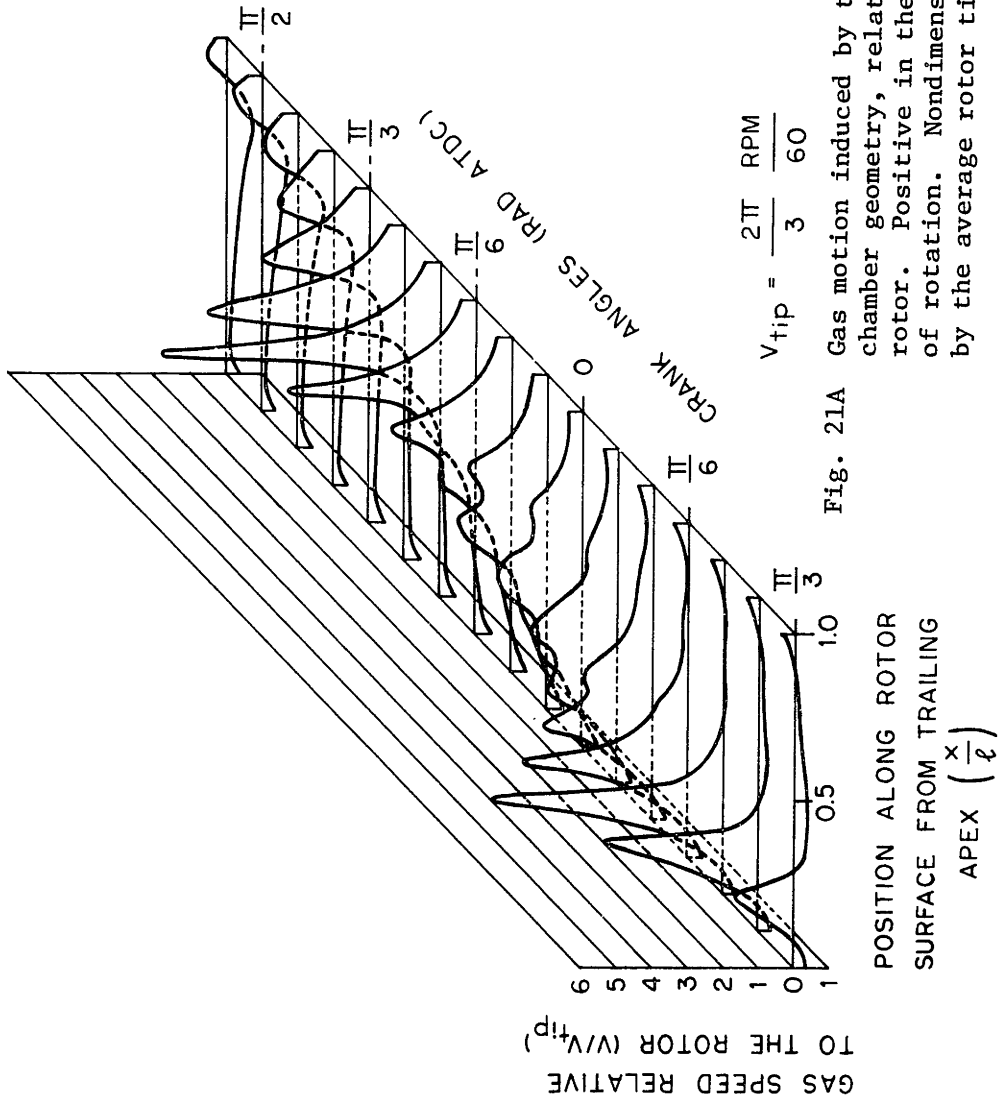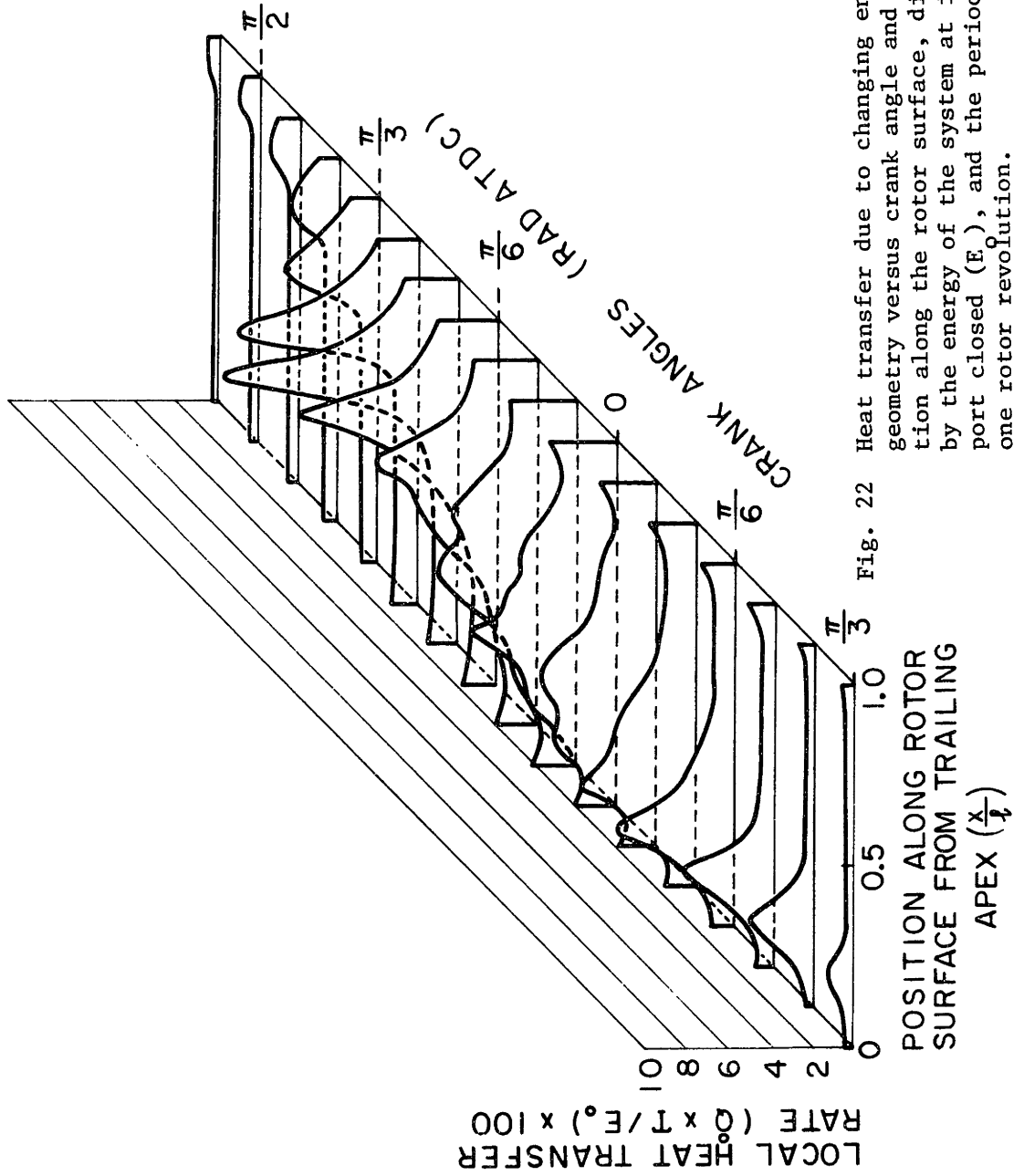
Fig. 22 Heat transfer due to changing engine geometry versus crank angle and position along the rotor surface, divided by the energy of the system at intake port closed (E_c), and the period T of one rotor revolution.
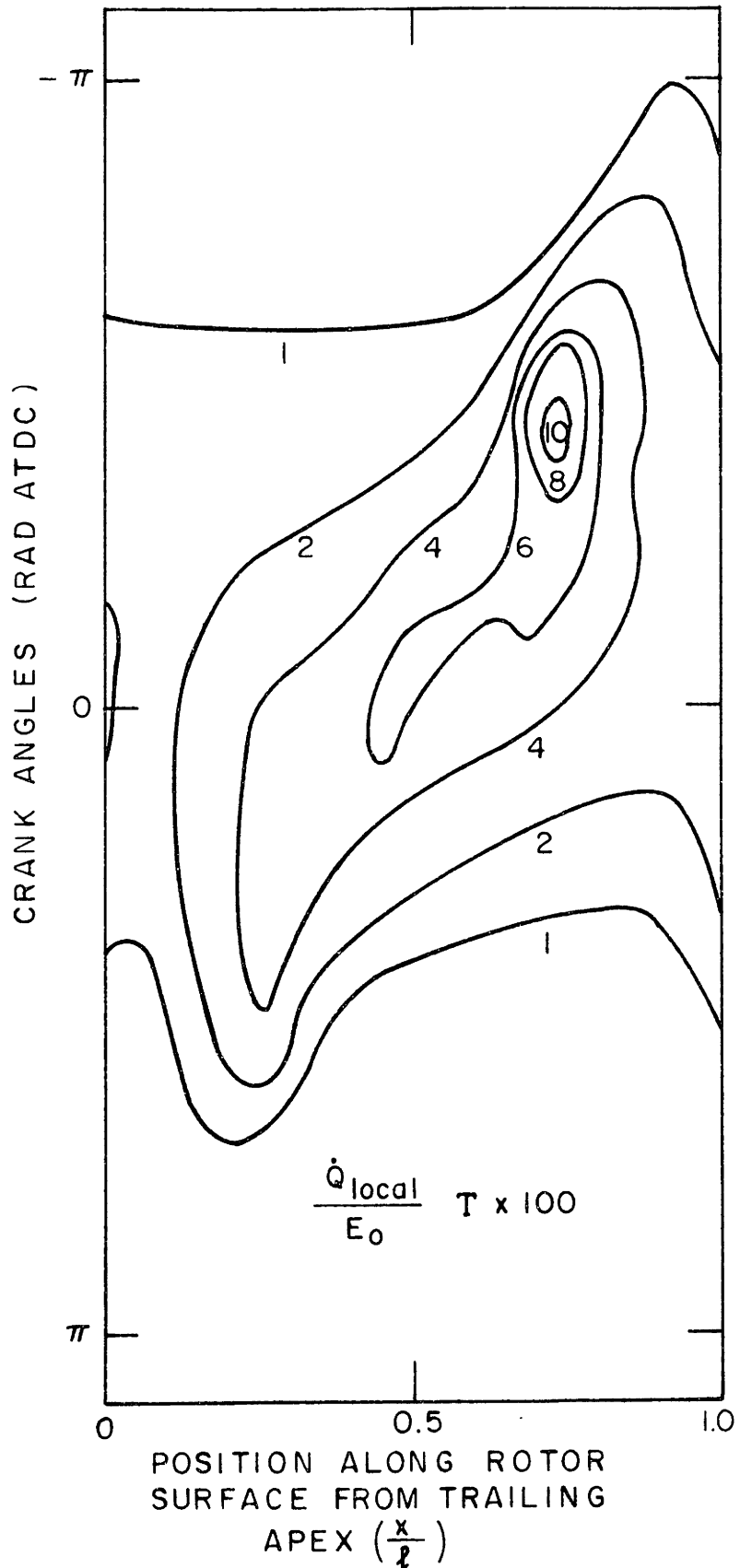
Fig. 23 Contour plot of the previous case.
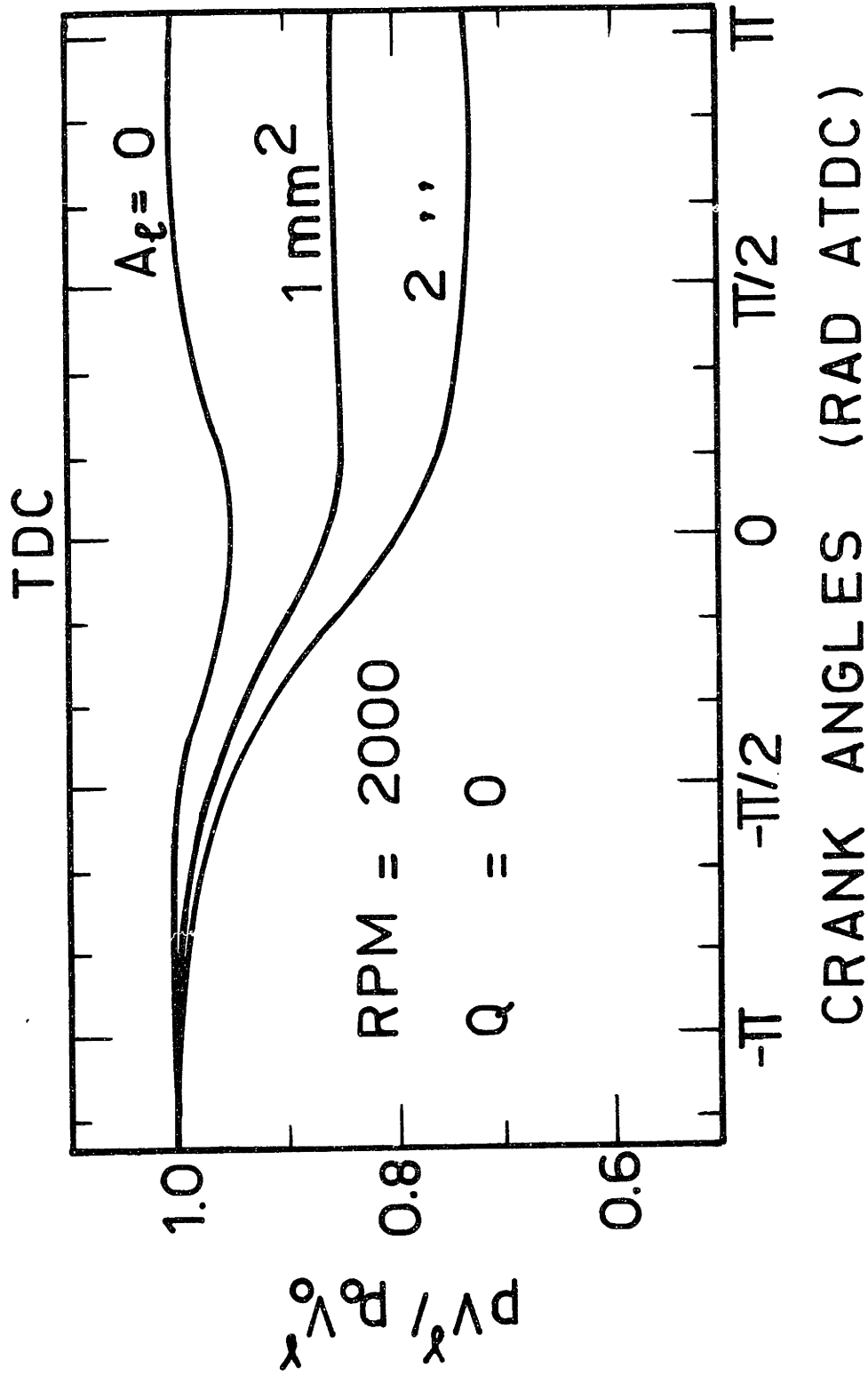
Fig. 24 Change in pV^γ with leakage area (A_ℓ) at constant speed and zero heat transfer.
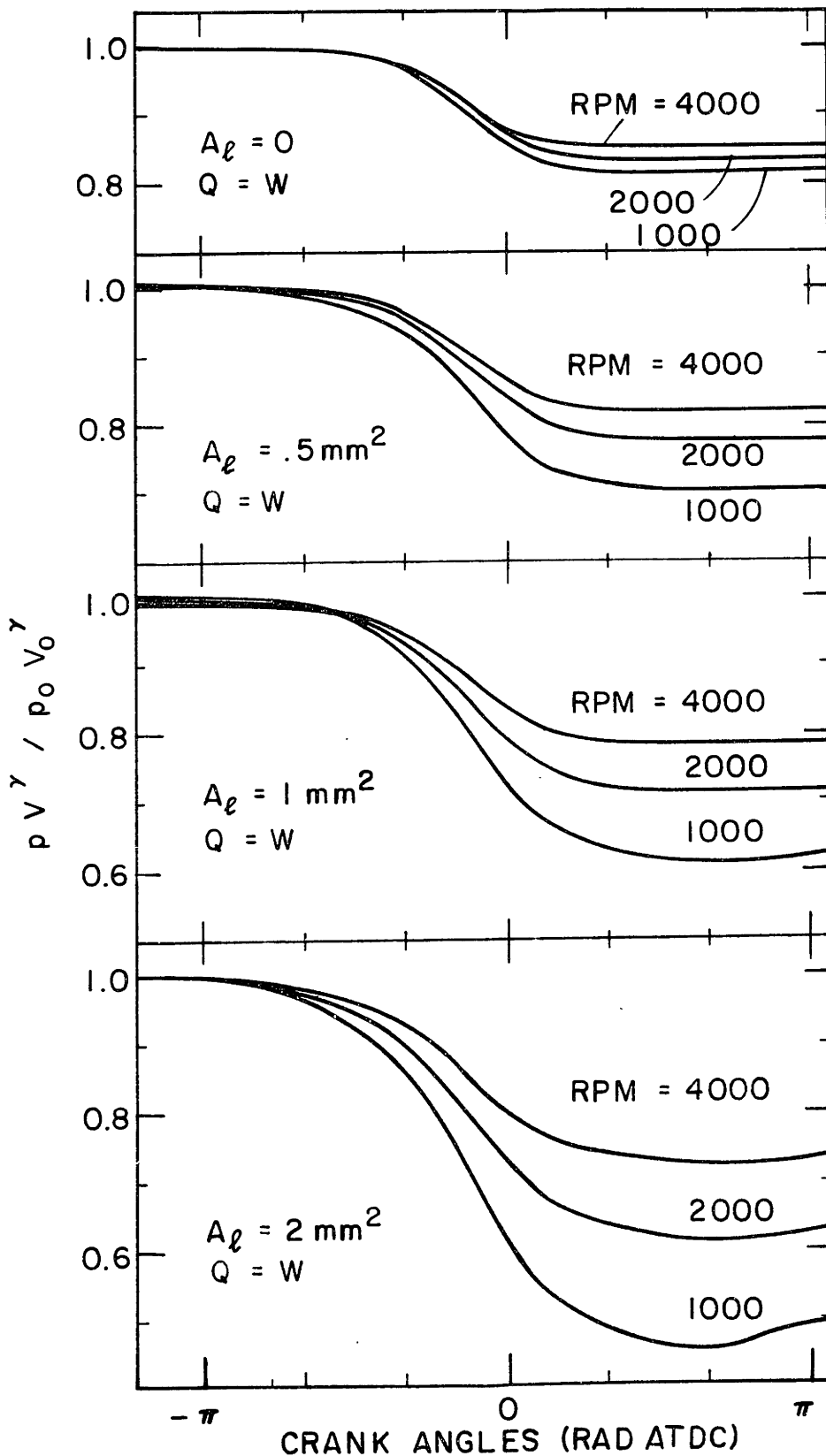
Fig. 25 Change in pV^γ with leakage and speed holding the heat transfer coefficient to the value given by Woschni.
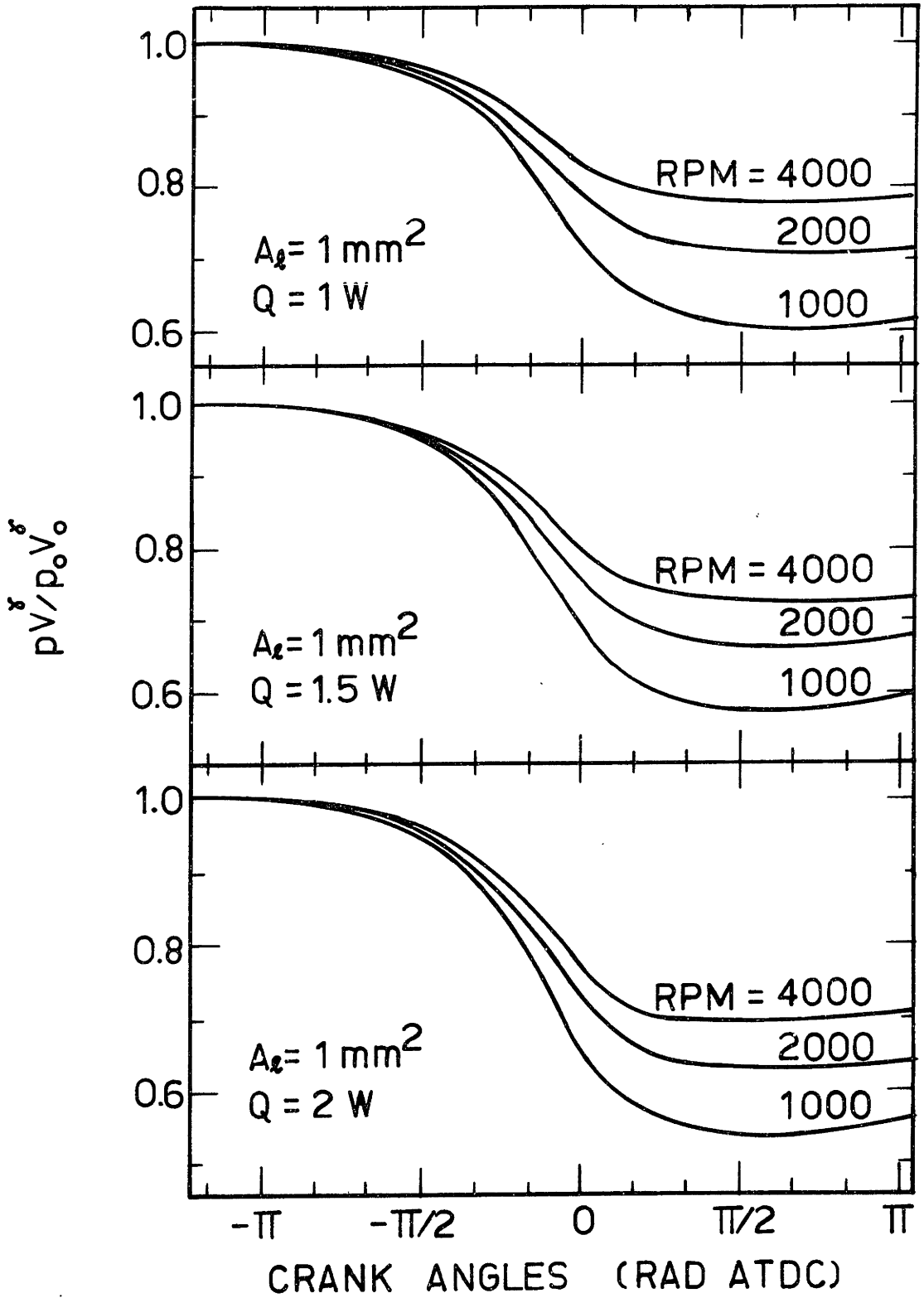
Fig. 26 Change in pV^γ with heat transfer and speed holding constant
the leakage.
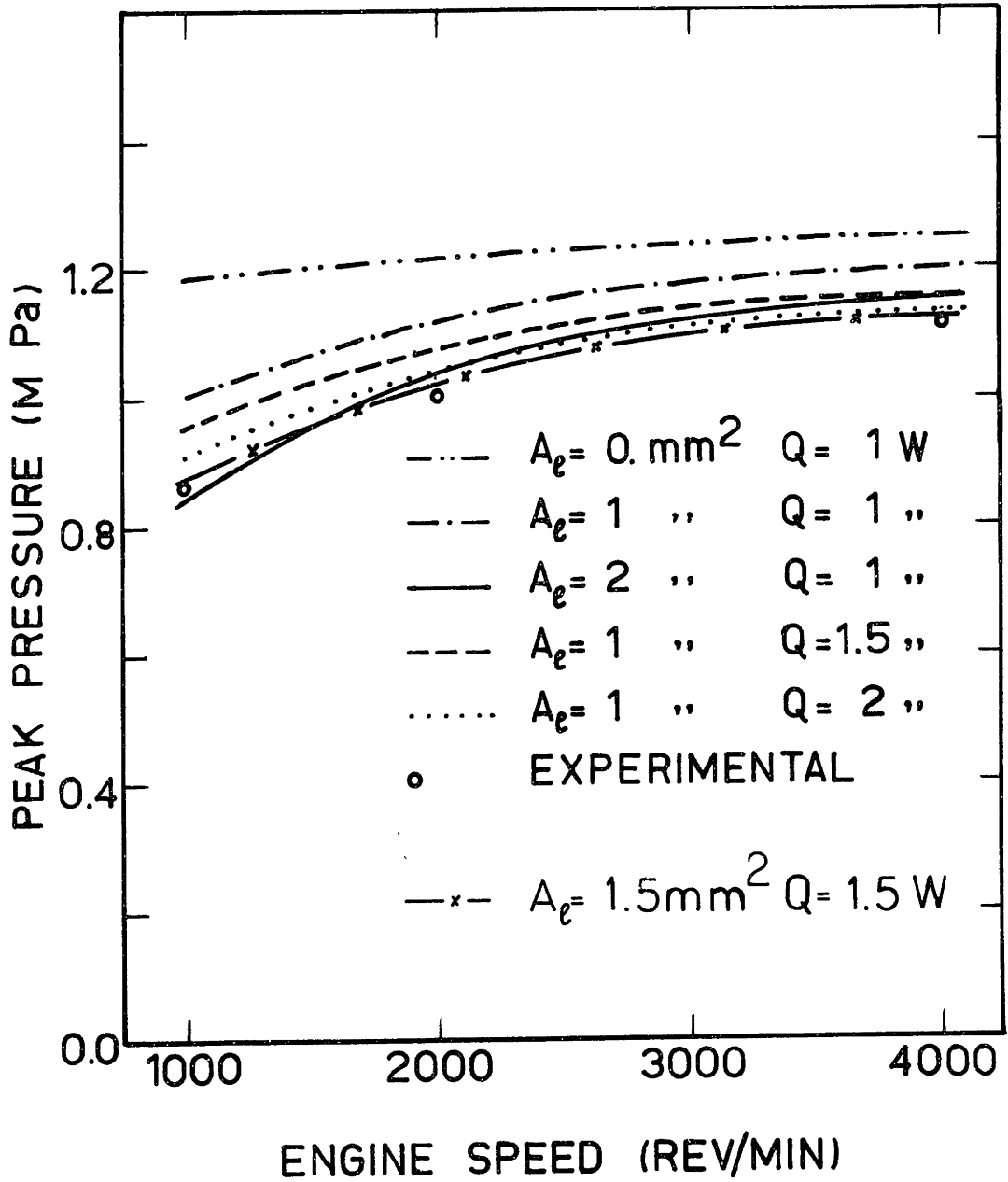
Fig. 27 Dependence of peak pressure from leakage and heat transfer.
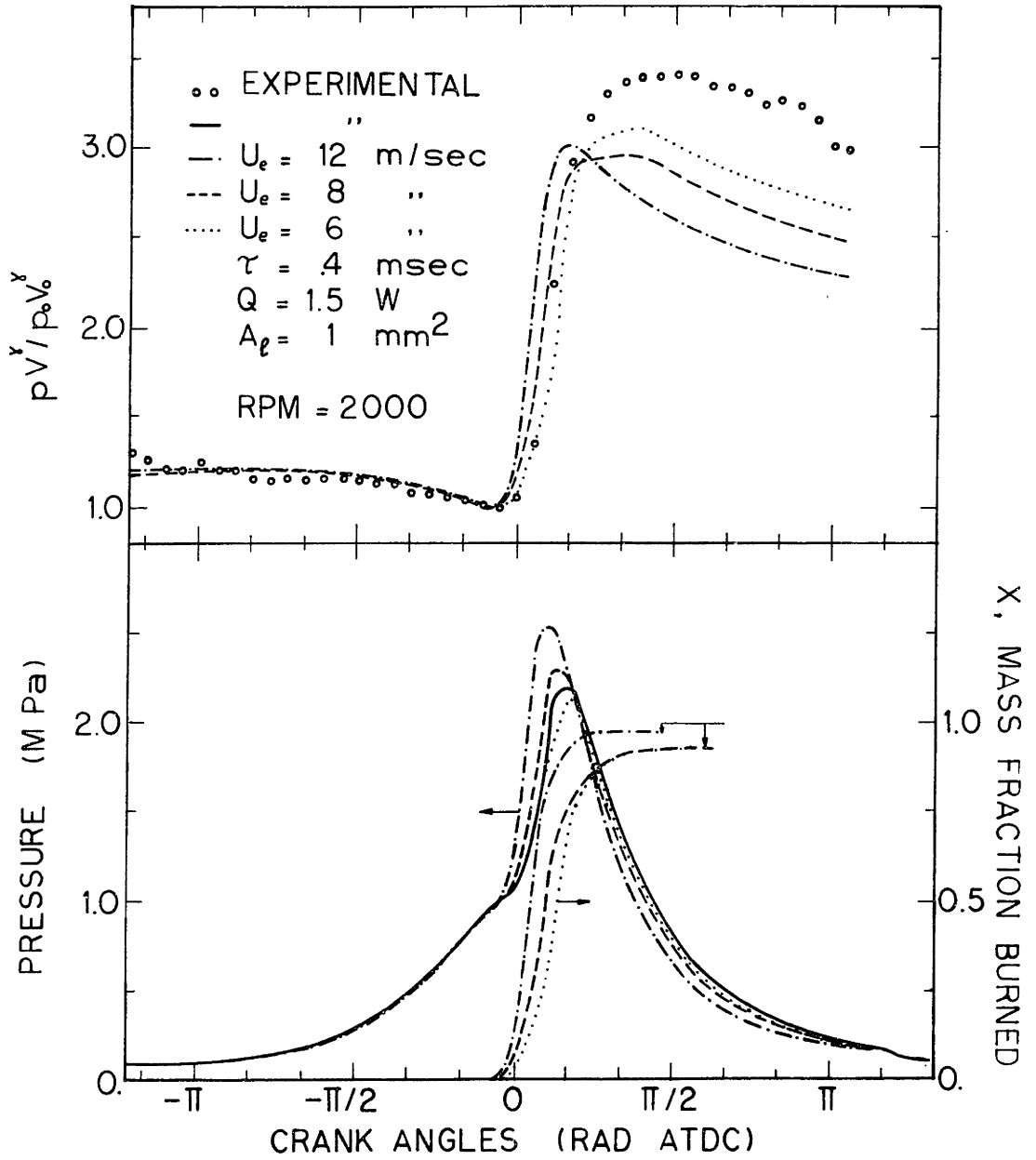
Fig. 28 Effect of the entrainment speed on pV^γ, pressure, and mass
fraction burned, during firing conditions, holding other
parameters constant.
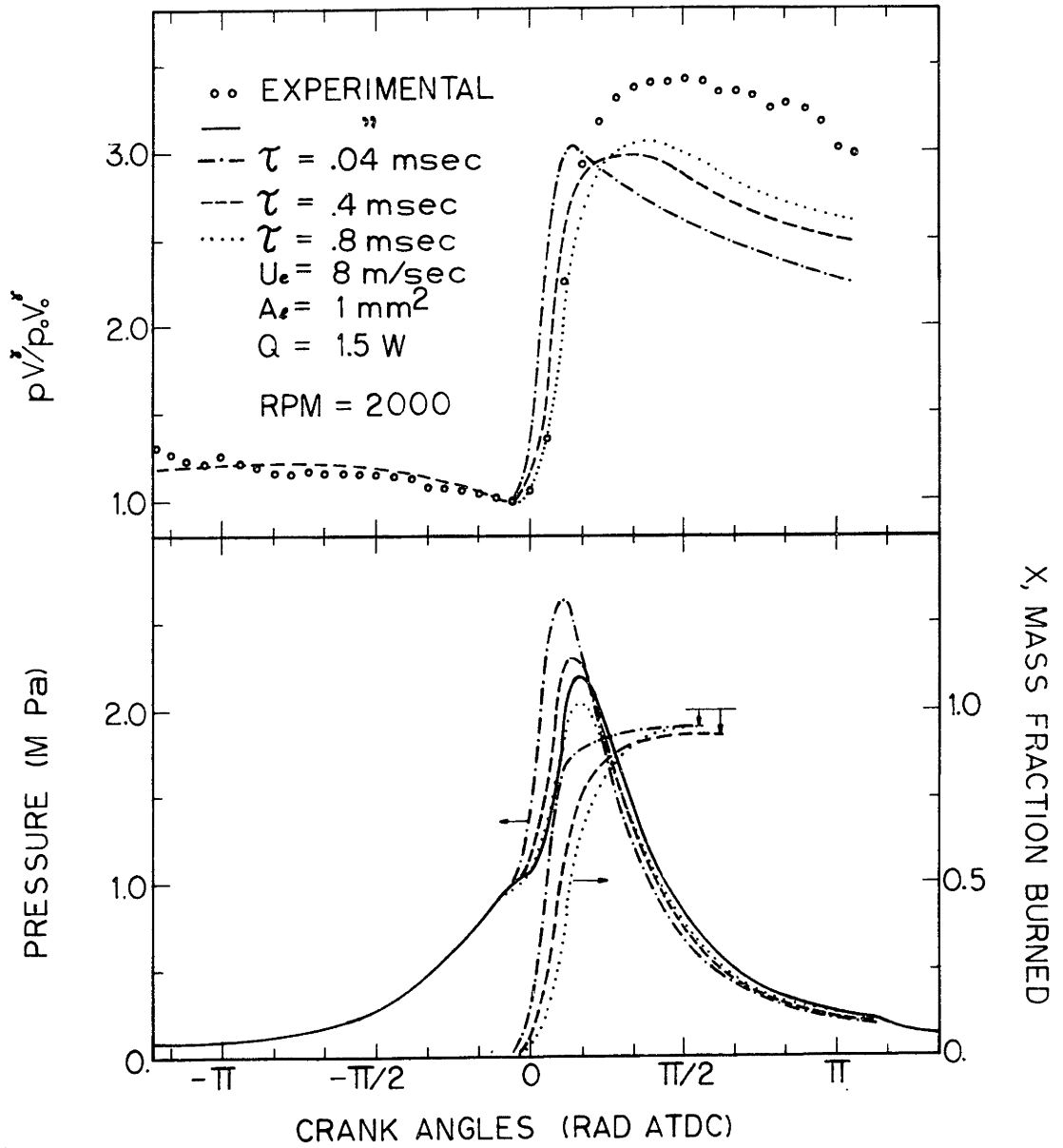
Fig. 29 Effect of burning time on pV^{γ}, pressure, and mass fraction burned, during firing conditions, holding other parameters constant.
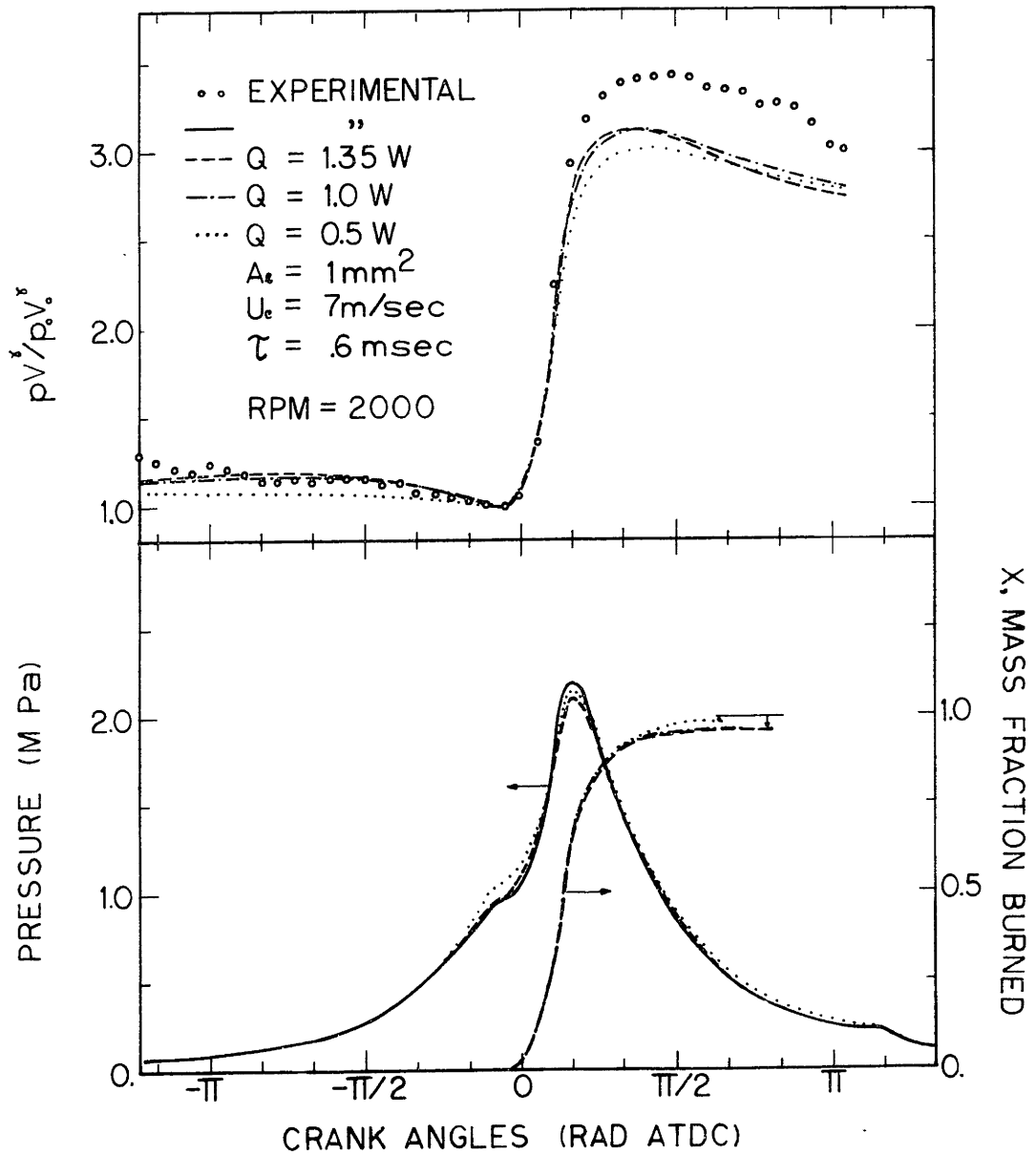
Fig. 30 Effect of heat transfer coefficient on pV^γ, pressure, and mass fraction burned, during firing conditions, holding other parameters constant.
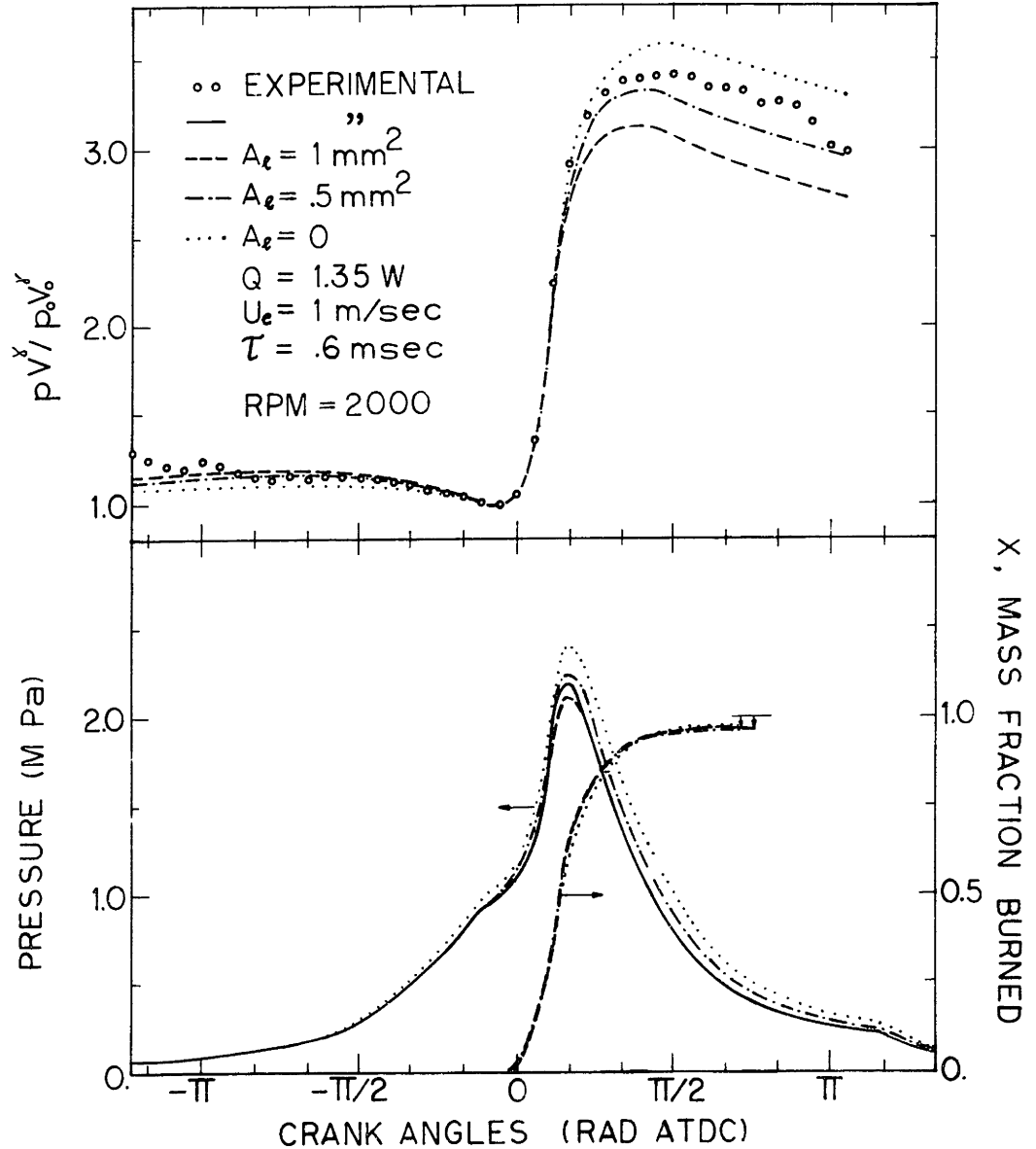
Fig. 31 Effect of leakage area on pV^γ, pressure, and mass fraction burned, during firing conditions, holding other parameters constant.
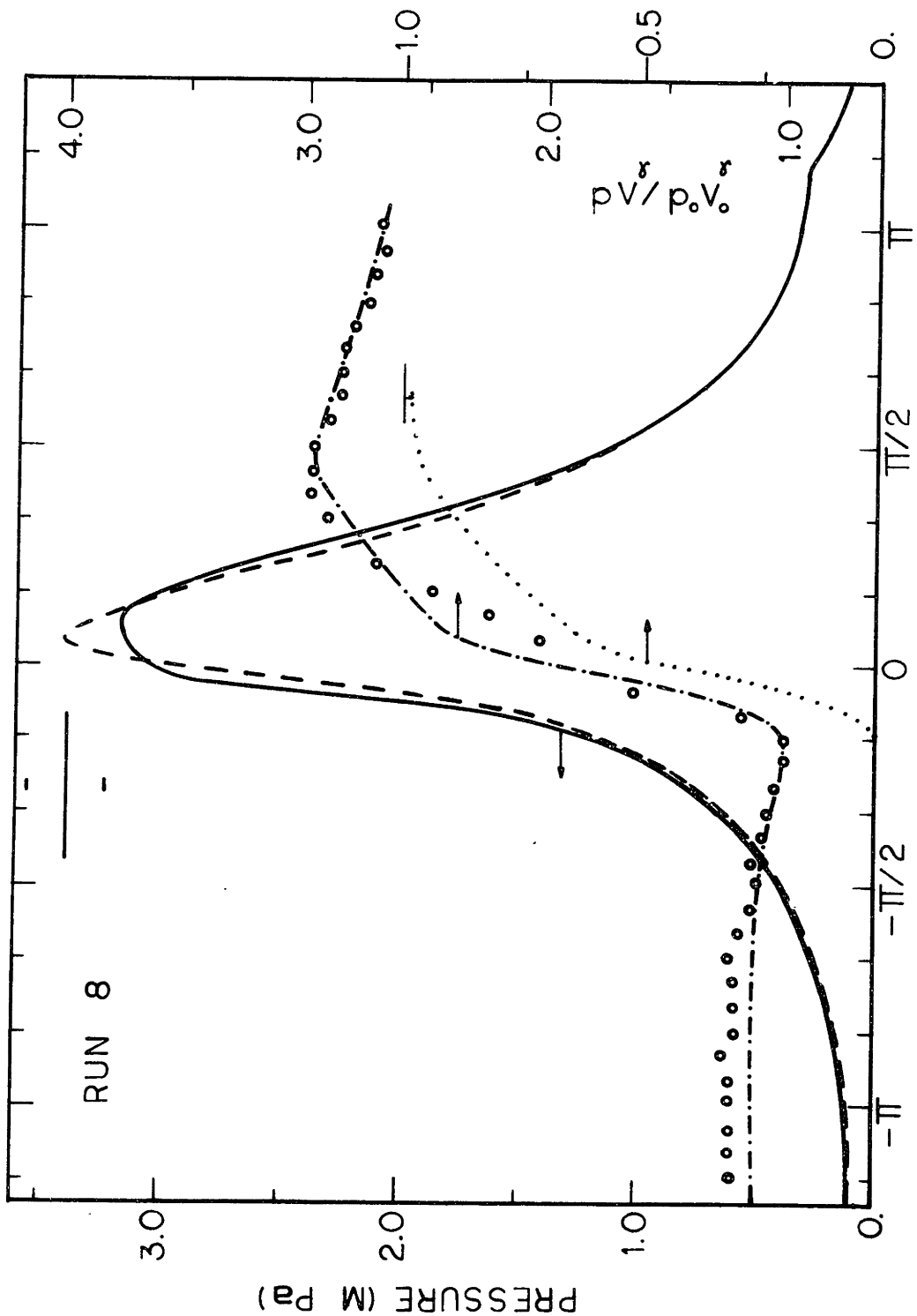
Fig. 32 Comparison between theory and experiments for Run 8 .
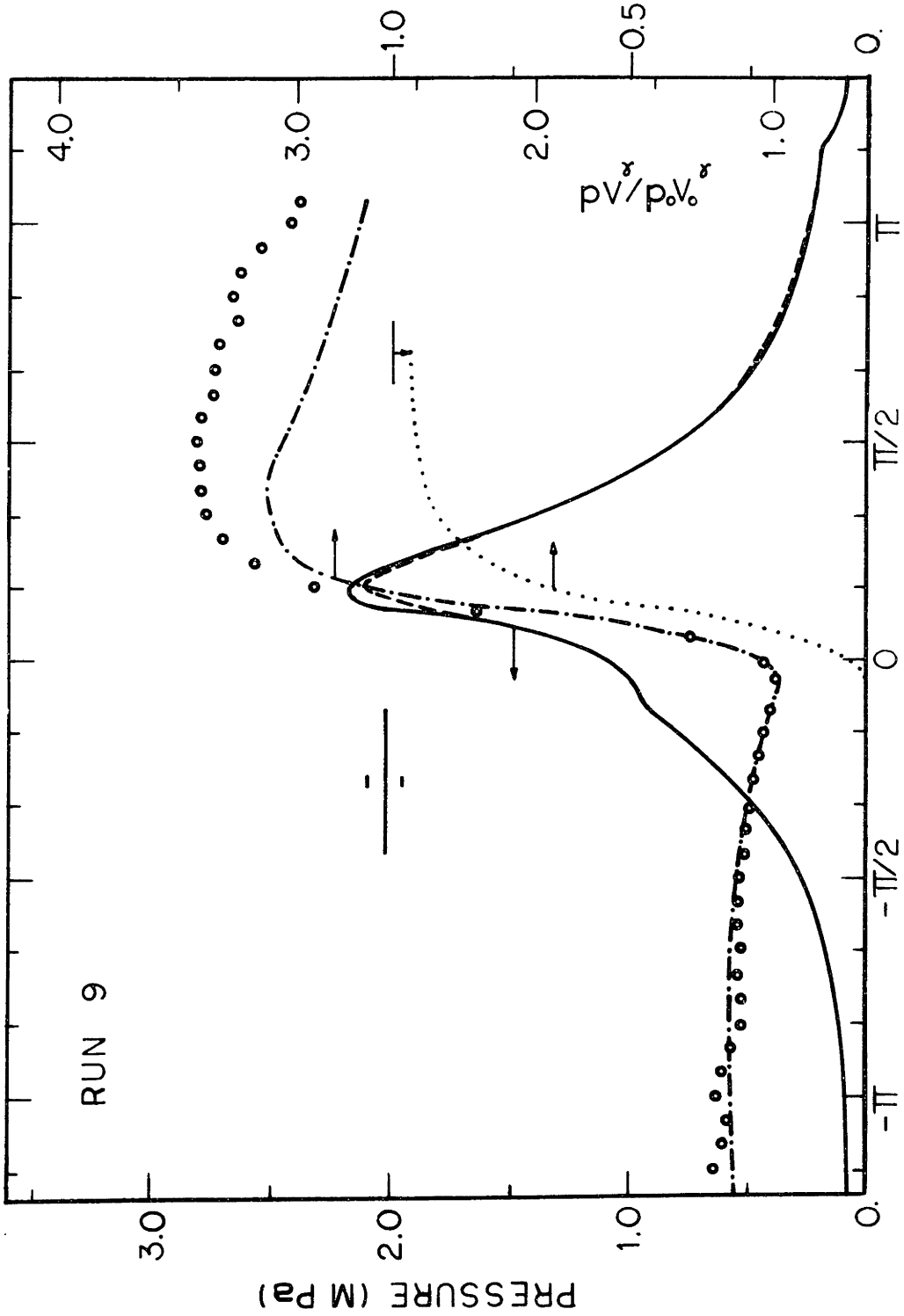
Fig. 33 Comparison between theory and experiments for Run 9 .
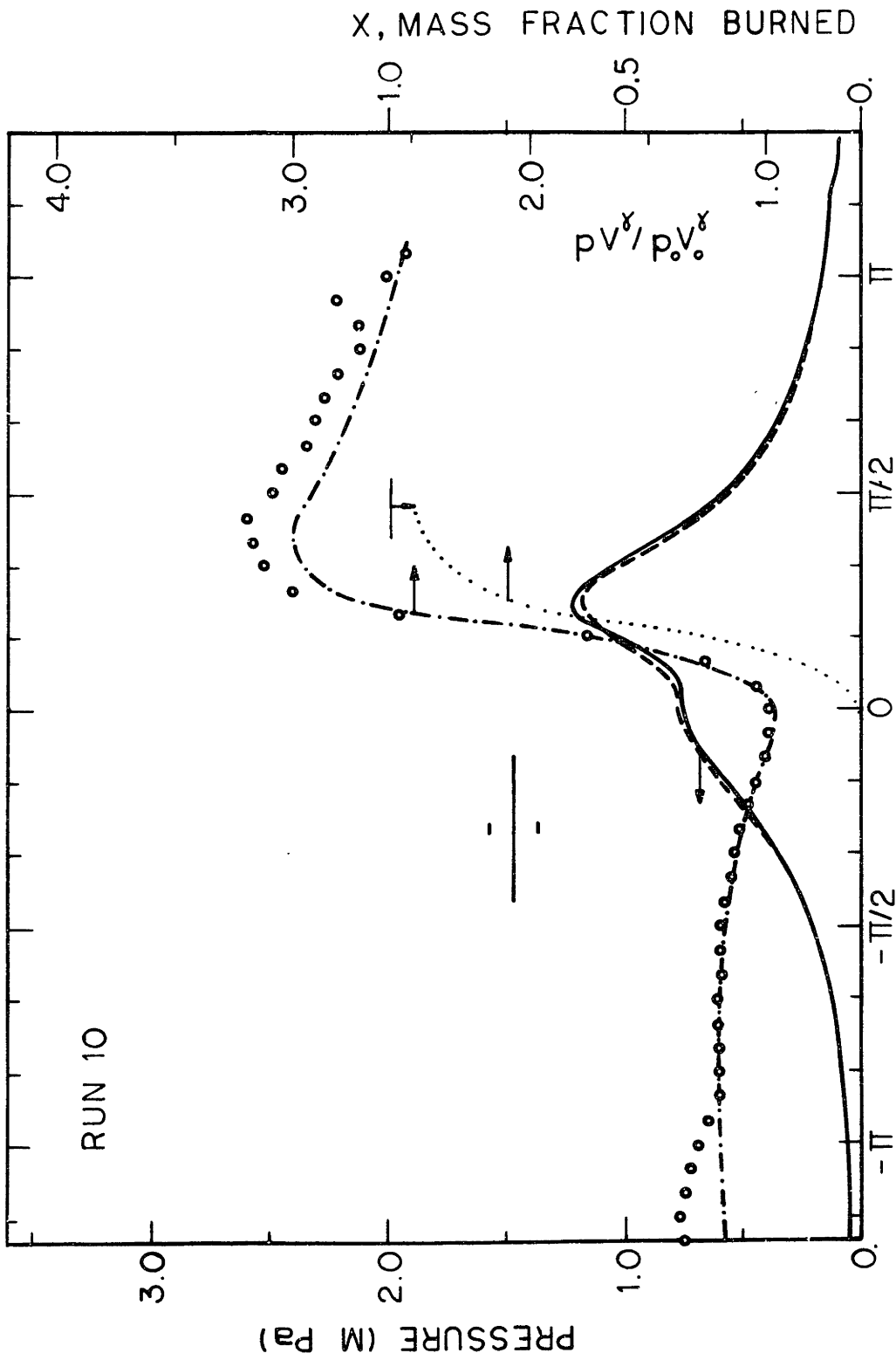
Fig. 34 Comparison between theory and experiments for Run 10 .
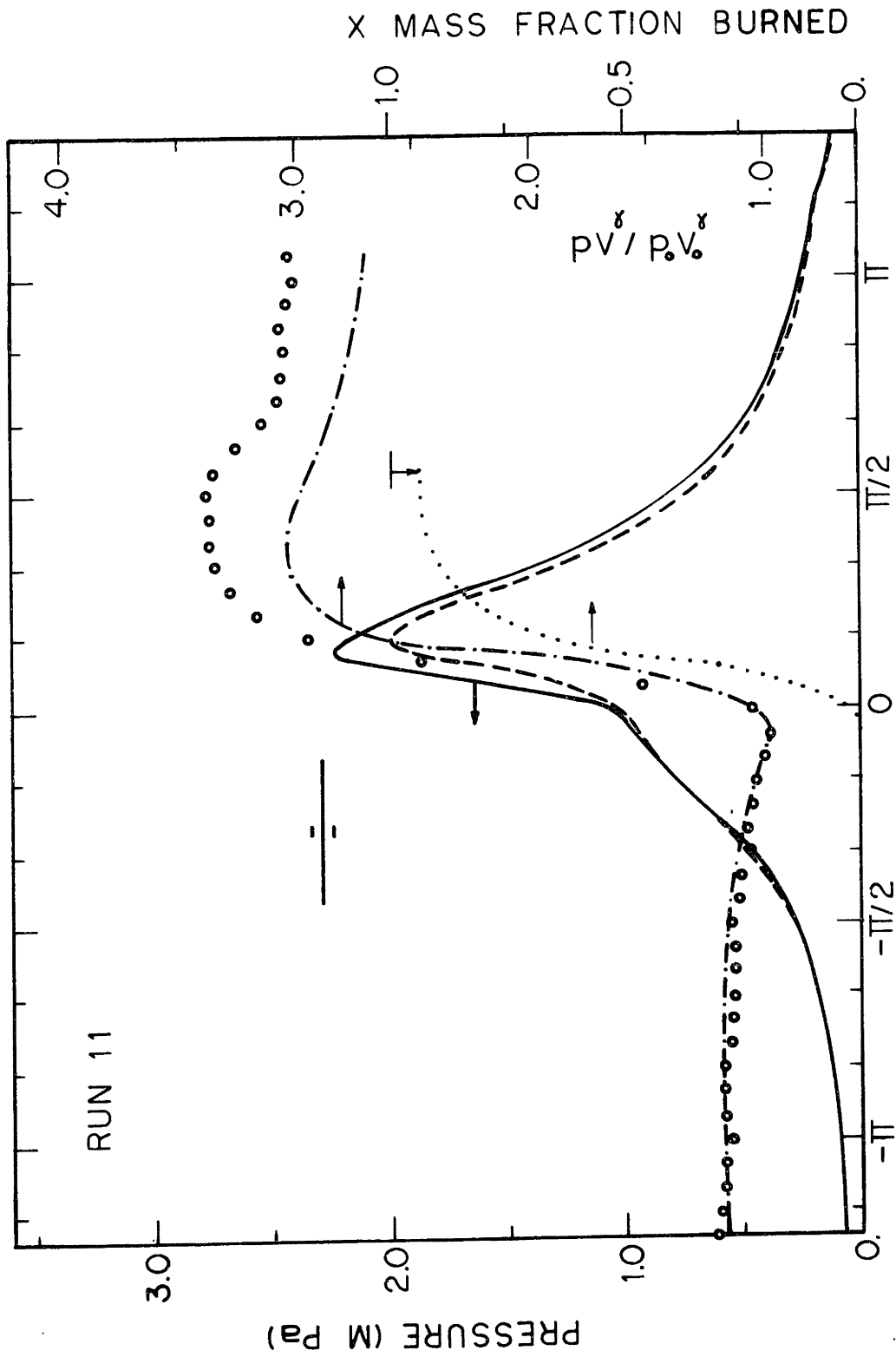
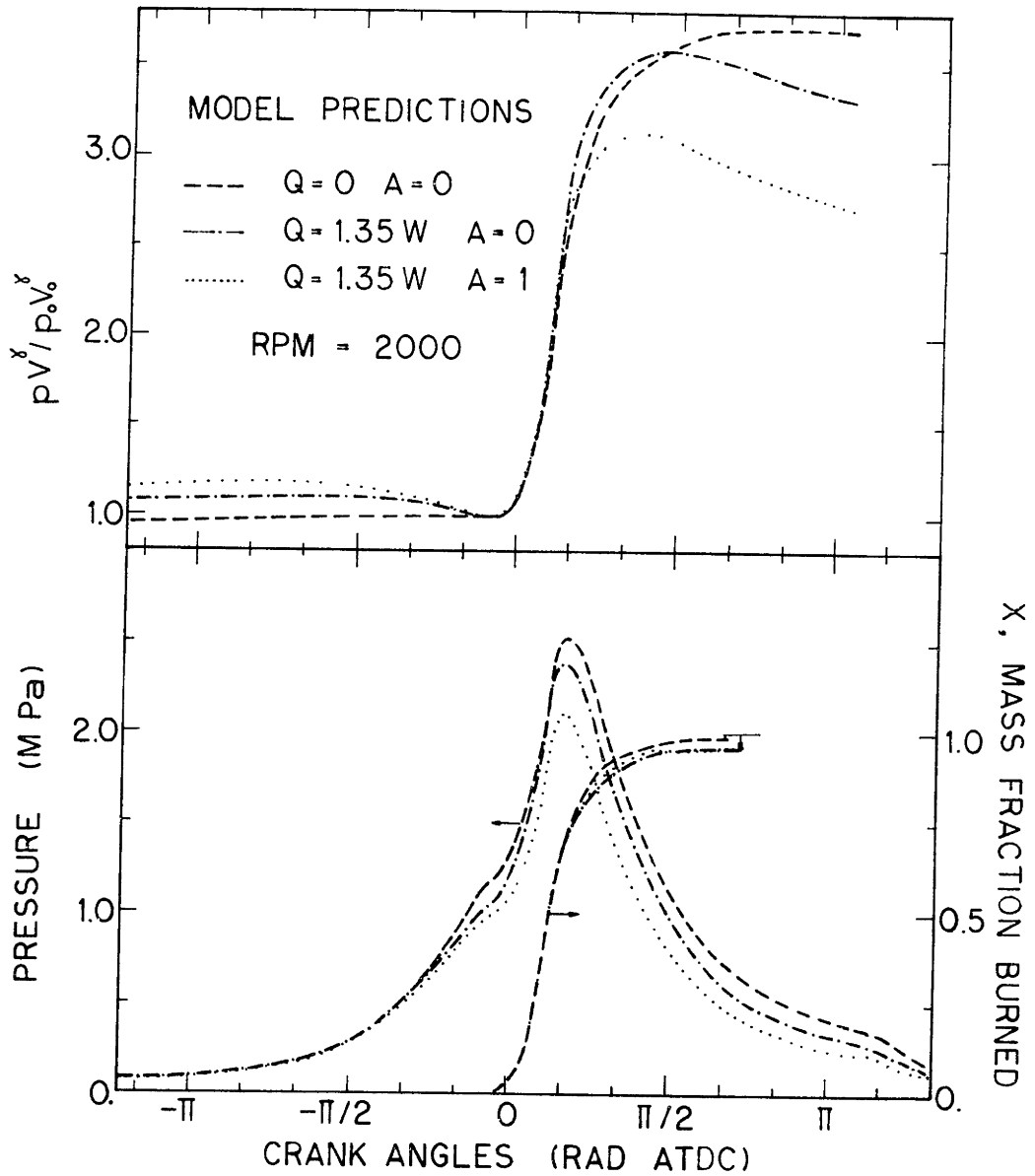Fig. 35 Comparison between theory and experiments for Run 11 .
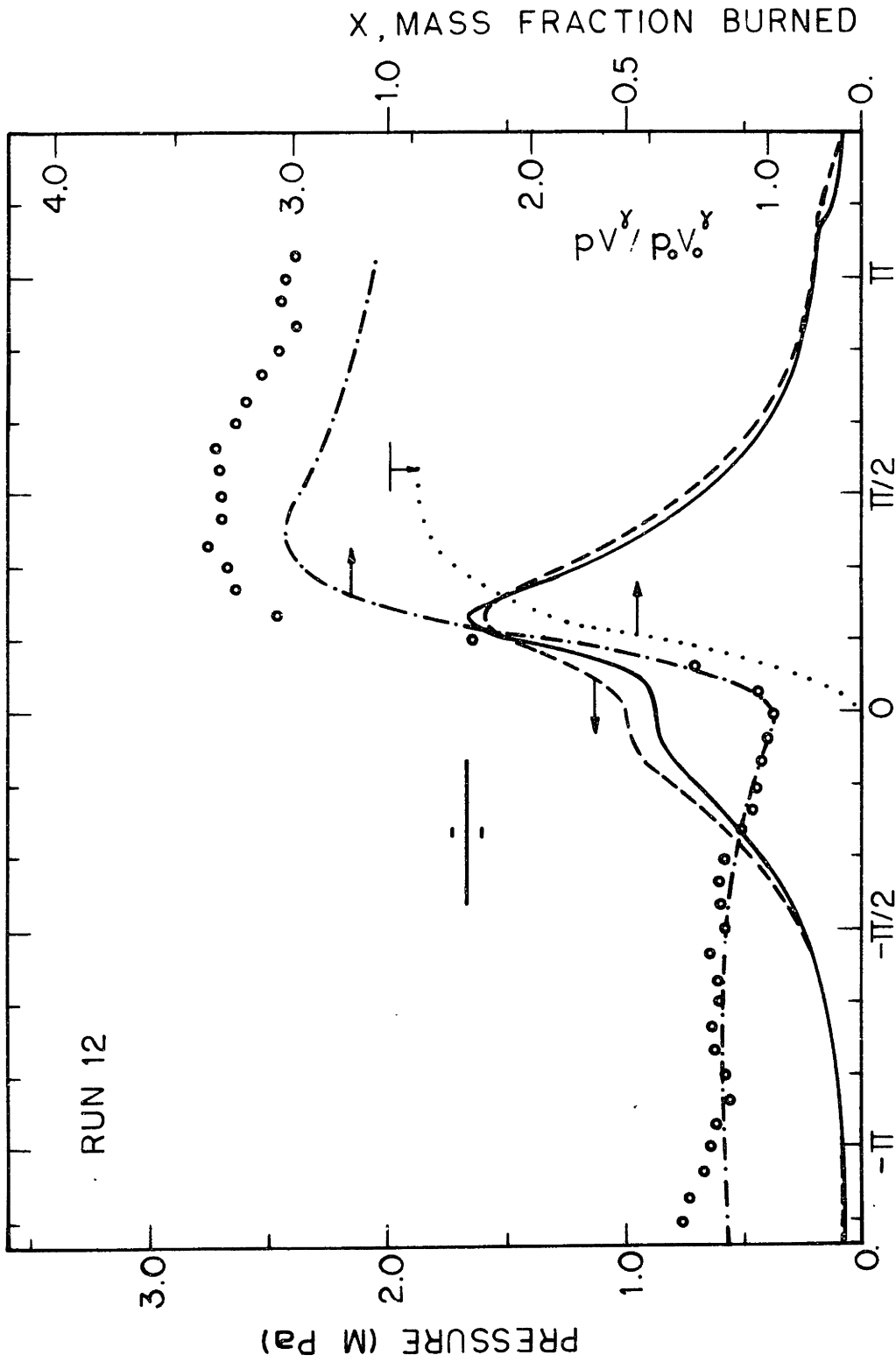
Fig. 36 Comparison between theory and experiments for Run 12 .
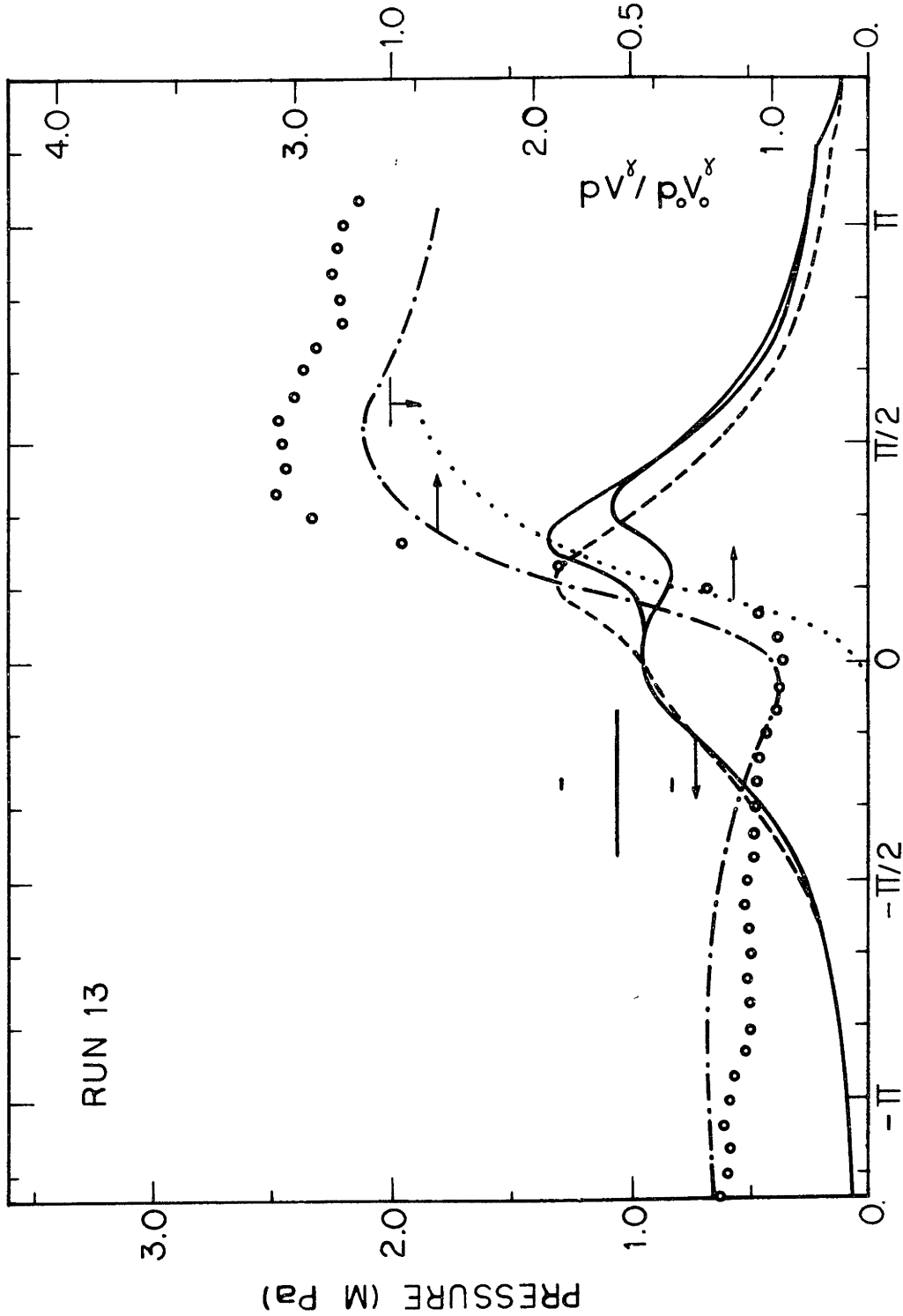
Fig. 37 Comparison between theory and experiments for Run 13.
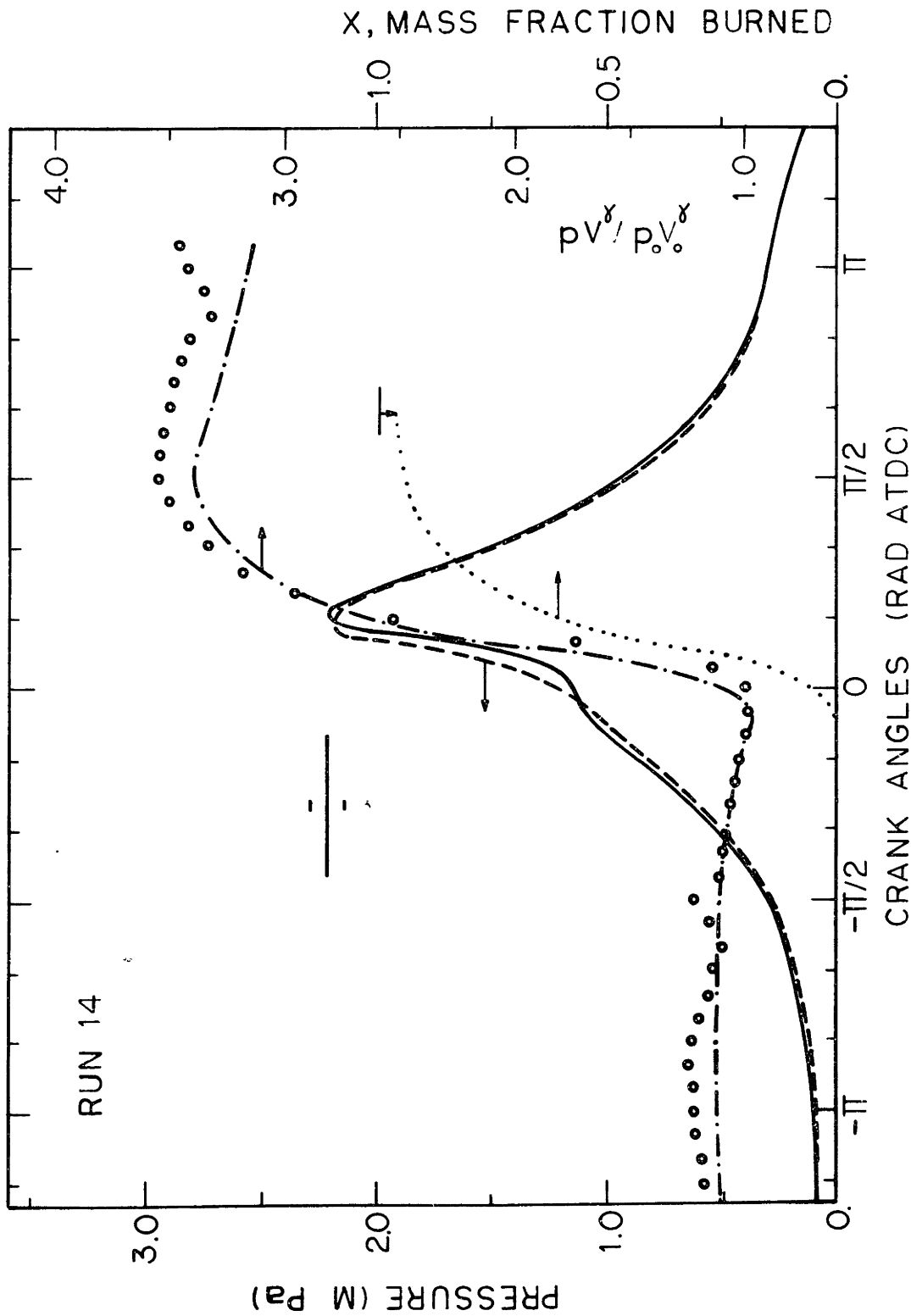
Fig. 38 Comparison between theory and experiments for Run 14 .

Fig. 39 Effect of elimination of losses on engine performances.
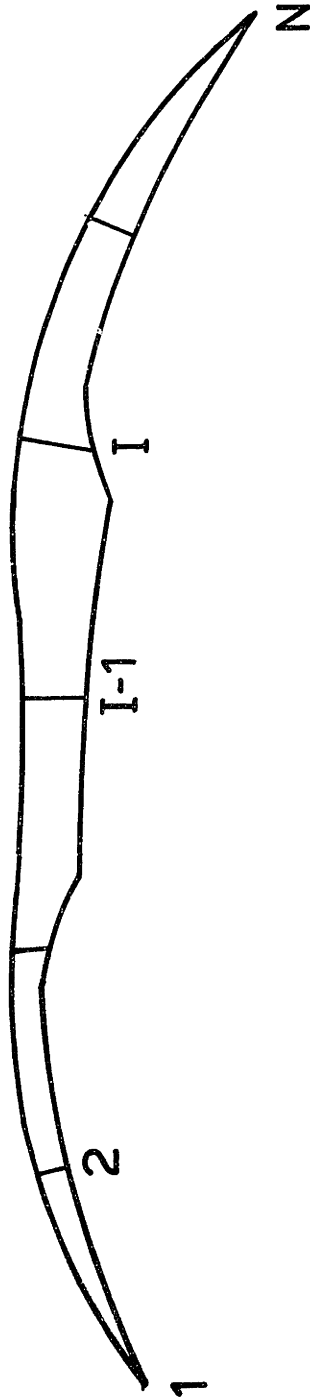
Fig. B1 Schematic representation of the control elements
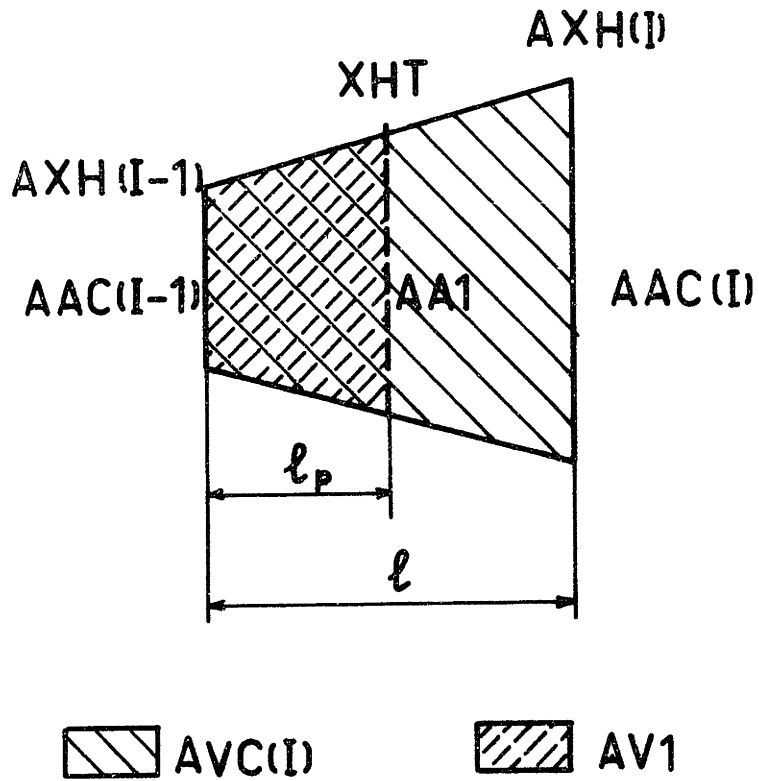and relative running indexes.

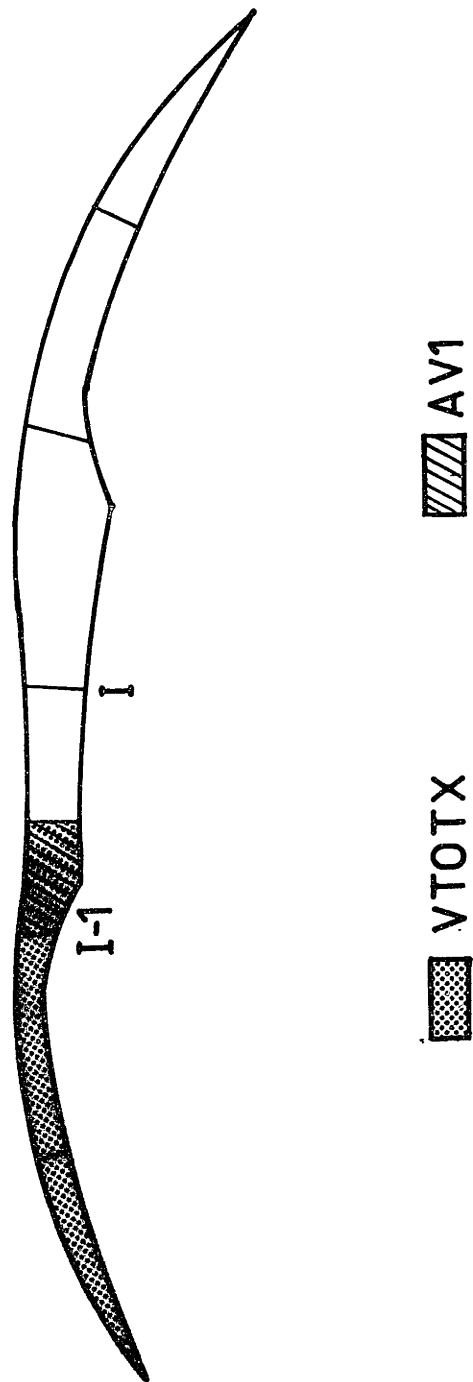Fig. B2 Partition of a control element into subelements.

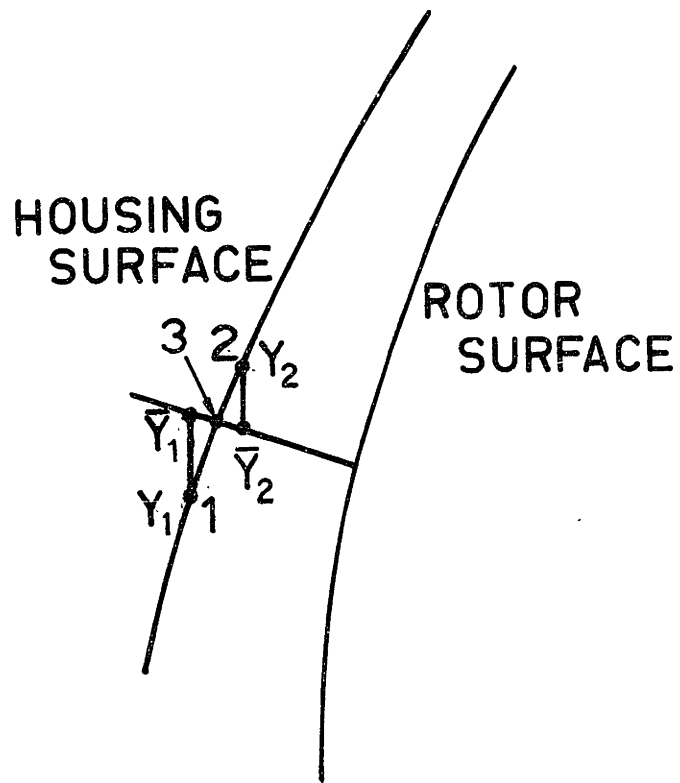Fig. B3 Determination of the volume enclosed in a control subelement (AV1)

Fig. E1 Determination of the intersection between a perpendicular to
the rotor profile and the housing.

BIOGRAPHICAL NOTES ON GUIDO A. DANIELI

Born in Torino (Italy), october the 1st 1946

Degrees:

1. Diploma di Laurea in Ingegneria Meccanica, Universita' degli Studi di NAPOLI, april 1971

2. M.S. in M.E., M.I.T., june 1973

3. Mech. Eng. Deg., M.I.T., september 1974

Work and Research Experience:

1. Italian Air Force Officer, 1970-71

2. Full time graduate student at M.I.T. from fall 1971

   a. Sloan Research Trainee, spring and summer 1972

   b Research Assistant, Dept of Mech. Eng., from fall 1972

3. Professore Incaricato of "Disegno Meccanico" and of "Macchine" at the Universita' degli studi della Calabria, Cosenza (Italy) from spring 1975

Papers:

1. "Il Problema della Sincronizzazione in Campo Automobilistico", 1971, Tesi di Laurea

2. "A Model of Combustion for the Wankel Engine", Term paper, Course 2.092, 1972

3. "Measurements of Nitric Oxide Concentrations in a Wankel Engine Compared with a Chemical Kinetic Model", M.S. in M.E. thesis, 1973

4. G.A.Danieli, C.R.Ferguson, J.B.Heywood, and J.C.Keck, "Predicting the Emissions and Performance Characteristcs of a Wankel Engine", S.A.E. Transaction, Vol   (1974), paper 740186

5. C.R.Ferguson, G.A.Danieli, J.B.Heywood, and J.C.Keck, "Time Resolved Measurements of Exhaust Composition and Flow Rate in a Wankel Engine", S.A.E. paper 750024, 1975

6. "Pressure Measuring Techniques in I.C.E.", Sloan Automotive Lab Internal Report, 1975

7. G.A.Danieli, C.R.Ferguson, J.B.Heywood, and J.C.Keck, "Analysis of Performance Losses in a Wankel Engine", I.M.E. Conference on "Combustion in Engines", 1975